Ministry of Higher Education and Scientific Research
Hassiba Ben Bouali University of Chlef
Faculty of Science and Technology
Department of Electrical Engineering

THESIS

Submitted in fulfillment of the requirements for the degree of

DOCTORATE (LMD)

Field: Electrotechnics

Specialty: Electrical Networks
by

Nesrine LABDOUNI

Title :

Nitrogen Oxides Reduction by Using Cold Plasma Discharge

(Réduction des Oxydes d'azote par Plasma Froid de Décharge)

Defended on **27/04/2026**, in front of the jury composed of:

Bachir BELMADANI	Professor	University of Chlef	Chair
Djilali BENYOUCEF	Professor	University of Chlef	Supervisor
Toufik TAHRI	Professor	University of Chlef	Examiner
Mohamed MOSTEFAOUI	MCA	University of Chlef	Examiner
Abdelatif GADOUM	MCA	University of Ouargla	Examiner
Hocine TEBANI	MCA	University of Chlef	Guest
Abdelkadir BELHADJ DJILALI	MCA	University of Chlef	Guest


In the Name of Allah, the Entirely Merciful, the Especially Merciful
بسم الله الرحمن الرحيم

Acknowledgments

All praise is due to ***Allah***, whose guidance and strength made the completion of this research possible.

I would like to express my sincere gratitude to my supervisors, Pr. **Djilali Benyoucef** and Dr. **Hocine Tebani**, from the Department of Electrical Engineering at the University of Chlef, for their invaluable guidance, continuous support, and constructive feedback throughout the course of this study.

I am also grateful to the members of the doctoral committee: the chair, Pr. **Bachir BELMADANI** from the University of Chlef, and the jury members: Pr. **Toufik Tahri**, Dr. **Mohamed Mostefaoui** from University of Chlef and Dr. **Abdelatif Gadoum** from University of Ouargla, as well as Dr. **Abdelkadir Belhadj Djilali** from University of Chlef. I sincerely appreciate the time and expertise they devoted to the evaluation of this thesis, as well as their insightful comments and suggestions.

My appreciation extends to all those who contributed, directly or indirectly, to the realization of this research. Their assistance, collaboration, and support are gratefully acknowledged.

Finally, I express my deepest gratitude to my family, particularly my parents, for their unwavering support, patience, and encouragement throughout my academic journey. Their constant presence and confidence have been an enduring source of motivation.

إهداء

إلى من كان دعاؤهما سرَّ قوتي، ونبضَ عزيمتي، وسندَ مسيرتي
إلى من كانا دعائي قبل أن يكونا سندي
إلى والديَّ الكريمين

أطال الله في عمرهما وجزاهما عني خير الجزاء

إلى إخوتي وأخواتي

من جاهدوا حتى يكون يومي مكللًا بالفخر لهم لا لنفسي

إلى من وعدتُ الله أن أكون لهم كما أحبّوا

إلى رفقاء السنين وأصحاب الشدائد والأزمات
إلى كل من كان عونًا وسندًا في هذا الطريق، بكلمة طيبة أو دعاء صادق

إليكم جميعًا أهدي ثمرة هذا الجهد، وهذا الإنجاز الذي ما كان ليكتمل إلا بتوفيق الله ثم بدعائكم

أدامكم الله لروحي، وحفظكم ملاذًا أنتمي إليه

أسأل الله أن يجعله علمًا نافعًا، وعملًا خالصًا لوجهه الكريم، وأن يبارك لي فيما تعلمت، وأن يكون حجةً لي لا عليّ.

**نسرين لعبدوني **

Abstract

This thesis reports a detailed numerical investigation of nitrogen oxides (NO_x) mitigation using a dielectric barrier discharge (DBD) reactor operating at atmospheric pressure. The study examines the electrical behavior of the discharge, including voltage–current characteristics, discharge power, and specific energy density, and investigates their relationship with NO_x removal performance. Simulations were performed for various working gas compositions (69% N_2, 20% O_2, and 1% Ar), and a simulated exhaust gas containing NO, under different operating conditions such as applied voltage(10kV), excitation frequency(3kHz), and NO flow rate. The numerical model was developed and implemented using COMSOL Multiphysics to analyze the coupled plasma dynamics and chemical kinetics involved in the discharge process. Particular attention is given to the temporal development of micro-discharges in order to elucidate the plasma-chemical pathways responsible for the generation of reactive species, including atomic oxygen, ozone, and electronically excited molecules of nitrogen and oxygen. These species are shown to govern the oxidation of NO and its subsequent transformation into NO_2, N_2O_5, and other less hazardous nitrogen compounds. The simulations were carried out for atmospheric-pressure gas mixtures composed of N_2, O_2, Ar, and NO under optimized operating conditions. The results indicate that higher applied voltages, combined with the presence of low oxygen fractions, markedly increase the formation of oxidative radicals, thereby improving NO conversion efficiency. In addition, the effect of argon admixture is analyzed, revealing its role in enhancing electron-impact processes and discharge homogeneity, which in turn leads to improved plasma reactivity. The obtained results demonstrate a NO reduction efficiency reaching approximately 99% under optimal operating conditions, confirming the strong potential of DBD plasma technology for air pollution control. The energetic performance of the process is evaluated to assess its suitability for large-scale implementation. Overall, the outcomes confirm that non-thermal plasma generated by DBD reactors constitutes an effective, energy-efficient, and environmentally sustainable approach for NO_x reduction. The reactor demonstrates significant removal efficiencies, underscoring its potential for advanced air purification. Finally, strategies for reactor optimization and prospects for coupling DBD technology with catalytic systems are discussed.

Keywords: Cold plasma; Dielectric barrier discharge (DBD); Nitrogen oxides (NO_x); Air pollution control; Numerical modeling; Plasma chemistry; Atmospheric-pressure plasma.

Résumé

Cette thèse présente une étude numérique détaillée de la réduction des oxydes d'azote (NO_x) à l'aide d'un réacteur à décharge à barrière diélectrique (DBD) fonctionnant à pression atmosphérique. L'étude analyse le comportement électrique de la décharge, notamment les caractéristiques tension–courant, la puissance de décharge et la densité d'énergie spécifique, ainsi que leur influence sur les performances d'élimination des NO_x. Les simulations ont été réalisées pour différents mélanges gazeux composés de 69% N_2, 20% O_2 et 1% Ar, ainsi qu'un gaz simulant les fumées contenant du 10% NO, sous diverses conditions de fonctionnement telles que la tension appliquée(10kV), la fréquence d'excitation(3kHz) et le débit de NO. Le modèle numérique a été développé et implémenté à l'aide du logiciel COMSOL Multiphysics afin d'étudier la dynamique du plasma et la cinétique chimique couplées au sein du réacteur DBD. Une attention particulière a été portée au développement temporel des micro-décharges afin d'identifier les mécanismes plasma-chimiques responsables de la génération des espèces réactives, telles que l'oxygène atomique, l'ozone et les molécules excitées d'azote et d'oxygène. Ces espèces jouent un rôle essentiel dans l'oxydation du NO et sa transformation en NO_2, N_2O_5 et d'autres composés azotés moins nocifs. Les résultats montrent que l'augmentation de la tension appliquée, associée à de faibles fractions d'oxygène, favorise fortement la formation des radicaux oxydants et améliore ainsi l'efficacité de conversion du NO. L'effet de l'ajout d'argon a également été étudié, révélant son rôle dans l'amélioration des processus d'impact électronique et de l'homogénéité de la décharge, ce qui conduit à une réactivité plasma plus élevée. Les résultats obtenus montrent une efficacité de réduction du NO atteignant environ 99 % dans des conditions optimales de fonctionnement, confirmant ainsi le fort potentiel de la technologie DBD pour le contrôle de la pollution atmosphérique. Les performances énergétiques du procédé ont également été évaluées afin d'examiner sa faisabilité pour des applications à grande échelle. Globalement, cette étude confirme que le plasma non thermique généré par les réacteurs DBD constitue une solution efficace, écoénergétique et durable pour la réduction des NO_x. Enfin, des perspectives d'optimisation du réacteur ainsi que le couplage de la technologie DBD avec des systèmes catalytiques sont proposés.

Mots-clés : Plasma froid ; Décharge à barrière diélectrique (DBD); Oxydes d'azote (NO_x); Dépollution de l'air; Modélisation numérique; Chimie plasma; Plasma à pression atmosphérique.

ملخص

تقدّم هذه الأطروحة دراسة عددية مفصلة لخفض أكاسيد النيتروجين (NO_x) باستخدام مفاعل التفريغ بالحاجز العازل (DBD) العامل تحت الضغط الجوي. شملت الدراسة تحليل السلوك الكهربائي للتفريغ، بما في ذلك خصائص الجهد، التيار، قدرة التفريغ، وكثافة الطاقة النوعية، بالإضافة إلى دراسة علاقتها بكفاءة إزالة أكاسيد النيتروجين. وقد أُجريت المحاكاة لعدة خلطات غازية تتكون من الآزوت ($69\%N_2$)والأكسجين($20\%\ O_2$) والأرجون($1\%Ar$) ، إضافة إلى غاز يحاكي غازات العادم المحتوية على$10\%NO$ ، وذلك تحت ظروف تشغيل مختلفة مثل الجهد المطبق(10kV)، تردد الإثارة(3kHz)، ومعدل تدفقNO. تم تطوير النموذج العددي باستخدام برنامج COMSOL Multiphysicsلدراسة ديناميكية البلازما والحركية الكيميائية المقترنة داخل مفاعل DBD. وقد تم التركيز بشكل خاص على التطور الزمني للتفريغات الدقيقة لفهم المسارات البلازمية الكيميائية المسؤولة عن توليد الأنواع النشطة، مثل الأكسجين الذري، والأوزون، والجزيئات المثارة للآزوت والأكسجين. وتلعب هذه الأنواع دورًا أساسيًا في أكسدة غاز NO وتحويله إلى NO_2 و N_2O_5ومركبات آزوتية أخرى أقل ضررًا .أظهرت النتائج أن زيادة الجهد المطبق، مع استعمال نسب منخفضة من الأكسجين، تؤدي إلى تعزيز تكوين الجذور المؤكسدة وبالتالي تحسين كفاءة تحويل .NO كما تمت دراسة تأثير إضافة غاز الأرجون، حيث تبين أنه يساهم في تعزيز عمليات التصادم الإلكتروني وتحسين تجانس التفريغ، مما يؤدي إلى زيادة فعالية البلازما .وقد بينت النتائج المحصل عليها أن كفاءة إزالة NO بلغت حوالي ٪99 تحت شروط تشغيل مثالية، مما يؤكد الإمكانات الكبيرة لتقنية البلازما غير الحرارية في التحكم في تلوث الهواء. كما تم تقييم الأداء الطاقوي للعملية لدراسة إمكانية تطبيقها على نطاق صناعي واسع. وبصفة عامة، تؤكد هذه الدراسة أن البلازما غير الحرارية المتولدة بواسطة مفاعلات DBDتمثل تقنية فعالة وموفرة للطاقة وصديقة للبيئة من أجل تقليل أكاسيد النيتروجين. وفي الأخير، تم اقتراح آفاق مستقبلية لتحسين تصميم المفاعل وربط تقنية DBD بالأنظمة التحفيزية لزيادة الكفاءة وتقليل النواتج الثانوية.

الكلمات المفتاحية :البلازما الباردة؛ التفريغ ذو الحاجز العازل(DBD) ؛ أكاسيد النيتروجين (NO_x)؛ تنقية الهواء؛ النمذجة العددية؛ كيمياء البلازما؛ البلازما عند الضغط الجوي.

List of Abbreviations

DBD : Dielectric Barrier Discharge

NTP : Non-Thermal Plasma

EEDF : Electron Energy Distribution Function

LEA : Local Energy Approximation

LFA : Local Field Approximation

OES : Optical Emission Spectroscopy

RF : Radio Frequency

NOx : Nitrogen Oxides

NO : Nitric Oxide

NO_2 : Nitrogen Dioxide

N_2O_5 : Dinitrogen Pentoxide

SOx : Sulfur Oxides

VOC : Volatile Organic Compounds

ODE : Ordinary Differential Equation

PDE : Partial Differential Equation

FEM : Finite Element Method

PIC : Particle-in-Cell

DM : Drift–Diffusion Model

CC : Continuity Equation

HV : High Voltage

AC : Alternating Current

List of Symbols

t : Time (s)

x : Spatial coordinate (m)

p : Pressure (Pa)

T : Gas temperature (K)

T_e : Electron temperature (eV or K)

n : Number density (m^{-3})

n_e : Electron density (m^{-3})

n_i : Ion density (m^{-3})

E : Electric field (V/m)

V : Electric potential / Applied voltage (V)

I : Discharge current (A)

P : Power (W)

f : Frequency (Hz)

μ_e : Electron mobility ($m^2 \cdot V^{-1} \cdot s^{-1}$)

μ_i : Ion mobility ($m^2 \cdot V^{-1} \cdot s^{-1}$)

D_e : Electron diffusion coefficient ($m^2 \cdot s^{-1}$)

D_i : Ion diffusion coefficient ($m^2 \cdot s^{-1}$)

Γ_e : Electron flux ($m^{-2} \cdot s^{-1}$)

Γ_i : Ion flux ($m^{-2} \cdot s^{-1}$)

k_j : Rate coefficient of reaction j

ε : Mean electron energy (eV)

n_ε : Electron energy density ($eV \cdot m^{-3}$)

φ : Electrostatic potential (V)

ε_0 : Vacuum permittivity (F/m)

ε_r : Relative permittivity

dg : Gas gap distance (m)

dd : Dielectric thickness (m)

A : Electrode area (m^2)

Q : Accumulated surface charge (C)

List of Figures

Chapter I: Overview of Nitrogen Oxides (NO_x) and Their Reduction Methods

Chapter II: Fundamentals and Applications of Dielectric Barrier Discharge Plasma

Chapter III: Modeling and Simulation Results of Air DBD Discharge

Chapter IV: Application of DBD Plasma for NO Reduction in Air

List of Tables

Chapter I: Overview of Nitrogen Oxides (NO_x) and Their Reduction Methods

Chapter II: Fundamentals and Applications of Dielectric Barrier Discharge Plasma

Chapter III: Modeling and Simulation Results of Air DBD Discharge

Chapter IV: Application of DBD Plasma for NO Reduction in Air

Table of Contents

Chapter II: Fundamentals and Applications of Dielectric Barrier Discharge Plasma

Chapter III: Modeling and Simulation Results of Air DBD Discharge

General Introduction

General Introduction

Air pollution remains one of the most critical environmental challenges of the 21st century, driven by rapid industrialization, intensive transportation systems, and increasing global energy demand. Among the various atmospheric contaminants, nitrogen oxides (NO_x) occupy a central position due to their major contribution to tropospheric ozone formation, photochemical smog, acid rain, and fine particulate matter ($PM_{2.5}$). With international regulations becoming increasingly stringent, the development of efficient and environmentally friendly NO_x reduction technologies has become an active area of scientific research. This thesis addresses this challenge through the study and modeling of dielectric barrier discharge (DBD) plasma as a promising non-thermal technology for NO_x reduction in air.

a) Antecedents

The emission of nitrogen oxides originates primarily from high-temperature combustion processes, including vehicular engines, power plants, gas turbines, and industrial furnaces. Historically, conventional mitigation techniques such as Selective Catalytic Reduction (SCR) and Selective Non-Catalytic Reduction (SNCR) have dominated the field due to their relatively high efficiency in converting NO_x into benign products like N_2 and H_2O. However, these technologies require elevated temperatures, expensive catalysts, and strict operating conditions, which limit their applicability particularly in small and medium scale systems or in applications involving fluctuating exhaust streams.

During the last three decades, advances in plasma science have opened new perspectives for addressing atmospheric pollution. Non-thermal (or cold) plasmas, characterized by energetic electrons and near-ambient gas temperatures, offer the ability to drive chemical reactions that are otherwise unattainable under normal conditions. Dielectric Barrier Discharges, first developed in the 19th century for ozone generation, have reemerged as a powerful tool for environmental applications due to their ability to generate highly reactive species without significant gas heating. The combination of historical knowledge on gas discharges and recent progress in plasma diagnostics and modeling sets the foundation for the present work.

b) Motivation

The motivation behind this thesis lies in the need to develop sustainable alternatives to conventional NO_x abatement technologies. Cold plasmas, and in particular DBD systems,

operate under atmospheric pressure, require no expensive catalysts, and can be activated instantaneously. They are capable of producing reactive oxygen and nitrogen species (O, O_3, N, N_2*) that react promptly with nitrogen oxides to convert them into less harmful compounds. Moreover, DBD reactors are relatively simple in design, scalable, and compatible with hybrid plasma catalytic systems.

Despite their advantages, several challenges remain. The efficiency of NO_x reduction strongly depends on electrical parameters (voltage, frequency, and waveform), reactor geometry, and gas composition. Additionally, the presence of competing reactions may lead to the formation of undesired by-products such as ozone or nitrous oxide (N_2O). As a result, understanding the physicochemical mechanisms governing DBD operation and the optimal conditions for NO removal requires comprehensive modeling and simulation.

This thesis aims to address this gap by developing a detailed 1D fluid model capable of capturing the temporal and spatial dynamics of charged and neutral species, electron energy, and chemical pathways relevant to NO_x reduction.

c) Literature Review

Plasma technology has attracted growing attention over recent decades due to its wide applicability across numerous scientific and industrial fields. Its versatility has enabled advancements in ozone generation, polymer surface modification, CO_2 laser excitation, environmental pollution control, plasma-assisted gas conversion, excimer lamps, plasma display panels, and medical disinfection technologies [1-3]. Among the various plasma sources, dielectric barrier discharges (DBDs) operating at atmospheric pressure are particularly attractive because they allow the generation of non-thermal plasmas under relatively simple operating conditions.

Several experimental studies have reported the formation of diffuse and filamentary plasmas in atmospheric-pressure discharges using a variety of gas compositions, including pure oxygen [4-6], argon–oxygen mixtures [7-8], argon–nitrogen mixtures [9], oxygen–nitrogen mixtures [10], pure argon [11], and pure nitrogen [12-13]. These investigations highlight the strong dependence of discharge characteristics on gas composition, emphasizing the need for a detailed understanding of the underlying physical and plasma-chemical processes governing DBD operation.

A thorough understanding of discharge physics and plasma chemistry is essential for further progress in plasma-based technologies. In particular, the composition of gas mixtures plays a critical role in determining discharge behavior, energy efficiency, and dominant chemical pathways in DBD reactors. Consequently, recent studies have focused on optimizing gas mixtures to enhance plasma performance for industrial and environmental applications [14]. In this context, nitrogen-based mixtures containing oxygen, nitric oxide, and argon have gained interest due to their relevance to air pollution control and NO_x abatement. The addition of argon is known to influence electron energy distribution functions and ionization processes, thereby enhancing the generation of reactive species through electron-impact reactions with molecular gases.

DBD reactors have been extensively investigated for the removal of nitrogen oxides (NO_x) from gas streams. Early work demonstrated the feasibility of using non-thermal plasmas as standalone systems for NO_x decomposition [15- 20]. Subsequent studies explored the synergistic coupling of DBD reactors with catalysts or adsorbents to further improve removal efficiency and selectivity [16, 21–27]. For example, the study reported in [22] examined non-thermal plasma treatment under very low-temperature conditions representative of flue gases from power plants and showed effective removal of gaseous pollutants. Reactor design parameters, including electrode geometry, dielectric material, electrode length and diameter, and discharge configuration, were also found to significantly affect NO removal performance [23].

In addition to reactor design, operating conditions and gas composition strongly influence NO_x abatement efficiency. The effects of oxygen concentration, NH_3/NO molar ratio, and discharge power were investigated in [24], where it was demonstrated that low-oxygen conditions combined with high discharge power could achieve NO_x removal efficiencies as high as 98.5%. More recently, numerical and experimental approaches have been increasingly employed to elucidate plasma chemistry mechanisms. A zero-dimensional kinetic modeling study combined with experimental validation [25] revealed a strong sensitivity of NO and N_2O formation to oxygen concentration and power input in N_2–O_2 plasmas, with a peak in NO production observed at approximately 4% O_2. Excellent agreement between modeled and measured species concentrations was reported.

Cold plasma techniques have also been applied to the treatment of flue gases, where NO was shown to be effectively oxidized to NO_2 and subsequently to N_2O_5, facilitating downstream catalytic reduction at lower temperatures [26]. The presence of hydrocarbons in the gas stream was found to further enhance oxidation efficiency. Complementary modeling studies have

examined the role of oxygen concentration on nitrogen oxide conversion using zero-dimensional plasma chemistry models, demonstrating that NO conversion efficiency strongly depends on O_2 levels and exhibits optimal behavior at specific concentrations [27].

Despite the extensive experimental and modeling efforts reported in the literature, several gaps remain. In particular, the combined effects of voltage and frequency on NO removal mechanisms in realistic N_2–O_2–Ar–NO gas mixtures are not yet fully understood, especially under atmospheric-pressure DBD conditions. Moreover, many numerical studies rely on simplified kinetic schemes or reduced-dimensional models that do not fully capture spatiotemporal plasma dynamics. In light of these limitations, the present work aims to provide a comprehensive numerical investigation of dielectric barrier discharge behavior in N_2–O_2–Ar–NO mixtures, with particular emphasis on the influence of operating frequency and applied voltage on electron dynamics, plasma chemistry, and NO elimination efficiency.

d) Objectives

The overarching goal of this research is to investigate the potential of dielectric barrier discharge plasma for the removal of nitrogen monoxide (NO) in air, using a 1D fluid modeling approach.

The specific objectives are:

- ✓ To analyze the physical principles and chemical mechanisms governing DBD operation, particularly those relevant to the generation of reactive species involved in NO oxidation and reduction.
- ✓ To develop a robust 1D fluid model of air DBD plasma, incorporating continuity equations, electron energy transport, Poisson's equation, and a representative set of chemical reactions.
- ✓ To characterize the temporal and spatial behavior of electrons, ions, radicals, and excited species under various electrical conditions (frequencies, voltages, waveforms).
- ✓ To evaluate the efficiency of NO removal in N_2–O_2–Ar–NO mixtures under different operating conditions.
- ✓ To identify the dominant chemical pathways and optimal conditions that maximizes NO conversion while minimizing undesired by-products.
- ✓ To contribute to the design and optimization of operating conditions of plasma systems to combat environmental pollution, with potential applications in industrial emission control and clean technologies.

e) Organization

The thesis is structured into four chapters, each addressing a major component of the research

Chapter I: Overview of Nitrogen Oxides (NO_x) and Their Reduction Methods

This first chapter presents background information on air pollution, the formation and impacts of NO_x, and conventional mitigation techniques. The fundamentals of cold plasma science are introduced, highlighting non-thermal plasma as an innovative method for pollution control.

Chapter II: Fundamentals and Applications of Dielectric Barrier Discharge Plasma

In the second chapter, an in-depth overview of plasma created by Dielectric Barrier Discharge plasma is provided, including discharge physics, micro-discharge behavior, chemical pathways, and the formation of reactive species. Applications of DBD reactors such as ozone generation, surface treatment, and pollutant removal are discussed, with emphasis on their role in NO_x reduction.

Chapter III: Modeling and Simulation Results of Air DBD Discharge

The third chapter describes the physical assumptions, governing equations, boundary conditions, and numerical methods used to simulate DBD plasma. The coupling between electron energy, particle charges species transport, dielectric surface charge, the electric and the voltage distribution in the gap discharge, and plasma chemistry forms the core of the modeling framework.

Chapter IV: Application of DBD Plasma for NO Reduction in Air

The last chapter presents the simulation results, analyzing the influence of frequency and voltage on discharge behavior, species formation, and NO conversion. Spatial and temporal distributions of key radicals are examined, and the dominant chemical mechanisms responsible for NO removal are identified. The chapter concludes with recommendations for optimizing DBD reactors for environmental applications.

This thesis will conclude with a comprehensive synthesis of the main accomplishments and the difficulties encountered throughout the work. In addition, potential avenues for future investigations will be outlined.

f) Graphical Abstract:

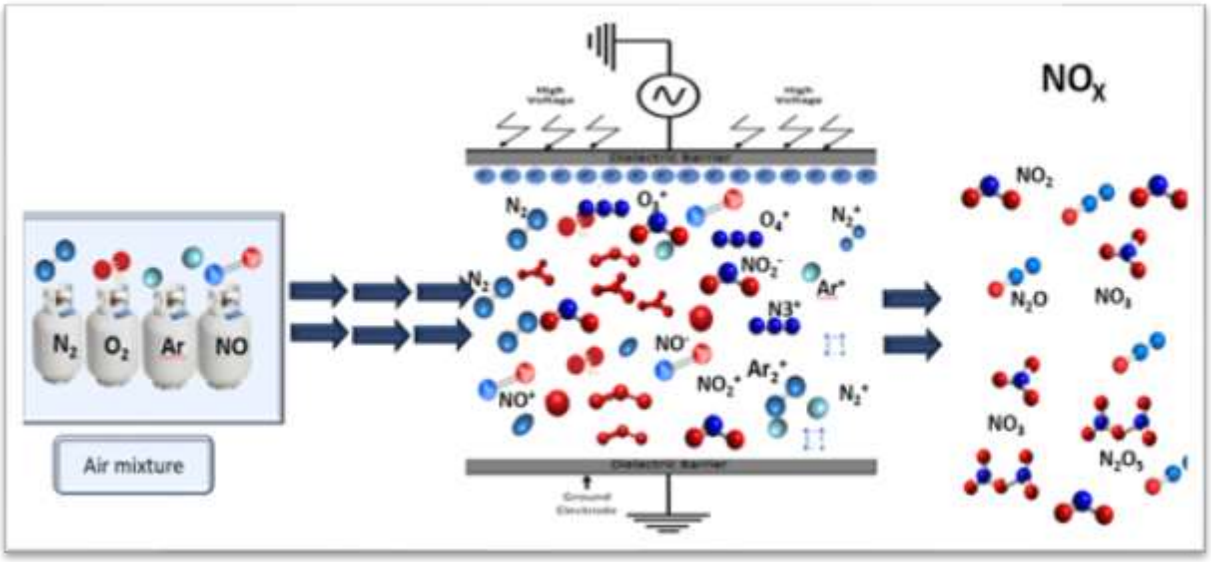

References

[1] Z. Fang, *et al.*, "Polyethylene terephthalate surface modification by filamentary and homogeneous dielectric barrier discharges in air," *IEEE Transactions on Plasma Science*, vol. 37, no. 5, pp. 659-667, 2009.

[2] C. Zhang, *et al.* "Surface treatment of polyethylene terephthalate films using DBD excited by repetitive unipolar nanosecond pulses in air at atmospheric pressure," *IEEE transactions on plasma science*, vol. 38, no.6, pp.1517-1526, 2010.

[3] S. Rath, S. Kar, "Microwave atmospheric pressure plasma jet: a review," *Contributions to Plasma Physics*, vol. 65, no. 2, p. e202400036, 2025.

[4] D. Benyoucef, M. Yousfi, "Particle modelling of magnetically confined oxygen plasma in low pressure radio frequency discharge," *Physics of Plasmas*, vol. 22, no. 1, 2015.

[5] N. Labdouni, D. Benyoucef, H. Tebani, "Numerical Simulation of Atmospheric Dielectric Barrier Discharge in Oxygen gas using COMSOL Multiphysics," *The third National Conference on Materials Science and Engineering*, Chlef, Algeria, June 11-12th, 2025.

[6] N. Labdouni, D. Benyoucef, H. Tebani, "Ozone Generation via Dielectric Barrier Discharge in The Atmosphere," *The 1st National Conference on Energy and its Applications*, Medea, Algeria, 18 December 2024.

[7] N. Labdouni, D. Benyoucef, H. Tebani, "Fluid Modeling Study on The Effects of Argon Addition to Oxygen for Ozone Generation," *The second International Conference on Physics of Semiconductor Devices, Renewable Energies and Environment*, Bechar, Algeria, 11-13 Novembre 2024.

[8] N. Labdouni, D. Benyoucef, H. Tebani, "Numerical Study of Ozone Generated by Dielectric Barrier Discharge in O2-Ar Mixture," *The 3rd edition of the international conference on materials science and engineering and their impact on the environment*, Sidi-Bel-Abbes, Algeria, 29-30-May 2024.

[9] N. Labdouni, *et al.*, "Analysis of Atmospheric Pressure Dielectric Barrier Discharges in Nitrogen-Argon Mixture," *The Third International Conference on Materials, Energy & Environment*, El Oued, Algeria, April 21-22, 2025.

[10] K. Liu, *et al.*, "Study on the Physical and Chemical Characteristics of DBD: The Effect of N_2/O_2 Mixture Ratio on the Product Regulation," *Plasma Chemistry and Plasma Processing*, vol. 39, no. 5, pp. 1255-1274, 2019.

[11] N. Labdouni, D. Benyoucef, H. Tebani, "Electrochemical Kinetic Modeling of an Argon Gas Dielectric Barrier Discharge," *The 1st National Conference for Applied Sciences and Engineering*, ENSTA, Algeria, 17-18 November 2024.

[12] N. Labdouni, D. Benyoucef, H. Tebani, "Plasma Chemistry of Nitrogen in Dielectric Barrier

Discharge Using COMSOL Multiphysics," *First international Seminar in Materials and Engineering Structures,* Ghelizane, Algeria, 26-27 October, 2024.

[13] P. Talebizadeh, *et al.*, "The role of non-thermal plasma technique in NOx treatment: A review," *Renew. Sustain. Energy Rev.*, vol. 40, pp. 886–901, Dec. 2014.

[14] B. S. Rajanikanth, D. Sinha, "Achieving better NOx removal in discharge plasma reactor by field enhancement," *Plasma Sci. Technol*., vol. 10, no. 2, pp. 198–202, 2008.

[15] T. Matsumoto, *et al.*, "Exhaust gas treatment using nano seconds pulsed discharge," *in Proc. IEEE Pulsed Power Conf.*, Jun./Jul. 2009, pp. 1035–1040, 2009.

[16] T. Matsumoto, D. Wang, T. Namihira, and H. Akiyama, "Energy efficiency improvement of nitric oxide treatment using nanosecond pulsed discharge," *IEEE Transactions on Plasma Science*, vol. 38, no. 10, pp. 2639–2643, 2010.

[17] S. Mohapatro and B. S. Rajanikanth, "Study of pulsed plasma in a crossed flow dielectric barrier discharge reactor for improvement of NOx removal in raw diesel engine exhaust," *Plasma Sci. Technol.*, vol. 13, no. 1, p. 82, 2011.

[18] T. Q. Vinh, *et al.*, "Fundamental study of NOx removal from diesel exhaust gas by dielectric barrier discharge reactor," *J. Mech. Sci. Technol.*, vol. 26, no. 6, p. 1921, 2012.

[19] B. M. Penetrante, et al., "Comparison of electrical discharge techniques for NOx reduction," *IEEE Transactions on Plasma Science*, vol. 23, no.4, pp. 679–687, 1995.

[20] Y. S. Mok, *et al.*,"Abatement of nitrogen oxides by combined plasma-photocatalysis process," *IEEE Transactions on Plasma Science*, vol. 30, no. 1, pp. 164–165, 2002.

[21] J. C. Whitehead, "Plasma–catalysis: the knowns and unknowns," *Journal of Physics D: Applied Physics*, vol. 49, no. 24, p. 243001, 2016.

[22] H. H. Kim, "Nonthermal plasma processing for air-pollution control: A strategic survey," *IEEE Transactions on Plasma Science*, vol. 32, no. 1, pp. 100–112, 2004.

[23] A. Taleb-Bendiab, *et al.*, "Zero-dimensional modeling of nitrogen oxide conversion in a N_2/O_2 DBD plasma," *J. Phys.: Conf. Ser.*, vol.596, no. 1, p. 012015, 2015.

[24] A.G. Chmielewski, *et al.*, "Operational experience of the electron beam flue gas treatment plant," *Radiation Physics and Chemistry*, vol. 71, no. 1-2, pp. 439–442, 2004.

[25] H. Wang, H., *et al.* "Effect of oxygen concentration and NH_3/NO molar ratio on NOx removal from flue gas by a DBD reactor," *J. Hazard. Mater.*, vol. 192, pp. 986–991, 2012.

[26] J. Van Durme, *et al.* "Post-plasma catalytic technology for volatile organic compounds abatement," Applied Catalysis B: Environmental, vol. 78, no. 3-4, pp. 324–333, 2008.

[27] I. S. Medjahdi, *et al.* "Numerical Modeling of Impact Effect of Chemical Reactions on Nitrogen Oxide Conversion in N_2/O_2 Mixtures Under Various X% O_2 Concentrations," *IEEE Transactions on Plasma Science*, vol. 49, no. 3, pp. 1181-1189, 2021.

Chapter I

Overview of Nitrogen Oxides (NOx) and Their Reduction Methods

I.1. Introduction

Air pollution has become one of the most pressing environmental challenges worldwide, largely driven by rapid industrialization, urban expansion, and the growing demand for energy. The continuous emission of harmful pollutants into the atmosphere poses serious threats to environmental quality and human health. Among these pollutants, nitrogen oxides (NO_x), primarily nitric oxide (NO) and nitrogen dioxide (NO_2), are of particular concern due to their significant contribution to photochemical smog, acid rain, ground-level ozone formation, and respiratory diseases. These compounds are mainly produced during combustion processes in power plants, transportation systems, and various industrial activities. To mitigate NO_x emissions, several conventional control strategies have been developed and implemented, including combustion optimization, Selective Catalytic Reduction (SCR), and Selective Non-Catalytic Reduction (SNCR). Despite their widespread application, these technologies suffer from notable limitations such as high operational costs, complex system requirements, and the potential generation of secondary pollutants. As a result, there is a growing demand for alternative treatment methods that are both energy-efficient and environmentally sustainable.

In this framework, plasma-based technologies, particularly cold plasma generated by dielectric barrier discharge (DBD) systems, have attracted increasing attention as promising solutions for air pollution control. Cold plasma discharges are capable of producing a wide range of highly reactive oxygen and nitrogen species under ambient conditions, enabling effective NO_x decomposition without the need for elevated temperatures. Accordingly, this chapter presents an overview of air pollution and its principal sources, examines the formation, impacts, and conventional abatement techniques of nitrogen oxides, and introduces the fundamental principles of plasma technology with a focus on cold plasma discharges as innovative tools for atmospheric depollution.

I.2. Nature and Sources of Atmospheric Pollution

Every day, we inhale approximately 15,000 liters of air, making it the most essential element for sustaining life. The average composition of dry air consists of 78% nitrogen (N_2), 21% oxygen (O_2), and 1% of other gases, mainly argon (Ar) and carbon dioxide (CO_2). Many other constituents are present at much lower concentrations. Among these constituents, an atmospheric pollutant can be defined as a substance present at a concentration significantly higher than its natural level, producing measurable harmful effects on humans, animals, plants, and materials through deposition or interactions with surfaces.

The origin of atmospheric pollution is diverse, as it involves both biogenic or natural sources (such as volcanic eruptions, dust, and emissions of volatile organic compounds from plants) and anthropogenic sources associated with human activity (transportation, industry, agriculture, households, etc.). The latter has grown considerably since the first industrial revolution. Atmospheric pollution includes several families of pollutants, classified according to their nature and the degree of dispersion of their components. These include:

- **Inorganic Pollutants**: nitrogen oxides (NO_x) and sulfur oxides (SO_x), ozone (O_3), hydrogen sulfide (H_2S), ammonia (NH_3), etc.
- **Organic Pollutants**: saturated, unsaturated, cyclic and polycyclic hydrocarbons, aldehydes, ketones, sulfur- and chlorine-containing compounds. Most of these are classified as volatile organic compounds (VOCs).
- **Aerosols**: particles, soot, smoke, etc. [1-2].

I.2.1. Major Atmospheric Pollutants

Atmospheric pollutants may occur in gaseous, liquid, or solid form, and their harmful effects are linked either to their intrinsic physicochemical properties or to the toxic substances adsorbed onto the surface of suspended particles. These pollutants originate from both natural processes, such as volcanic eruptions, desert dust storms, or biogenic emissions and human activities including industrial operations, transportation, and domestic energy use. In reality, the atmosphere contains a highly complex mixture of hundreds of chemical compounds, ranging from major pollutants released in significant quantities to trace species that, despite their low concentrations, can have profound environmental and health impacts due to their reactivity or persistence. Among these pollutants, nitrogen oxides (NO_x) are of particular concern, as they play a central role in atmospheric chemistry by contributing to smog formation, acid rain, ground-level ozone production, and secondary particulate matter. Given their environmental significance and direct relevance to human health, this study focuses specifically on nitrogen oxides as the primary target for investigation and control. In the following section, the major categories of primary pollutants will be briefly introduced to provide context for the discussion of NO_x [3–6], figure I.1 shows the major atmospheric pollutants.

- Nitrogen Oxides (NO_x)
- Carbon Oxides (CO_x)
- Sulfur Dioxide (SO_2)
- Polycyclic Aromatic Hydrocarbons (PAHs)
- Toxic Heavy Metals
- Suspended and Fine Particles (PM_{10} and $PM_{2.5}$)
- Volatile Organic Compounds (VOCs)

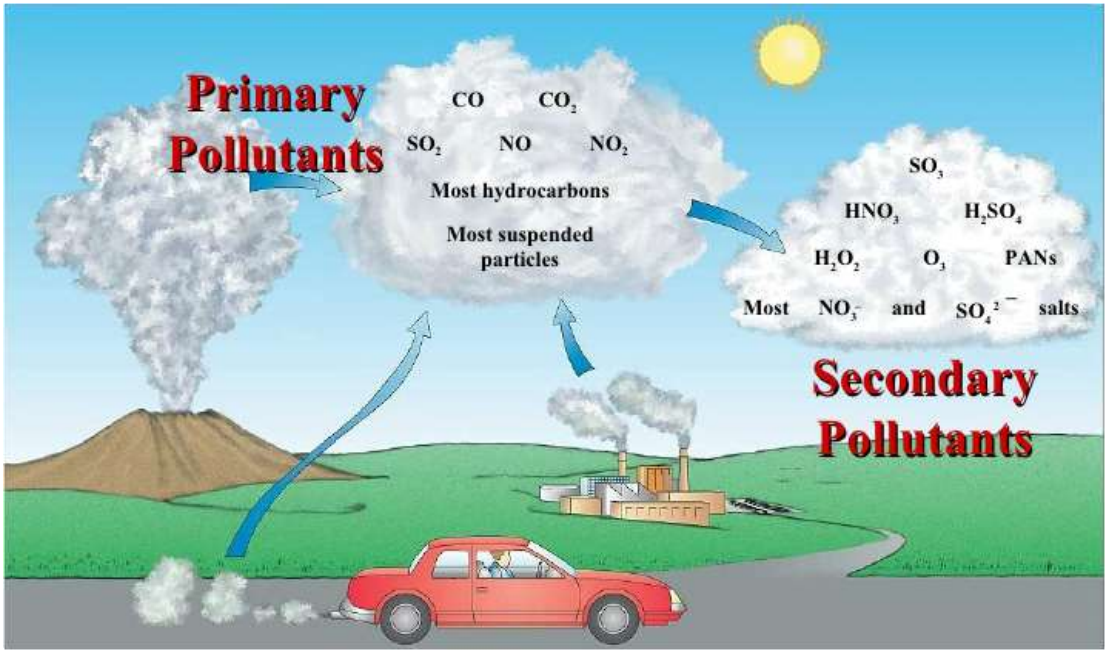

Fig I.1. *Major Atmospheric Pollutants [3]*

I.3. Nitrogen Oxides (NOx): Sources and Environmental Impact

I.3.1. Chemical Nature of NOx

Nitric Oxide (NO):

Nitric oxide is a colorless, odorless gas primarily generated during high-temperature combustion processes, where atmospheric nitrogen (N_2) reacts with oxygen (O_2). Major sources include vehicle engines, industrial furnaces, and power plants. Although NO itself is relatively inert and has low solubility in water, it serves as a key precursor in atmospheric chemistry. In the presence of oxygen and other oxidants, NO is readily converted to nitrogen dioxide (NO_2). It also reacts with ozone (O_3), thereby influencing the balance of tropospheric ozone concentrations. Despite its short atmospheric lifetime, NO is critically important because of its role as an initial product of thermal and fuel-bound nitrogen oxidation [7].

Nitrogen Dioxide (NO_2):

Nitrogen dioxide is a reddish-brown gas with a pungent, acrid odor. It can be directly emitted from combustion sources but is more commonly formed through the oxidation of NO in the atmosphere. Unlike NO, NO_2 is highly reactive and plays multiple roles in air pollution chemistry. It is directly harmful to human health, as it is a strong respiratory irritant capable of penetrating deep into the lungs. From an atmospheric point of view, NO_2 is a primary contributor

to the formation of ground-level ozone (O_3) through photochemical reactions under sunlight. It also participates in the formation of secondary particulate matter ($PM_{2.5}$) via the generation of nitrates. Furthermore, NO_2 absorbs visible light, contributing to urban haze and the characteristic brownish coloration of smog [8].

Other Nitrogen Oxides:

Although less abundant, other nitrogen oxides also have environmental relevance. Nitrous oxide (N_2O), commonly known as "laughing gas," is a powerful greenhouse gas with a global warming potential nearly 300 times greater than carbon dioxide (CO_2) and a long atmospheric lifetime (~120 years). While traditionally considered harmless in air pollution studies, its role in stratospheric ozone depletion and climate change has made it a growing concern. Higher oxides, such as dinitrogen tetroxide (N_2O_4), dinitrogen trioxide (N_2O_3), and dinitrogen pentoxide (N_2O_5), are generally unstable under ambient conditions but act as intermediates in atmospheric chemistry, particularly in nighttime reactions and the formation of nitric acid (HNO_3) [8].

I.3.2. Sources of NOx Emissions

The primary sources of NOx emissions include both natural and anthropogenic (human-caused) activities [9], figure I.2 shows the different sources of NOx emissions.

Anthropogenic sources:

- Transportation: Combustion of fuels in vehicles is one of the largest contributors to NOx emissions, especially in urban areas with heavy traffic.
- Industrial combustion processes: Factories, power plants, and refineries burn fossil fuels, releasing large amounts of NOx.
- Agriculture: Agricultural machinery and livestock, especially cattle, contribute to NOx emissions.
- Residential heating: Wood stoves, heating appliances, and coal-fired heating systems also produce NOx.

Natural sources:

- Lightning: Lightning strikes can cause nitrogen in the atmosphere to react with oxygen, producing NOx.
- Wildfires: Combustion of organic material in wildfires releases NOx into the atmosphere.

- Soil emissions: Soil microbes, particularly in wetlands, can release nitrogen compounds, contributing to NOx formation.

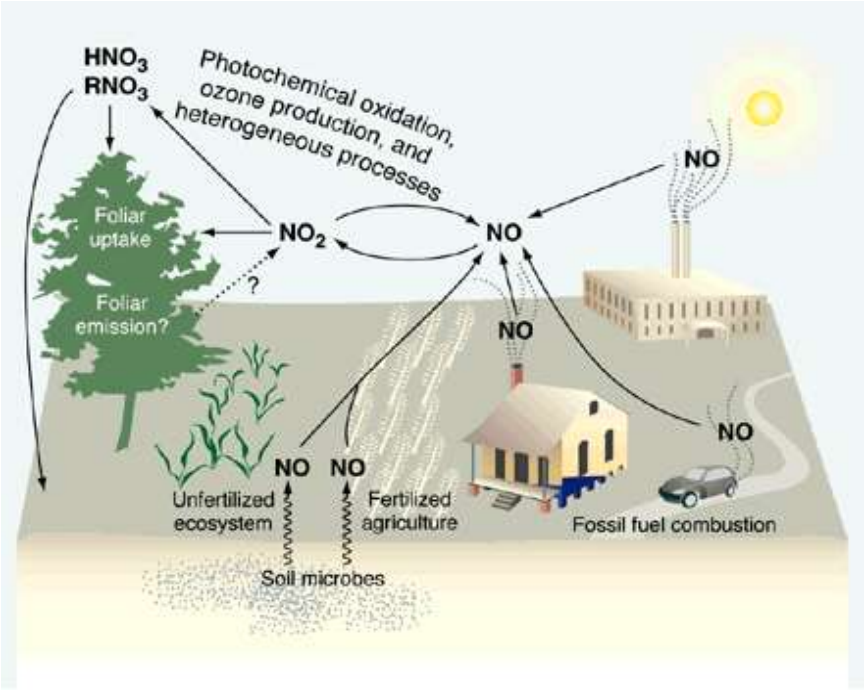

Fig I.2. *Different Sources of NOx Emissions [10].*

I.3.3. Environmental Impacts of NOx

NOx has significant effects on both air quality and ecosystems [11]:

- Formation of Ground-Level Ozone (Tropospheric Ozone): NOx, along with volatile organic compounds (VOCs), reacts in the presence of sunlight to form ground-level ozone, a key component of smog. Ground-level ozone is harmful to human health and vegetation.
- Acid Rain: NOx combines with water vapor and other compounds to form nitric acid (HNO_3), which contributes to acid rain. Acid rain can damage aquatic ecosystems, soil, forests, and buildings.
- Particulate Matter (PM): NOx can react with other pollutants to form fine particulate matter (PM2.5), which is harmful to human health when inhaled.
- Global Warming: Although NOx is not a direct greenhouse gas, its role in the formation of ozone contributes to global warming because ozone is a potent greenhouse gas.

I.3.4. Health Impacts of NOx

NOx has several detrimental effects on human health (see figure I.3), especially in areas with high pollution levels:

- Respiratory Issues: NOx can irritate the respiratory system, leading to conditions such as asthma, bronchitis, and other chronic obstructive pulmonary diseases (COPD).
- Increased Mortality: Long-term exposure to high levels of NOx is associated with an increased risk of heart disease, lung cancer, and premature death.
- Vulnerable Populations: Children, the elderly, and individuals with preexisting respiratory or cardiovascular conditions are more susceptible to the health impacts of NOx.

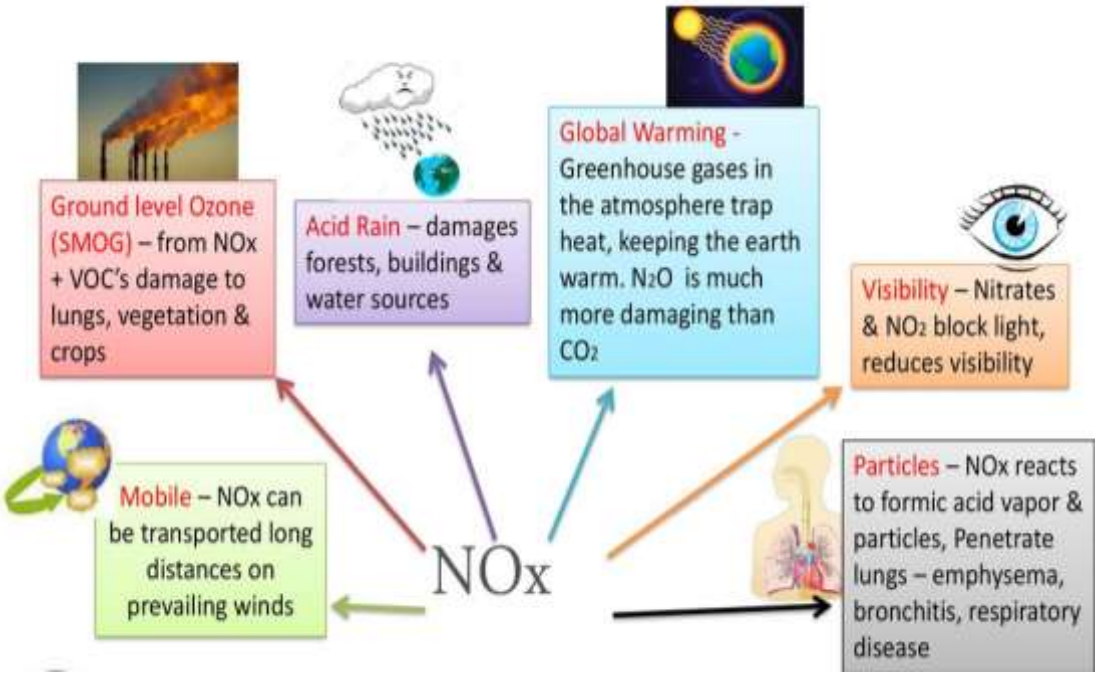

Fig I.3. *Environmental and Health Impacts of NOx [11].*

I.3.5. Formation of NO_x: Detailed Mechanisms

NOx formation primarily occurs in two ways: thermal NO_x formation and fuel NO_x formation [12], in addition to prompt formation:

Thermal NOx

- **Process:** This is the most common form of NO_x generated in high-temperature combustion processes. At temperatures greater than 1,300°C (2,372°F), nitrogen (N_2) from the air reacts with oxygen (O_2) to form nitric oxide (NO).

The reaction is as follows:

$$N_2 + O_2 \rightarrow \text{high temperature} \quad 2NO \qquad \text{(I.1)}$$

- **Thermal NO_x Contribution:** It's produced in engines, power plants, and industrial combustion sources. The higher the combustion temperature, the greater the production of thermal NO_x.

Fuel NOx

- **Process:** This occurs when nitrogen compounds present in the fuel itself, particularly in fossil fuels (like coal, oil, or natural gas), combine with oxygen during combustion. This type of NOx forms at lower temperatures than thermal NOx.

  The main reactions involve the conversion of nitrogen in fuel (e.g., nitrogen in coal) into NO and NO_2.

Prompt NO_x

- **Process:** This is a rapid reaction between nitrogen (N_2) and hydrocarbons (CH) in the combustion process, especially in engines and internal combustion devices. This type of NO_x is generally formed in fuel-rich combustion zones, where there's an abundance of hydrocarbons.

  The reaction can be represented as:

$$CH + N_2 \rightarrow HCN + N \quad \text{(I.2)}$$

$$4HCN + 5O_2 \rightarrow 4NO+4CO+2H_2O \quad \text{(I.3)}$$

I.3.6. Secondary NOx Formation (Photochemical Reactions)

- **NO and Ozone Formation:** When NO (produced from the combustion process) mixes with ozone (O_3) under sunlight, it forms nitrogen dioxide (NO_2):

$$NO+O_3 \rightarrow NO_2+O_2 \quad \text{(I.4)}$$

This interaction is critical in the formation of smog and can increase the concentrations of ozone in the troposphere, which is harmful to human health and the environment.

I.4. Conventional Gas Treatment Techniques

Several conventional techniques are commonly employed for the depollution of gaseous emissions [13–15]:

I.4.1. Filtration

The fundamental step in the separation and pretreatment of polluted effluents consists of separating a discontinuous solid or liquid phase from a continuous gaseous or liquid phase by passing the fluid under pressure through a semi-permeable membrane, which retains the particles on the surface, or through a porous medium which traps the undesirable matters (see figure I.4).

I.4.2. Adsorption

The physical process in which gaseous pollutants are transferred onto the surface of an adsorbent, driven by weak Van der Waals forces, the adsorption can be reversible, allowing desorption and regeneration of the adsorbent, or irreversible, requiring replacement.

I.4.3. Absorption

A method in which a pollutant gas is captured within a liquid phase, often referred to as "gas scrubbing", for particulate capture, inertia and impaction dominate, while for gaseous pollutants, thermodynamic and chemical interactions between the carrier gas, the pollutant, and the liquid govern the process.

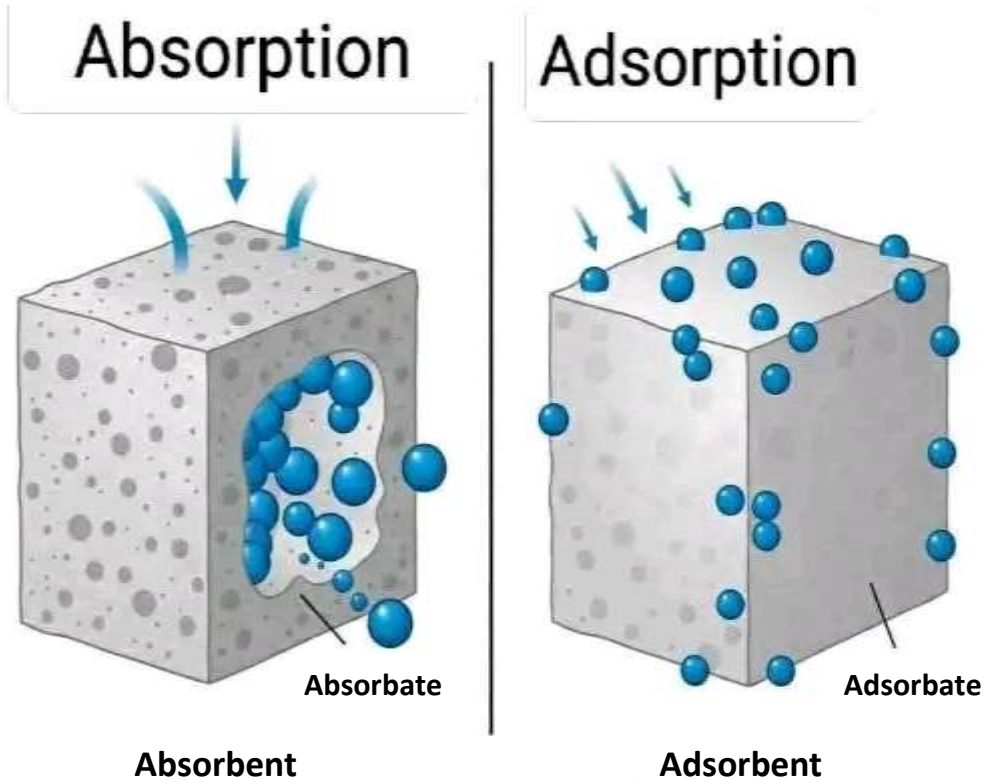

Fig I.4. *Absorption and Adsorption Techniques.*

I.4.4. Cryogenic Trapping

Based on the physical properties of matter at very low temperatures (below 200 K), This technique induces condensation, fractional distillation, gas cooling and liquefaction, or cryogenic absorption/adsorption, enabling efficient pollutant removal.

I.4.5. Combustion

It is primarily applied to exhaust gases containing hydrocarbons; the pollutants are oxidized at high temperatures (900–1200 K) into inert, non-polluting compounds. Effective application requires knowledge of the type and concentration of the pollutant to prevent uncontrolled ignition and ensure uniform reaction conditions in the gas stream.

I.5. Plasma-Based Pollution Control Techniques

Plasma-based pollution control techniques [15, 16, 17] are generally divided into two groups. The first group relies on thermal plasmas (plasma torches or electric arcs) to raise the gas temperature (500–1200 K), thereby promoting specific reduction reactions. The second group uses non-thermal (non-equilibrium) plasmas, which seed the gas with excited and radical species to initiate chemical kinetics for pollutant transformation.

Techniques requiring elevated gas temperatures include:

I.5.1. Selective Catalytic Reduction (SCR) is one of the most effective and widely used technologies for NO_x control. In this process, a reducing agent typically ammonia (NH_3) or urea is injected into the flue gas stream, where NO_x is selectively reduced to molecular nitrogen (N_2) and water (H_2O) in the presence of a catalyst. Common catalysts include vanadium titanium oxides and zeolite-based materials. SCR systems operate efficiently within a temperature window generally ranging from 250 to 450 °C. Despite their high removal efficiencies, often exceeding 90%, SCR installations are associated with high capital and maintenance costs, catalyst deactivation, and the risk of ammonia slip.

I.5.2. Selective Non-Catalytic Reduction (SNCR), also known as *Thermal DeNO$_x$,* eliminates the need for a catalyst by relying solely on thermal activation. In this technique, ammonia or urea-based reagents are injected directly into the combustion chamber or flue gas at elevated temperatures, typically between 850 and 1100 °C. Under these conditions, NO_x is reduced to nitrogen and water through homogeneous gas-phase reactions. Although SNCR systems are simpler and less expensive than SCR, their NO_x removal efficiency is comparatively lower

(usually 30–60%) and highly sensitive to temperature fluctuations, which may lead to unreacted ammonia emissions.

I.5.3. Non-Selective Catalytic Reduction (NSCR) is an earlier technology that has been in use since the mid-20th century, particularly in stationary engines and industrial exhaust treatment. This method employs hydrocarbon-based reducing agents, such as carbon monoxide (CO) or unburned hydrocarbons, in the presence of a catalyst to reduce NO_x. Unlike SCR, NSCR does not selectively target NO_x, as oxygen competes with NO_x for the reducing species. Consequently, NSCR requires near-stoichiometric or fuel-rich conditions and is generally unsuitable for oxygen-rich exhaust gases.

I.5.4. RAPRENO$_x$ process is a high-temperature reduction technique closely related to Thermal DeNO$_x$. It involves the injection of isocyanic acid (HNCO) or cyanuric acid as the reducing agent. At elevated temperatures, these compounds decompose to form reactive intermediates that facilitate the reduction of NO_x to nitrogen. While effective under controlled conditions, the RAPRENO$_x$ process faces practical challenges related to reagent handling, operational safety, and process optimization.

These thermal methods are not well suited for treating toxic effluents present at low concentrations in large gas volumes (e.g., exhaust gases), since they heat molecules non-selectively, resulting in high energy and financial costs

More recently, research in several countries has focused on cold (non-thermal) plasmas [18], that is can induce similar chemical reduction processes as thermal methods, but without significant gas heating, while also enabling the simultaneous removal of multiple pollutants. They are particularly well suited for treating exhaust gases where toxic species are highly diluted. Crucially, the treatment process is driven by electronic energies (several thousand Kelvin), rather than bulk gas temperature, which remains nearly unchanged. Economically, the main advantage lies in the fact that electrical power is primarily used to generate energetic electrons. These electrons transfer their energy during collisions with neutral species, creating radicals and chemically active excited species, without unnecessary heating of the gas.

While oxidation of NO to NO_2 is relatively easy to achieve in plasma, complete removal of both NO and NO_2 (i.e., conversion to N_2 and O_2) requires a delicate balance of radical concentrations and residence time. In some cases, undesirable by-products like N_2O or O_3 may form, which must be carefully controlled through reactor design and process optimization.

I.6. Cold Plasma Pollution Control Techniques

I.6.1 Plasma Fundamentals

This section is devoted to defining the concept of plasma, presenting the type of plasmas of discharge studied, and providing a brief description of the mechanisms responsible for their generation by electrical discharge [19, 20].

I.6.1.1. What is Plasma?

Unlike solids, liquids, and gases, plasmas exhibit high electrical conductivity and collective behavior governed by long-range electric and magnetic fields [21-23]; The term *plasma* was introduced by Langmuir in 1929 to describe ionized gases that are quasi-neutral, containing nearly equal numbers of positive and negative charges [24]. Although plasma constitutes about 99% of the visible Universe, it is relatively rare on Earth under normal conditions and is usually generated artificially through electrical discharges or electromagnetic fields. Depending on their degree of ionization, plasmas are generally classified into two categories: thermal plasmas, which are in thermodynamic equilibrium, and non-equilibrium cold plasmas, where energetic electrons coexist with a near-room-temperature bulk gas. We can now define more precisely what a plasma is. A plasma is a gas that is partially or fully ionized [21]. It is therefore composed of electrons, positively or negatively charged ions, neutral particles, excited species, and photons (Figure I.5).

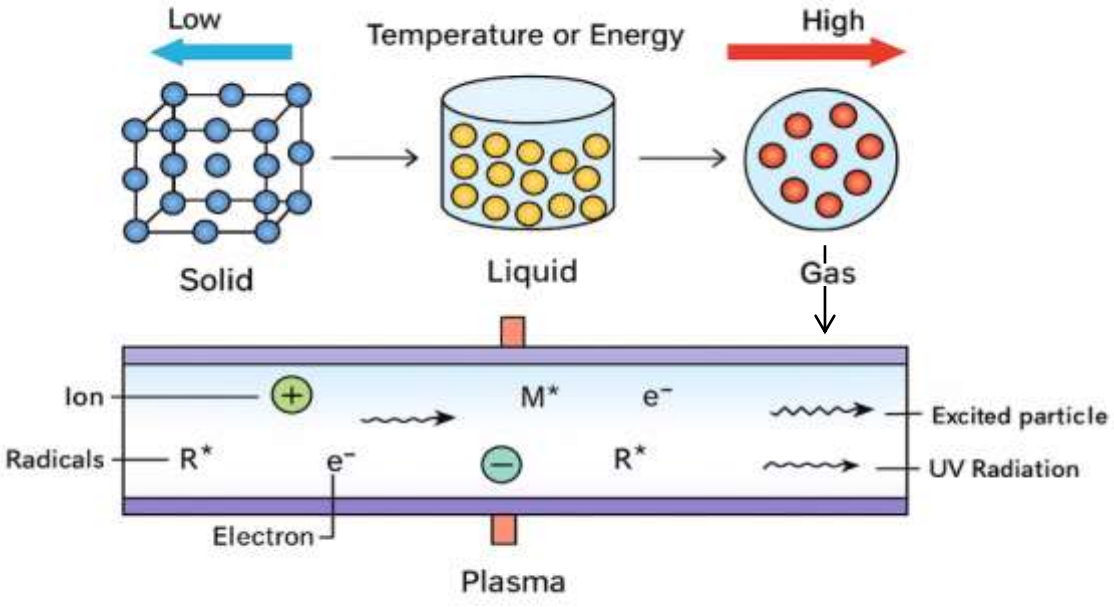

Fig I.5. *Fundamental State of Matter [22].*

I.6.1.2. Plasma in Our Life

Plasma is not only a fundamental state of matter in the Universe but also an essential part of our daily lives. In nature, plasmas manifest as lightning, auroras, and solar winds that continuously interact with Earth's atmosphere. Artificial plasmas are equally significant: they power lighting systems like fluorescent and neon lamps, and are used in plasma display technologies [25]. Industrially, plasmas play a critical role in semiconductor manufacturing, thin-film deposition, and surface modification, thanks to their ability to activate chemical reactions under controlled non-equilibrium conditions. In environmental applications, non-thermal plasmas are being developed for ozone generation, pollution control, and advanced water purification particularly in degrading persistent organic contaminants and wastewater treatment [26-27]. Medical applications of non-thermal atmospheric plasmas have also seen rapid growth, from sterilization, wound healing, and dermatological treatments to emerging roles in cancer therapy and plasma-activated liquid technologies [28-29]. These natural phenomena and technological applications underscore that plasma, beyond its cosmic prevalence, serves as a versatile and indispensable tool in contemporary science, healthcare, and environmental technology. Plasmas can be characterized according to two key parameters: the electron density (n_e) and the electron temperature (T_e). By representing these parameters in a diagram, two main categories of plasmas can be distinguished: hot plasmas and cold plasmas. The distribution of plasmas in this parameter space is shown in figure I-6.

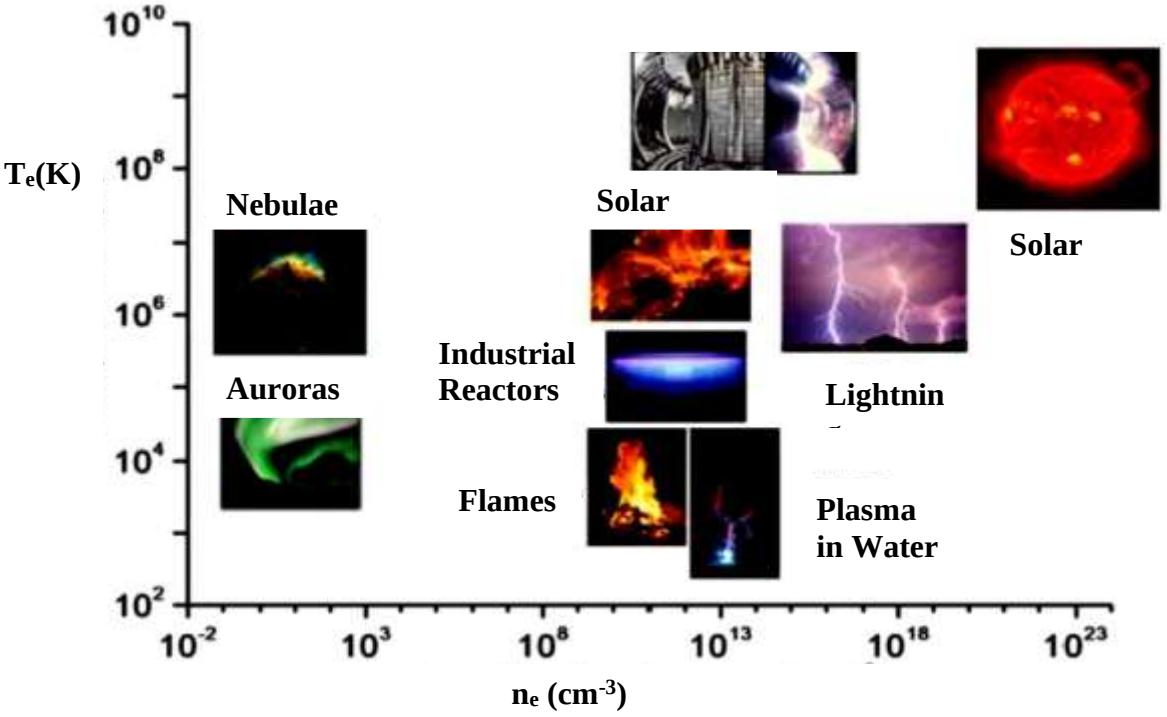

Fig I.6. *Diagram of Plasmas in the Space T_e/n_e [30].*

I.6.1.3. Classification of Plasmas

One of the key characteristics of plasma related to the electron density is its degree of ionization α , which is defined as:

$$\alpha = \frac{n_e}{n_e + N} \tag{I.5}$$

where n_e is the electron density and N is the density of neutral species.

Based on the degree of ionization and the electron temperature (T_e), plasmas can be classified into the two main categories previously defined: hot plasmas (thermal plasma) and cold plasmas (also referred to as non-thermal plasmas). Hot plasmas are fully ionized and exhibit temperatures higher than 10^6 K such as those found in the solar core, lightning, and fusion reactors. In contrast, cold plasmas are non-equilibrium systems where ions and neutrals remain at relatively low temperatures (typically below 1000 K), while the minority electron population reaches much higher temperatures in the range of 10,000 to 50,000 K. The degree of ionization for such plasmas typically lies between 10^{-6} and 10^{-2}.

The plasmas investigated in this thesis belong to the category of cold (non-thermal) plasmas.

I.6.1.3.1. Thermal Plasmas

Thermal plasmas, also called equilibrium plasmas, are characterized by local thermodynamic equilibrium (LTE), where electrons, ions, and neutrals have approximately the same temperature and their velocity distributions follow Maxwell Boltzmann statistics. They are typically generated under high-pressure and high-density conditions, resulting in temperatures ranging from several thousand to tens of thousands of kelvins. Examples include electric arcs, plasma torches, and fusion plasmas. Thermal plasmas are widely applied in industrial processes such as plasma spraying, cutting, welding, and waste treatment [31].

I.6.1.3.2. Cold (Non-Thermal) Plasmas

Cold plasmas, also called non-equilibrium plasmas, are distinguished by a strong temperature disparity between electrons and heavy species (ions and neutrals). While electron energies can reach several electron volts (equivalent to thousands of kelvins), the bulk gas remains close to room temperature. This non-equilibrium feature allows cold plasmas to initiate fast chemical reactions without globally heating the system, making them ideal for temperature

sensitive applications. Today, cold atmospheric plasmas (CAPs) are being extensively investigated for sterilization, wound healing, cancer therapy, dermatology, water purification, and environmental decontamination [26 -28].

To generate this type of plasma, an electric field can be applied to accelerate electrons, which then produce ionizing collisions and thereby create a plasma. In our study, this is the type of plasma we investigated. Cold plasmas have a wide range of applications, including lighting tubes, microelectronic etching, thin film deposition, gas lasers, as well as pollutant and surface treatment. Later in this thesis, we will present possible applications of the specific types of this plasma studied.

For environmental applications such as NO_x treatment, non-thermal plasma is preferred due to its ability to initiate chemical reactions at low gas temperatures, avoiding thermal NO formation and saving energy.

I.6.2. Cold Plasma Generation Techniques

Two main techniques can be used to generate cold plasma at atmospheric pressure:

I.6.2.1. Electron Beam Techniques: (electron beam irradiation of exhaust gases) first developed in the 1970s by the Japanese company EBARA, later extended in Germany and the United States in the 1980s. This process oxidizes NOx and SO_2 into HNO_3 and H_2SO_4, which are subsequently neutralized with a base, yielding solid residues that can be recovered via mechanical filters or electrostatic precipitators and reused as fertilizer salts.

In this approach, electrons are first created and accelerated under vacuum conditions. These highly energetic electrons are then introduced into the target gas through a semiconductor window. Once inside the gas, which is at atmospheric pressure, the energetic electrons initiate plasma formation by colliding with gas molecules and inducing ionization [32].

I.6.2.2. Electrical Discharge Techniques: (Non-equilibrium electrical discharges**,** including corona discharges, dielectric barrier discharges (DBD), surface discharges, and glidarc discharges).

In this case, electrons are directly created and accelerated at atmospheric pressure within the gas volume to be treated, through the application of a high voltage between two electrodes. These electrons collide with the gas molecules, and ionization of the molecules or atoms occurs.

Ionization takes place when a molecule or atom acquires sufficient energy either from an external excitation source or via collisions with other energetic particles [32].

A gas always initially contains a small number of electrons and ions, formed for instance by collisions with cosmic rays or radioactive radiation interacting with the gas. These free charges are accelerated by the applied electric field, and new charged particles may subsequently be created when they collide with atoms and molecules in the gas or with the surfaces of the electrodes. This process leads to an avalanche of charged particles, which is eventually balanced by charge losses, resulting in the establishment of a steady-state plasma [33].

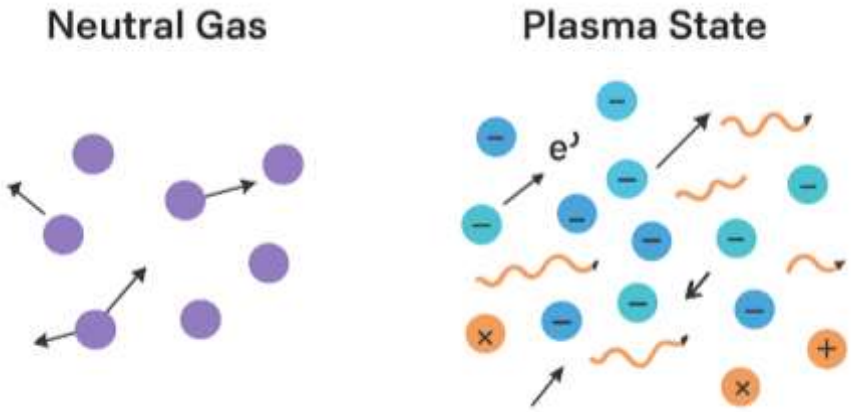

Fig I.7. *Representation of the difference between a Neutral Gas and a Plasma [33].*

I.6.3 Characteristic Scales and Processes in Plasmas

Plasma behavior is governed by a set of characteristic scales and elementary processes that control its dynamics, stability, and interaction with matter. These characteristic scales define the collective properties of the plasma, while the elementary processes determine how energy and particles are exchanged within the plasma and with its surroundings.

I.6.3.1. Plasma Oscillations

Plasma oscillations are high-frequency collective motions of the electron population around a nearly immobile ion background. When electrons are displaced, the electrostatic restoring force drives them back, creating oscillations at the plasma pulsation **(ω_p)**:

$$\omega_p = \sqrt{\frac{n_e e^2}{\varepsilon_0 m_e}} \tag{I.6}$$

where n_e is the electron density, e the elementary charge, ε_0 is the vacuum permittivity, and is m_e the electron mass. These oscillations are fundamental in determining plasma stability and wave propagation [34].

I.6.3.2. Debye Length

The Debye length (λ_D) characterizes the distance over which electrostatic interactions are screened in a plasma, It is defined as:

$$\lambda_D = \sqrt{\frac{\varepsilon_0 k_B T_e}{n_e e^2}} \tag{I.7}$$

where T_e is the electron temperature, n_e is the electron density, e is the elementary charge, ε_0 is the vacuum permittivity, and k_B is the Boltzmann constant.

Within a Debye sphere, the plasma behaves collectively, but beyond this scale, electrostatic potentials are shielded. A defining condition for a medium to be plasma is that the system size $L >> \lambda_D$ ensuring collective behavior [34].

I.6.3.3. Reactive Processes

The plasma generation process is based on the injection of a “plasma forming” gas into a chamber maintained either under partial vacuum or at atmospheric pressure [19]. Ionization processes can occur, for example, when the gas molecules are subjected to high energy radiation, an electric field, or high thermal energy. Free electrons are then accelerated, gain energy, and collide (elastically or inelastically) with gas molecules or atoms. Inelastic collisions lead to the ionization of gas molecules. As a result, the gas transitions from an electrically insulating state to a conducting state through the production of free charged species. The presence of ionized and excited species initiates a wide range of complex reactional processes (ionization, dissociation, emission, recombination, neutralization, de-excitation, attachment, etc.) [20].
In practice, several types of collisions can be distinguished:

I.6.3.3.1. Elastic Collisions

In these collisions, both kinetic energy and momentum are conserved. Heavy particles readily exchange their energy through elastic collisions, whereas in the case of a collision between an electron and a heavy particle, the fraction of energy transferred is very small. Consequently, an electron must undergo thousands of elastic collisions to lose its energy.

$$e^- + A \rightarrow e^- + A \quad \text{(I.8)}$$

I.6.3.3.2. Inelastic Collisions

Electrical discharges induce collisions between electrons emitted from the cathode toward the anode and the gas species. All inelastic collisions have an energy threshold: electrons must possess an energy greater than this threshold in order for the reaction to occur. After the collision, the electron loses the threshold energy. These collisions sustain the electrical discharge and give rise to primary and secondary processes such as excitation, dissociation, ionization, and attachment. Inelastic collisions are therefore the source of a large number of physico-chemical reactions, which in turn modify the macroscopic properties of the gas [19].

$$e^- + A \rightarrow e^- + A^* \quad \text{(I.9)}$$

where A^* represents the excited atom.

- **Charge Transfer Collisions**

In this process, a high-energy ion (A^+) becomes a fast neutral (A), while a neutral species (B), initially at the gas temperature, is transformed into a positive ion (B^+):

$$A^+ + B \rightarrow B^+ + A \quad \text{(I.10)}$$

- **Ionization**

In the case of low pressure or high pressure discharges, gas ionization is primarily due to electron molecule or electron atoms interactions. A collision between an electron and a molecule produces a scattered electron, an ejected electron, and a positive ion. Both electrons are subsequently accelerated by the electric field, leading to further ionization processes:

$$e^- + A \rightarrow 2e^- + A^+ \quad \text{(I.11)}$$

- **Electron Attachment**

According to the molecule or atom electron affinity, the electron can be captured by these last particles, leading to the formation of a negative ion. This process occurs primarily in electronegative gases:

$$e^- + A \rightarrow A^- \quad \text{(I.12)}$$

- **Electron Detachment**

The collision of a negative ion with a neutral species can result in the release of an electron, producing two neutral particles:

$$A^- + e^- \rightarrow A + 2e^- \tag{I.13}$$

- **Ion Conversion**

When an ion collides with a molecule, the impact may cause dissociation of the molecule and the formation of a new type of ion.

Table I.1 presents a set of representative reactions induced by electron impact during inelastic collisions [19].

Table I.1: Set of Reactions Induced by Electron Impact [19]

Type of Collision	Reaction
Electronic Impact Excitation	$A + e^- \rightarrow A^* + e^- \rightarrow e^- + A + h\nu$
Electron Impact Ionization	$A + e^- \rightarrow A^+ + 2e^-$
Electron Impact Dissociation	$AB + e^- \rightarrow e^- + A + B$
Dissociative Ionization	$AB + e^- \rightarrow A^+ + B + 2e^-$
Penning Ionization	$A^* + e^- \rightarrow A^+ + 2e^-$
Dissociative Attachment	$AB + e^- \rightarrow A^- + B$
Recombination	$A^+ + B + e^- \rightarrow A + B$
Radiative Recombination	$e^- + A^+ \rightarrow A^* + h\nu$
Electron Impact Detachment	$e^- + A^- \rightarrow A + 2e^-$

where **A** and **B** are chemical species (neutral particles, atoms, molecules, etc.)

I.6.4. Cold Plasma reactors

Cold plasma reactors are devices designed to generate non-equilibrium plasmas, where electrons are highly energetic while ions and neutral species remain near room temperature. Different reactor configurations have been developed to tailor plasma properties for specific applications such as surface modification, sterilization, environmental remediation, and biomedical treatments. The most common types include glow discharge, radio frequency

discharges, microwave discharges, corona discharges (pulsed and continuous), dielectric barrier discharges, and gliding arc systems.

I.6.4.1. Glow discharge

Glow discharge reactors are the simplest and most studied cold plasma sources. They consist of two electrodes at low pressure, where a DC voltage initiates a discharge characterized by distinct regions (cathode fall, negative glow, plasma region). Glow discharges are widely used in thin-film deposition, sputtering, surface cleaning, and analytical techniques such as glow discharge spectroscopy. Recent studies report their application in nanomaterial synthesis and plasma-assisted catalysis [35].

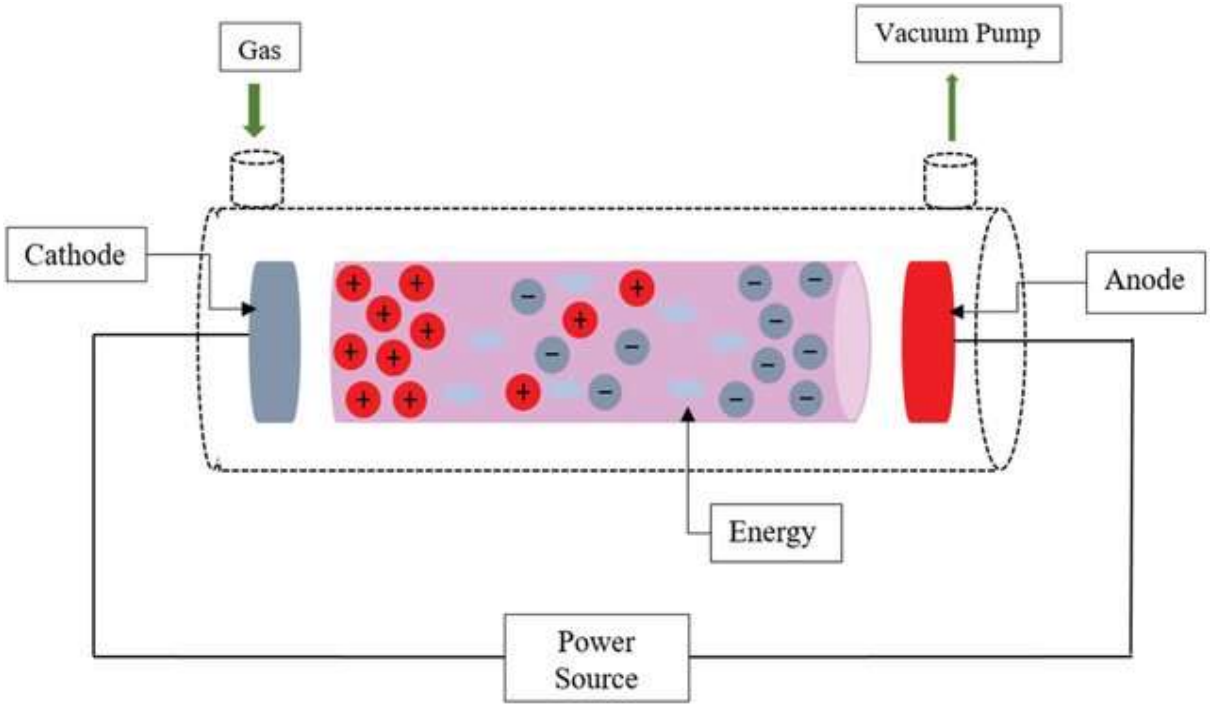

Fig I.8. *Glow Discharge Reactor [35].*

I.6.4.2. RF Discharge (Capacitive, Inductive)

RF discharges are generated by applying an alternating electric field, typically at 13.56 MHz, to electrodes. Two main modes exist; Capacitively Coupled Plasma, and Inductively Coupled Plasma (see fig. I.9).

- **Capacitively Coupled Plasma (CCP):** electrons gain energy from oscillating electric fields between two electrodes, commonly used in microelectronics, thin film processing, and biomedical devices.

- **Inductively Coupled Plasma (ICP):** energy is transferred via electromagnetic induction, generating denser plasmas with higher ionization efficiency. ICPs are widely used in spectroscopy and etching processes [35].

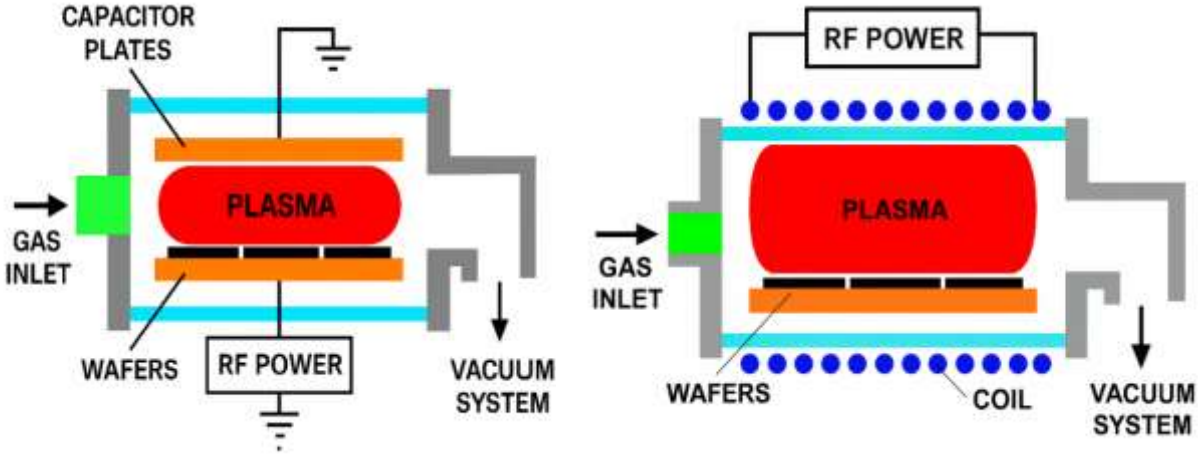

Fig I.9. *RF Discharge Reactor Design [35].*

I.6.4.3. Microwave Discharge

Microwave plasmas are produced when microwave radiation (typically 2.45 GHz) couples with a gas, leading to high electron densities and efficient ionization. Microwave discharges operate at low or atmospheric pressure and are applied in plasma chemistry, ozone generation, and biomedical treatments. They provide stable, uniform plasmas without electrodes, reducing contamination risks, the scheme of Microwave Reactor is represented in figure I.10 [36].

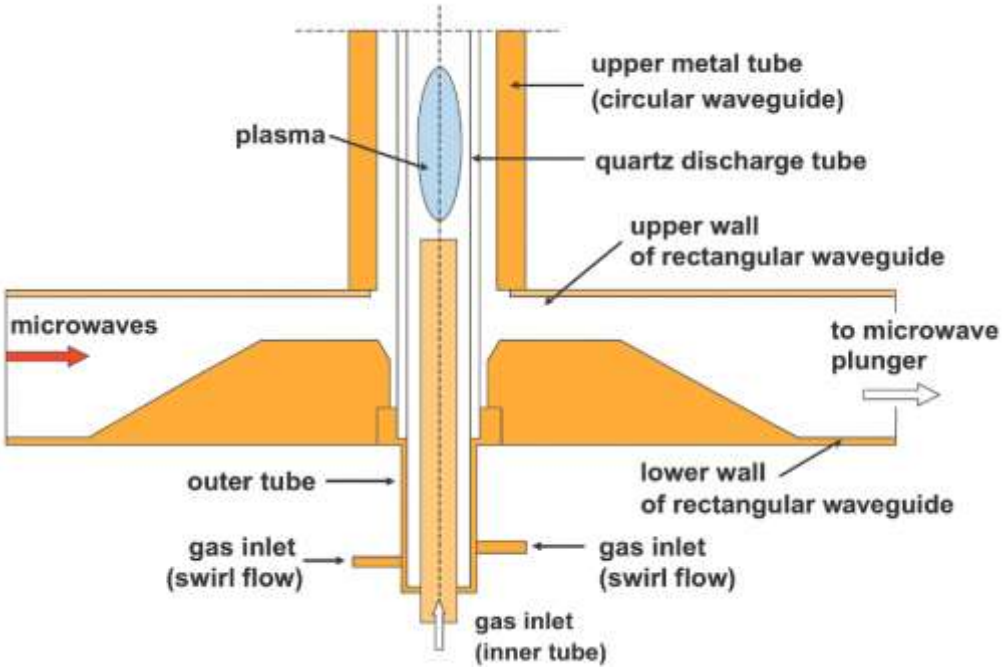

Fig I.10. *Microwave Discharge Reactor [36].*

I.6.4.4. Corona Discharge

Corona discharges occur when a high voltage is applied to asymmetric electrode geometries (sharp tips, wires) under atmospheric pressure, creating strong electric fields near the electrode surface. They are characterized by localized plasma regions around sharp electrodes. Corona discharges are widely used for ozone generation, flue gas treatment, and surface activation of polymers, the scheme of point to plane corona discharge reactor is shown in figure I.11 [37,38].

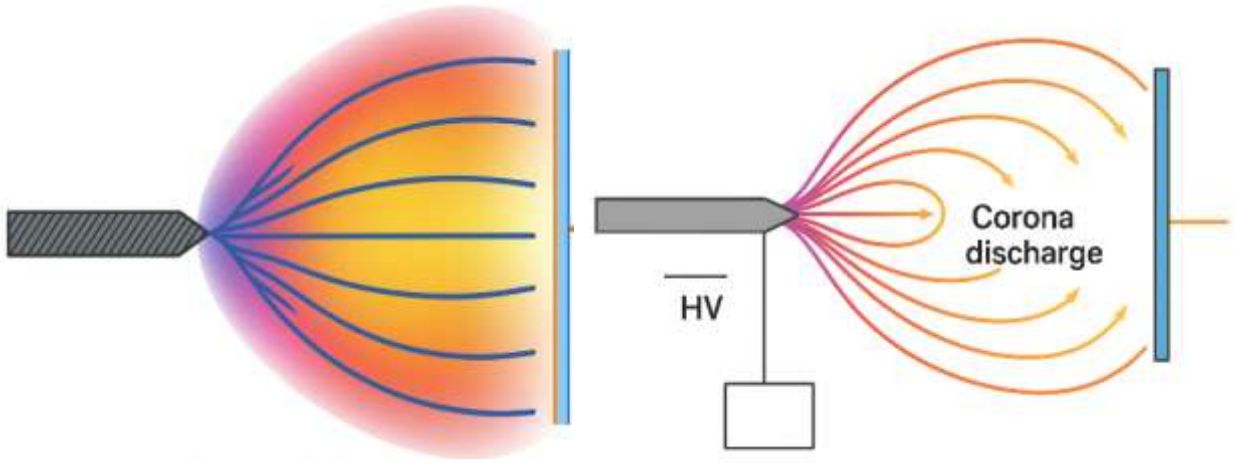

Fig I.11. *Corona Discharge Reactor [37,38].*

I.6.4.5. Pulsed Corona Discharge

A pulsed corona discharge uses short-duration, high-voltage pulses, which reduce electrode heating and enhance energy efficiency compared to continuous corona discharges. This configuration is especially effective for non-thermal plasma water treatment, decomposition of volatile organic compounds (VOCs), and plasma-assisted sterilization. Recent works emphasize pulsed corona discharges for environmental and biomedical applications due to their controllability and efficiency [36].

I.6.4.6. Dielectric Barrier Discharge

In DBD reactors, at least one electrode is covered with a dielectric material, which limits the discharge current and distributes the plasma into micro-discharges. DBDs operate at atmospheric pressure and are used in ozone generation, surface functionalization, plasma medicine, and CO_2 conversion. Their ease of scalability and ability to operate in ambient air make them among the most versatile cold plasma sources, the dielectric barrier discharge phenomena is shown in figure I.12 [27].

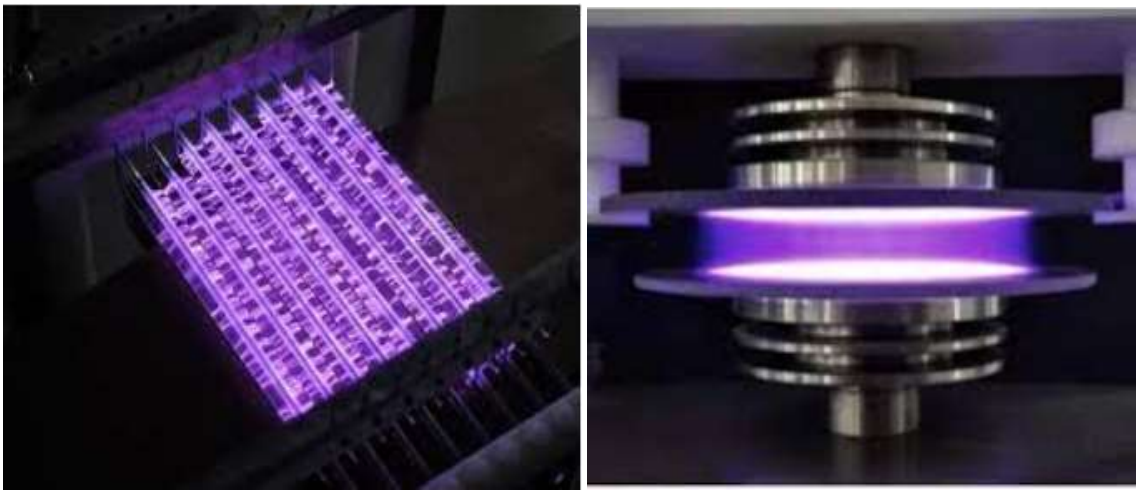

Fig I.12. *Dielectric Barrier Discharge Phenomena [27].*

I.6.4.7. Gliding Arc Discharge

Gliding arc discharges are non-equilibrium plasmas formed between diverging electrodes, where an arc is ignited and then "glides" along the electrode gap due to gas flow. They combine properties of both thermal and non-thermal plasmas: electrons remain hot, while bulk gas temperature is moderately elevated. Gliding arcs are widely applied in plasma-assisted combustion, gas reforming, and pollution control, the scheme of Gliding Arc Discharge Reactor is represented in figure I.13 [39].

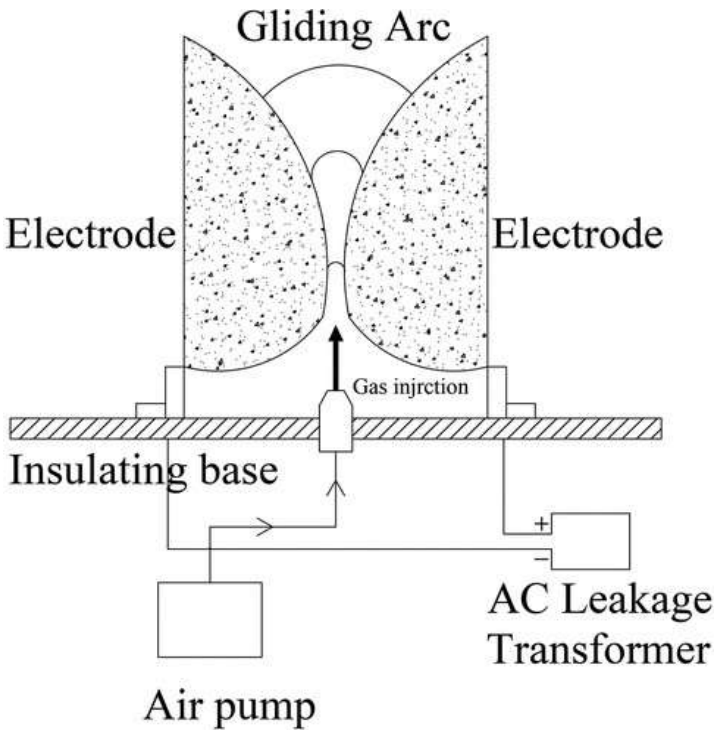

Fig I.13. *Gliding Arc Discharge Reactor [39].*

I.6.4.8. Gliding Arc Tornado Discharge

The gliding arc tornado (GAT) reactor is an advanced configuration where a gliding arc is stabilized and rotated by a strong vortex gas flow, forming a tornado like plasma structure. This geometry improves plasma gas mixing, increases energy efficiency, and provides longer residence times. Recent studies report its promising use in CO_2 conversion, syngas production, and plasma-assisted catalysis [39].

Table I.2 Comparative of Cold Plasma Reactors

Reactor Type	Operating Principle	Pressure Range	Typical Applications
Glow Discharge	DC voltage at low pressure; electron avalanches sustain stable plasma glow	Low pressure (0.1–10 Torr)	Thin-film deposition, sputtering, spectroscopy, nanomaterials synthesis
RF Discharge (CCP/ICP)	RF (13.56 MHz) field excites plasma; CCP uses electrodes, ICP uses induction coils	Low to medium (mTorr – few Torr)	Microelectronics, plasma etching, thin-film processing, biomedical devices
Microwave Discharge	Microwave radiation (2.45 GHz) couples with gas; electrode-less plasma generation	Low or atmospheric pressure	Ozone generation, plasma chemistry, biomedical sterilization, material processing
Corona Discharge	High voltage applied to sharp/asymmetric electrodes at atmospheric pressure	Atmospheric pressure	Ozone production, flue gas treatment, surface activation of polymers
Pulsed Corona Discharge	Short high-voltage pulses improve corona stability and reduce heating	Atmospheric pressure	VOC removal, wastewater treatment, sterilization
Dielectric Barrier Discharge (DBD)	At least one electrode covered with dielectric; limits current and forms micro-discharges	Atmospheric pressure	Ozone generation, surface modification, CO_2 conversion, plasma medicine
Gliding Arc Discharge	Arc ignited between diverging electrodes, carried by gas flow ('glides' along gap)	Atmospheric to moderate pressure	Plasma-assisted combustion, gas reforming, pollution control
Gliding Arc Tornado	Gliding arc stabilized and rotated by vortex gas flow, creating tornado-like discharge	Atmospheric to moderate pressure	CO_2 conversion, syngas production, plasma catalysis

Dielectric Barrier Discharge (DBD) was selected in this study as the core plasma technology due to its unique advantages in pollutant removal under atmospheric pressure

conditions. Unlike thermal plasmas, which require high energy input and elevated gas temperatures, DBD generates a non-thermal plasma where energetic electrons initiate chemical reactions without significantly heating the bulk gas. This allows efficient generation of reactive species such as radicals, excited molecules, and ozone, which are highly effective in oxidizing and decomposing nitrogen oxides (NO_x) at low energy cost. Furthermore, DBD reactors are relatively simple, compact, and flexible in design, making them suitable for integration into pollution control systems. Their ability to operate under ambient conditions with minimal secondary pollution makes DBD an attractive and sustainable solution for addressing NO_x emissions, which are the central focus of this research.

I.7. Conclusion

Atmospheric pollution represents a major challenge for both environmental sustainability and public health, with nitrogen oxides (NO_x) playing a central role in the formation of photochemical smog, acid rain, and other secondary pollutants. Although conventional control technologies such as Selective Catalytic Reduction (SCR) and Selective Non-Catalytic Reduction (SNCR) are commonly employed, their inherent limitations related to cost, operational complexity, and potential secondary emissions underscore the necessity for alternative mitigation strategies. In this context, plasma-based processes, particularly cold plasmas generated by dielectric barrier discharges (DBDs), have gained increasing attention as effective and flexible solutions for NO_x abatement. These systems enable the generation of highly reactive species under ambient conditions, allowing efficient pollutant removal without the need for high temperatures. Consequently, the following chapter focuses on the fundamental principles of dielectric barrier discharge plasma, with particular emphasis on its application in air pollution control.

References

[1] R. Meetham, D. W.Bottom, S. Cayton, "Atmospheric pollution: its history, origins and prevention,*"Elsevier,*2016.

[2] M. S. Callén, *et al*.," Nature and sources of particle associated polycyclic aromatic hydrocarbons (PAH) in the atmospheric environment of an urban area," *Environmental Pollution,* vol. *183*, pp. 166-174, 2013.

[3] D. K. Saini, S.K. Garg, M. Kumar,"Major air pollutants and their effects on plant and human health: a review," *Plant Archives (09725210),* vol. 19, no.2, 2019.

[4] M. J.Molina, L. T.Molina, "Megacities and atmospheric pollution," *Journal of the Air & Waste Management Association,* vol. 54, no. 6, pp. 644-680, 2004.

[5] H. T. Pham, "Contribution à l'étude de la dépollution de l'air chargé en composés organiques volatils par un procédé associant un plasma de décharge à barrière diélectrique impulsionnelle et des catalyseurs, " *Thèse de doctorat, Université d'Orléans,* 2014.

[6] A Touhami,‟ Dépollution de l'air des particules polluantes par décharge électrique, "*thèse de Magister, université USTO Oran,* 2007.

[7] K. J. Syed, E. Buchanan, "The nature of NOx formation within an industrial gas turbine dry low emission combustor," In *Turbo Expo: Power for Land, Sea, and Air*, vol. 4725, pp. 11-18.January, 2005.

[8] Z.Zhu,B.Xu, "Purification technologies for NOx removal from flue gas: a review," *Separations,* vol.9, no.10, p.307,2022.

[9] R. K. Srivastava, *et al.,* "Controlling NOx emission from industrial sources,"*Environmental progress*, vol. 24, no. 2, pp.181-197, 2005.

[10] Jena, "Inter-comparison of different NOx emission inventories and associated variation in simulated surface ozone in Indian region,"*Atmospheric Environment*, vol.117, pp.61-73, 2015.

[11] T. Boningari, P. G. Smirniotis,"Impact of nitrogen oxides on the environment and human health: Mn-based materials for the NOx abatement,"*Current Opinion in Chemical Engineering*, vol. 13, pp.133-141,2016.

[12] Z. Wang, X. Yang, "NOx Formation Mechanism and Emission Prediction in Turbulent Combustion: A Review,"*Applied Sciences,* vol. 14, no. 14,pp. 2076-3417, 2024.

[13] S. I. Medjahdi,"Modélisation de la cinétique chimique dans la réduction des oxydes d'azote par décharge couronne," *Thèse de doctorat, Université de Tlemcen*, 2009.

[14] S. Lachaud, "Décharge pointe-plan dans les mélanges gazeux correspondant aux effluents industriels : étude électrique et physico-chimique, application à la destruction du dioxyde

d'azote, " *Thèse de doctorat, Université de Toulouse,France,* 2002.

[15] D. Dubois, "Réalisation et caractérisation d'un réacteur plasma de laboratoire pour des études sur la dépollution des gaz d'échappement, " *Thèse de doctorat, Université de Toulouse III,* 2006.

[16] A. Abahazem, *et al.*, "Etude électrique et spectroscopique de la décharge couronne dans l'air à la pression atmosphérique pour la dépollution des gaz,"*J. Mater. Environ. Sci. vol.* 5,no. S2,pp.2544-2549,2014.

[17] A. Abahazem, "études expérimentales des décharges couronne pour la dépollution des gaz, " *thèse du doctorat, Université de Toulouse,* 2009.

[18] P. Gururani, *etal.*,"Cold plasma technology: advanced and sustainable approach for wastewater treatment,"*Environmental Science and Pollution Research,* vol. *28,* no. 46, pp. 65062-65082, 2021.

[19] J. A. Bittencourt,"Fundamentals of plasma physics,*"Springer Science & Business Media,*2013.

[20] L. Conde, "An Introduction to Plasma Physics and Its Space Applications,"*Basic Equations and Applications*. *IOP Publishing,*Vol.2, 2020.

[21] A. Valt, "Etude de deux procédés de polymérisation d'un précurseur gazeux dans unplasma radiofréquence basse pression et liquide déposé sur un substrat activé par décharge à barrière diélectrique à pression atmosphérique : application aux propriétés antifouling," *Thèse de Doctorat, Université Pierre et Marie Curie,* 2008.

[22] R. A. Eljalil, "Modélisation de là entre relation les paramètres procédé plasma et les caractéristiques de la qualité du matériau x textile par apprentissage de données physiques," *Thèse de doctorat, Université des sciences et Technologies de Lille,* Avril, 2010.

[23] M. Moisan,J. Pelletier, "The plasma state: Definition and orders of magnitude of principal quantities. In *Physics of Collisional Plasmas: Introduction to High-Frequency Discharges*, pp. 1-100. *Dordrecht: Springer Netherlands*, 2012.

[24] P. Mathew,*et al.,* "Fundamentals of Discharge Plasmas;"*In Research Methodologies and Practical Applications of Chemistry,* pp. 245-268. Apple Academic Press, 2019.

[25] K. D. Weltmann, "The future for plasma science and technology," *Plasma Processes and Polymers,* vol. *16*, no. 1, 1800118, 2019.

[26] A.Barjasteh,*et al*.,"Recent progress in applications of non-thermal plasma for water purification, bio-sterilization, and decontamination,"*Applied Sciences,* vol. 11, no. 8, p. 3372, 2021.

[27] A. Giardina, *et al*., "Air non-thermal plasma, a green approach for the treatment of contaminated water: the case of sulfamethoxazole,". *Frontiers in Environmental Chemistry,*

2024.

[28] T. Khalaf, *et al*.,"Cold atmospheric plasma (CAP): A revolutionary approach in dermatology and skincare,"*European Journal of Medical Research,* vol. 29, p. 487, 2024.

[29] F.O'Neill, L.O'Neill, P.Bourke,"Recent developments in the use of plasma in medical applications,"*Plasma,* vol. *7* no. 2, pp.284–299, 2024.

[30] L. Abdelhadi, "Modélisation Electrique d'une Décharge à Barrières Diélectriques DBD," *Mémoire de Magister*, *Université d'Oran des Sciences et de la Technologie (USTO-MB),* Décembre, 2014.

[31] B.Murphy, G.Arnoult,"Modelling of thermal plasmas: Recent developments and challenges," *Plasma Sources Science and Technology,* vol. 31, no. 12, 123001, 2022.

[32] N. Dubus, "Contribution à l'étude thermique d'un réacteur à décharge à barrière diélectrique," *Thèse de Doctorat, Ecole Supérieure d'Ingénieurs de Poitiers*, 2009.

[33] S. Bournet, "Fonctionnalisation de surface de polymères par plasma à la pression atmosphérique. Amination de surface et dépôt de couches minces par un procédé de décharge par barrière diélectrique," *Thèse de Doctorat, Université Toulouse III-Paul Sabatier*, 2009.

[34] F. F. Chen, "*Introduction to plasma physics and controlled fusion (3rd ed.)*."*Cham: Springer*, 2016.

[35] M. Bedoui, A. W. Belarbi, and S. Habibes, "Macroscopic modeling of the glowdielectric barrier discharge (GDBD) in helium," *European Journal of Electrical Engineering*, vol. 20, pp. 89-103, 2018.

[36] M. M. Tahiyat,*et al.*,"Striations in moderate pressure dc driven nitrogen glow discharge," *Journal of Physics D: Applied Physics*, vol. 55, no. 8, 085201,2021.

[37] D.Raouti, S. Flazi, D. Benyoucef, "Electrical modelling of a positive point to plane corona discharge at atmospheric pressure," *Contributions to Plasma Physics*, vol. 54, no. 10, pp. 851-858, 2014.

[38] D. Benyoucef, M. Yousfi, "Improved fictitious charge method for calculations of electric potential and field generated by point-to-plane electrodes," *Journal of Electrostatics*, vol. 76, p. 24-30, 2015.

[39] X. Gong, *et al*.,"Decomposition of volatile organic compounds using gliding arc discharge plasma," *Journal of the Air & Waste Management Association*, vol. 70, no. 2, pp. 138-157, 2020.

Chapter II

Fundamentals and Applications of Dielectric Barrier Discharge Plasma

II.1. Introduction

Dielectric barrier discharge (DBD) plasma has emerged as a promising non-thermal plasma technology for NO_x abatement. Operating under atmospheric pressure and near-ambient temperatures, DBDs produce a rich variety of reactive oxygen and nitrogen species capable of oxidizing or reducing NO and NO_2 without generating additional thermal NO_x. Their modular design, scalability, and compatibility with catalytic materials further enhance their potential for practical applications.

This chapter provides an in-depth overview of DBD plasmas and their relevance to NO_x reduction. It begins with a discussion of Electrical discharge fundamentals, followed by the physical and chemical mechanisms governing DBD operation. The unique chemical environment of DBDs, where short-lived radicals and long-lived species act synergistically in both plasma and post-discharge regions, is examined in detail. Furthermore, recent advances in DBD applications for pollution control are reviewed, including ozone generation, surface treatment, and pollutant reduction.

Despite significant progress, several knowledge gaps remain, particularly concerning plasma chemistry pathways, by-product formation, and reactor optimization for large-scale operation. Addressing these challenges requires both experimental investigations and numerical modeling approaches capable of capturing the coupled physics and chemistry of DBD plasmas. This context provides the scientific and technological foundation for the modeling framework developed in the following sections, which aims to better understand and optimize NO_x reduction under DBD conditions.

II.2. Historical Development of DBDs

To provide context for the evolution of this technology, the following table (Table II.1) outlines the major milestones in the development of Dielectric Barrier Discharges (DBDs), since its inception in the mid-19th century, the application of DBDs has transitioned from a specialized method for ozone production to a versatile solution for modern environmental and biomedical challenges.

This chronological overview highlights the transition from the first discovery, basic industrial chemistry, the breakdown of volatile organic compounds, biomedicine and screens, to the sophisticated plasma-assisted catalytic systems used today [1-12].

Table II. 1. Historical Development of DBD Technology.

Era	Key Milestone	Primary Application
1857	First Discovery (Siemens)	Proof of concept for ozone generation via dielectric barriers.
Early 1900s	Industrialization	Large scale ozone production for water treatment.
1960s–1970s	Surface Processing	Polymer activation, textile treatment, and thin film deposition.
1980s	Environmental Pivot	First use in flue gas cleaning (NOx and SO_2 removal).
1990s	VOC& CO reduction	Decomposition of volatile organic compounds and carbon monoxide.
2000s	Biomedical& Displays	Plasma medicine (wound healing, sterilization) and Plasma Display Panels.
2010s–Now	Plasma Catalysis	Synergy between plasma and catalysts for CO_2 and NOx conversion.

II.3. Definition and Characteristics of Dielectric Barrier Discharge (DBD)

A Dielectric Barrier Discharge (DBD) is a source of non-equilibrium cold plasma, i.e., an ionized gas that remains globally neutral in which the electrons possess a much higher energy or temperature (with an average energy of a few electron volts) than that of the ions and the neutral gas particles (approximately 300 K), which constitute the majority species [13].

The term DBD refers to discharge configurations in which a current flow between two metallic electrodes separated by a gas and at least one layer of insulating material. Depending on the intended application, two insulating layers may also be employed. Typical coplanar and cylindrical electrode configurations are illustrated in Figure II.1. Coplanar configurations are generally used for surface treatment applications, while cylindrical ones are more suitable for gas treatment. The plane–plane arrangement (c) in Figure II.1 has the advantage of avoiding direct contact between the plasma and the metallic electrodes, which is particularly useful when working with corrosive plasmas. Configuration (b) enables the simultaneous generation of a discharge on both sides of the dielectric, which is advantageous when the dielectric itself constitutes the material to be treated, as it allows processing of both surfaces at once. Commonly used dielectric materials include glass, quartz, ceramics, and silicone rubber, particularly in corona treatment applications [13].

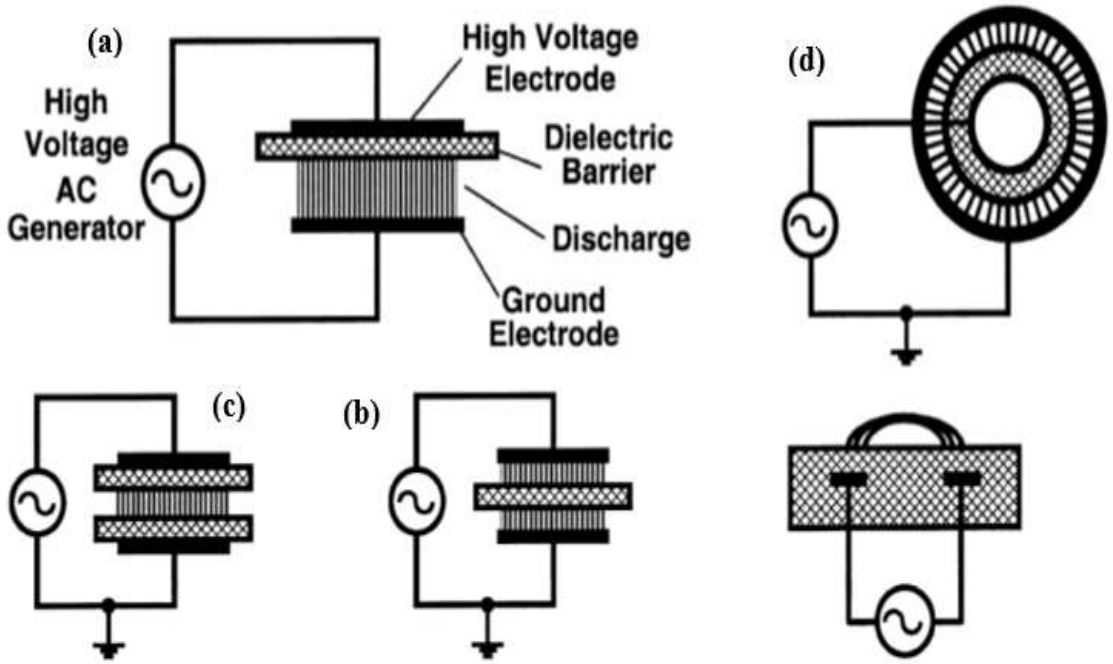

Fig II.1. *Current Configurations of DBD*

These discharges have the particular advantage of being able to operate at atmospheric pressure. However, under high-pressure conditions (and with larger inter-electrode gaps), the increase in current between two metallic electrodes generally leads to a transition into an arc regime [14], which is characterized by high temperatures that are detrimental to many applications. The role of the dielectric barriers is precisely to limit the current flowing through the discharge. The accumulation of charges from the plasma on the solid dielectric causes a reduction of the potential and the electric field applied to the gas, which results in the extinction of the discharge. Due to the presence of the solid dielectric, a DBD is inherently pulsed and requires excitation by alternating voltage power supplies. Typically, potential differences on the order of several tens of kilovolts and frequencies ranging from 1 Hz to 1000 kHz are applied to ignite the gas across an inter-electrode gap of only a few millimeters.

II.4. Basic Principle of DBD

The fundamental operating principle of dielectric barrier discharges (DBDs) relies on the use of at least one dielectric layer placed between two electrodes (Figure II.2.), across which a high alternating or pulsed voltage is applied. This dielectric barrier plays a crucial role in controlling the discharge process and ensuring the generation of a non-thermal plasma rather than a thermal arc.

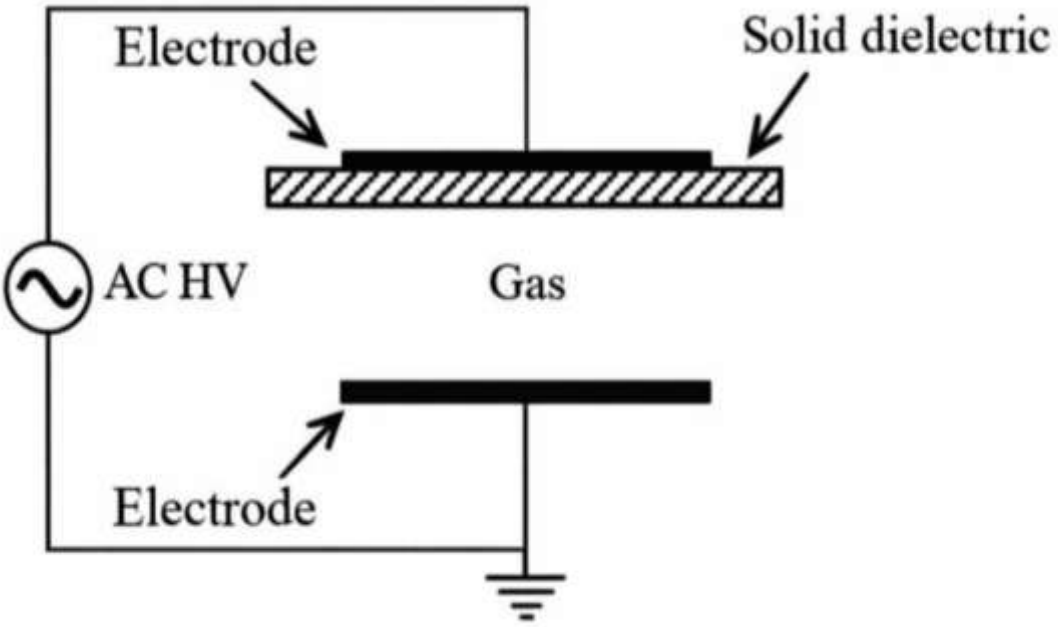

Fig II.2. *DBD with One Dielectric Layer*

When the applied voltage exceeds the breakdown voltage of the working gas (typically air, oxygen, nitrogen, or their mixtures), localized micro-discharges are initiated in the gap. These micro-discharges consist of short-lived plasma filaments with high electron density, which last only a few nanoseconds. During each micro-discharge, electrons are accelerated by the high electric field, producing ionization, excitation, and dissociation of gas molecules. This process leads to the formation of reactive species such as O, O_3, N, and excited N_2, which are central to applications like ozone generation, pollutant abatement, and surface modification

A distinctive feature of DBDs is the charge accumulation on the dielectric surface during each micro-discharge event. As charges deposit on the dielectric, they locally reduce the electric field, which quenches the discharge and prevents continuous current flow. This self-termination mechanism is essential for maintaining a cold, non-equilibrium plasma where electrons reach high energies (1–10 eV) while the bulk gas remains near room temperature. Unlike arcs or glow discharges, DBDs can therefore operate stably at atmospheric pressure without significant gas heating.

Overall, the operation of DBDs is based on three key elements: (i) the application of high-voltage AC or pulsed power, (ii) the formation of transient micro-discharges that generate reactive species, and (iii) the dielectric barrier, which prevents arcing and maintains plasma stability, the operating principle of the DBD is shown schematically in figure II.3.

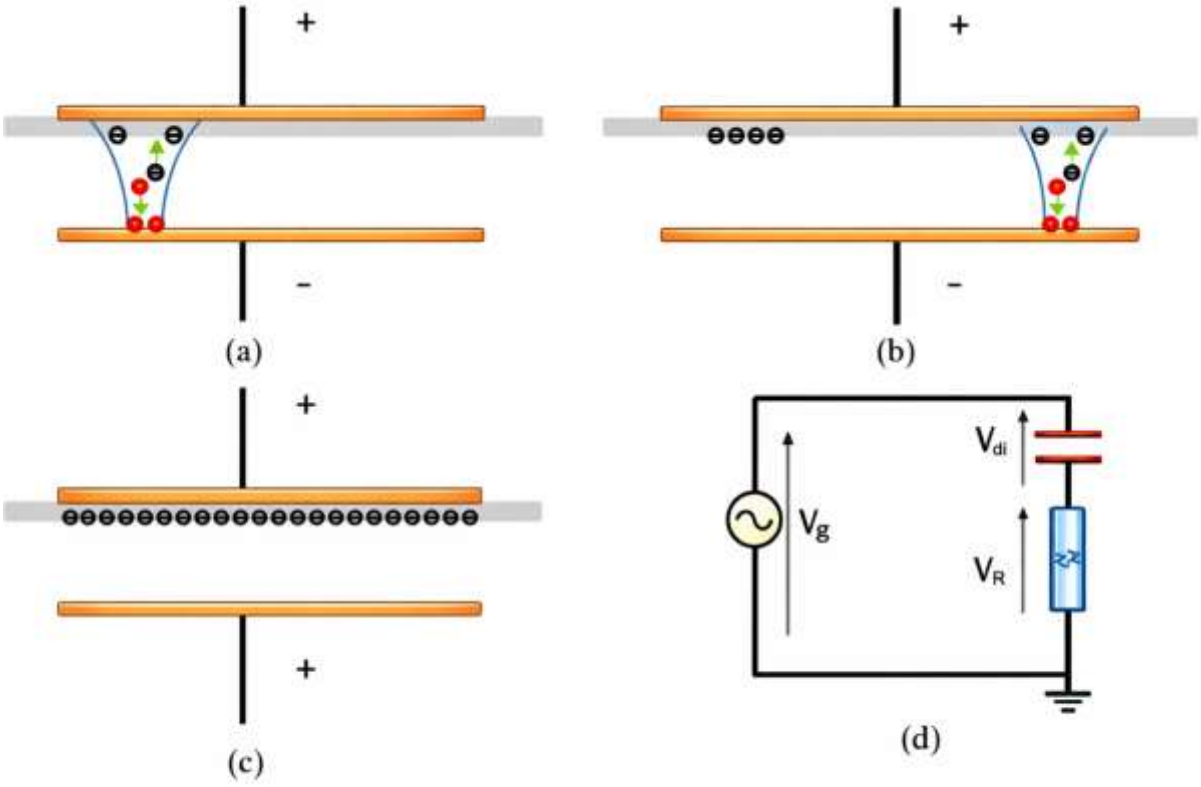

Fig II.3. *Operating principle of a DBD: (a) initiation of the first micro-discharge, (b) extinction of the initial micro-discharge and triggering of a new one, (c) reversal of the applied polarity on the electrodes, and (d) equivalent electrical circuit of a micro-discharge [15], [16].*

II.5. Electrical Characteristics of DBD

The electrical behavior of dielectric barrier discharges (DBDs) is central to their operation and directly influences their stability, efficiency, and chemical reactivity. Unlike continuous arc discharges, DBDs are characterized by a series of short-lived, spatially and temporally localized discharges that occur within each half-cycle of the applied voltage, ensuring non-equilibrium plasma conditions.

II.5.1. Voltage–Current Behavior

DBD reactors typically operate under sinusoidal or pulsed high voltages in the range of 5–30 kV, with frequencies between 1–1000 kHz, depending on the reactor geometry and application [15-16]. The current waveform reflects the formation of multiple micro-discharges per cycle, appearing as sharp current spikes superimposed on a capacitive displacement current. This characteristic current profile distinguishes DBDs from other non-thermal plasmas, such as coronas or gliding arcs.

II.5.2. Micro-discharges

The plasma formed in DBDs does not fill the gap uniformly; instead, each half-cycle produces numerous short micro-discharges, typically lasting 10–100 nanoseconds, and distributed randomly across the dielectric surface [15-16]. These micro-discharges appear as filamentary channels with high electron density (~10^{13}–10^{14} cm^{-3}), surrounded by regions of low ionization. Their transient and localized nature is crucial in preventing the transition to thermal arcs while allowing efficient generation of reactive species.

II.5.3. Charge Accumulation and Self-Termination

A defining feature of DBDs is the role of the dielectric barrier in accumulating surface charge during each micro-discharge event. As charges deposit on the dielectric surface, they locally reduce the electric field in the discharge gap, causing the micro-discharge to self-terminate within nanoseconds. This self-limiting mechanism prevents continuous current flow and arcing, thereby maintaining the plasma in a non-equilibrium state where the electron temperature (several eV) is much higher than the gas temperature (close to ambient) [15-16].

The combination of high-voltage excitation, nanosecond micro-discharges, and charge-controlled self-termination results in a plasma environment dominated by energetic electrons, weakly ionized gases, and abundant radicals. These features explain why DBDs are particularly effective for applications requiring selective chemistry, such as ozone generation, volatile organic compound decomposition, and NO_x reduction.

II.6. Different Types and Mechanisms of Dielectric Barrier Discharges

II.6.1. Positive Polarity DBD

When a positive voltage is applied to the powered electrode, electrons in the gas are accelerated toward the dielectric surface while positive ions move in the opposite direction, and because of the electrons have much higher mobility, they quickly accumulate on the dielectric, leading to strong surface charging.

The surface charge created by the dielectric barrier discharge effectively reduces the local electric field, interrupting the discharge after a few nanoseconds. Positive polarity discharges generally favor short-duration micro-discharges, characterized by narrow current pulses and lower discharge uniformity [17].

II.6.2. Negative Polarity DBD

For negative voltage polarity, the powered electrode acts as a cathode. Electrons are accelerated into the gap, while positive ions bombard the dielectric surface. This process enhances secondary electron emission from the dielectric and electrode surfaces, leading to longer and more stable micro discharges. Negative polarity discharges are often more effective for initiating streamers, as the enhanced electron emission sustains electron avalanches over longer distances [17].

II.6.3. Pulsed DBD

In addition to the conventional sinusoidal or alternating current (AC) excitations, pulsed voltage sources are increasingly employed in dielectric barrier discharge (DBD) systems. The use of pulsed operation introduces several important advantages, both from a physical and a chemical perspective, making it highly attractive for advanced plasma applications.

One of the primary benefits of pulsed excitation lies in the generation of short high voltage pulses on the nanosecond to microsecond timescale. Such short pulses produce higher values of the reduced electric field (E/N), which strongly influences the behavior of electrons in the discharge. This high reduced electric field accelerates electrons to energies sufficient for efficient excitation, dissociation, and ionization of gas molecules, thereby favoring electron driven reactions over thermal processes. This leads to a more energy efficient plasma where reactive species are formed with minimal power losses to gas heating.

A second advantage of pulsed operation is the effective suppression of gas heating, and because of each discharge event is confined to very short durations, there is insufficient time for significant thermal energy transfer to the bulk gas. As a result, the discharge remains in a non-thermal regime**,** characterized by hot electrons and relatively cold ions and neutrals. This property is crucial for applications where thermal damage must be avoided, such as in biological treatments or the processing of temperature sensitive materials.

Another key feature of pulsed DBD is the ability to achieve enhanced control over plasma chemistry. By adjusting pulse parameters such as width, frequency, amplitude, and repetition rate, it is possible to tailor the production of specific reactive species notably oxygen radicals (O), hydroxyl radicals (OH), and nitrogen species (N). These reactive species are highly desirable in many plasma-assisted processes, including sterilization, decontamination, and

environmental remediation. At the same time, pulsed operation helps to minimize the generation of undesired by-products, which improves selectivity and process efficiency.

Due to these combined advantages, pulsed DBD has found wide applicability across multiple fields. In plasma medicine, it enables localized treatment of tissues with reactive oxygen and nitrogen species (RONS) without causing thermal injury. In sterilization and disinfection, the method ensures effective microbial inactivation with minimal material degradation. For ozone generation, pulsed operation enhances ozone yield while reducing unwanted secondary reactions. Similarly, in plasma catalysis, pulsed DBDs improve catalyst plasma interactions, thereby enhancing conversion efficiency and selectivity in chemical processes. These characteristics make pulsed DBD a versatile and promising technology for both industrial and biomedical applications [20].

II.7. Mechanism of DBD Formation

A. Seed Electron Sources

The initiation of a dielectric barrier discharge (DBD) requires the presence of seed electrons, which act as the starting point for electron avalanche processes. In a neutral gas, the density of free electrons is naturally very low; however, several mechanisms can supply these initial electrons. One important source is cosmic rays and natural background radiation, which continuously produce a small but steady concentration of charged particles in the atmosphere. Although their contribution is weak, they are sufficient to trigger the very first ionization events when the applied electric field becomes high enough.

Another relevant mechanism is photoionization of impurities or background gas molecules by ultraviolet (UV) photons. These photons are generated by other micro discharges within the plasma and can ionize nearby neutral molecules, thereby creating additional seed electrons that facilitate spatial expansion of the discharge. Furthermore, secondary electron emission from dielectric or electrode surfaces also contributes significantly. When energetic ions or photons strike these surfaces, they can release electrons into the gap, reinforcing the pre ionization level of the system. Altogether, these different electron sources play a critical role in ensuring that the discharge can ignite at the onset of each half cycle of the applied voltage [18].

B. Streamer Mechanism

a. Electron Avalanche

Once seed electrons are present in discharge volume, they are accelerated by the strong local electric field applied across the gap. Under these conditions, electrons gain sufficient

kinetic energy to collide inelastically with neutral gas molecules. Each collision may ionize the molecule, producing a new electron and a positive ion.

$$e^- + M \rightarrow 2e^- + M^+ \quad \text{(II.1)}$$

This process repeats itself, and the number of free electrons grows exponentially as they drift in the opposite direction of the electric field. The phenomenon is known as an electron avalanche. The avalanche process is extremely rapid, occurring on nanosecond time scales, and it represents the first stage of the breakdown process in DBD systems.

b. Streamer Propagation

As the avalanche develops, space charge effects start to influence the local field distribution. The accumulation of positive ions at the tail and electrons in the head of the electric avalanche enhances the electric field locally, enabling the discharge to extend beyond its initial region of formation. This leads to the formation of a streamer, a thin, filamentary plasma channel that propagates through the gas gap.

The direction and dynamics of streamer propagation depend on the applied polarity. Positive streamers propagate toward the cathode, driven primarily by the strong local reduced electric field created by high energy electrons at the streamer tip. In contrast, negative streamers move toward the anode and are supported by photoionization processes ahead of the streamer, which provide new seed electrons in the propagation path. Streamers typically last only a few nanoseconds but occur repeatedly across the electrode surface during each half cycle of the applied AC voltage. They are the fundamental building blocks of filamentary DBD micro-discharges, whose collective effect results in the uniform non-thermal plasma that characterizes this type of discharge [19].

II.8. Types of DBD in Volume

II.8.1. Filamentary Discharge

The filamentary regime is the most common mode of dielectric barrier discharges (DBDs) at atmospheric pressure, particularly in air and molecular gases. In this regime, the plasma forms as a collection of numerous short-lived micro-discharges, or streamers, that appear randomly distributed across the electrode surface during each half cycle of the applied voltage. Each filament typically lasts for only a few nanoseconds, with diameters ranging from a few hundred micrometers to several millimeters. These filaments generate sharp current pulses superimposed on the displacement current, resulting in a highly non-uniform discharge structure [21]. Despite

their transient nature, the large number of filaments per cycle can make the plasma appear diffuse to the naked eye. The localized high energy density within each filament leads to strong production of reactive species, making filamentary DBDs highly effective for applications such as ozone generation, nitrogen oxides (NOx) removal, volatile organic compound (VOC) decomposition, and plasma-assisted combustion.

II.8.2. Homogeneous Discharges

Under specific operating conditions, DBDs can exhibit a homogeneous or diffuse regime, where the plasma is more evenly distributed throughout the discharge gap without the formation of discrete filaments. Achieving this regime typically requires the use of noble gases (e.g., helium, neon, argon) or gas mixtures that facilitate photoionization, as well as optimized operating conditions such as high-frequency excitation, small electrode gaps, and smooth dielectric surfaces [22].

Unlike filamentary discharges, homogeneous DBDs produce smoother current waveforms with fewer spikes, indicating more uniform conduction. This uniformity is advantageous for processes that require controlled plasma exposure and minimal localized heating, such as polymer surface treatment, thin-film deposition, sterilization, and biomedical applications [23]. Although more challenging to sustain in molecular gases at atmospheric pressure, homogeneous DBDs are increasingly studied for advanced applications that demand stable and uniform plasma characteristics.

II.9. Applications of Dielectric Barrier Discharges (DBDs)

The operating principle of DBD plasmas has two aspects, one physical and the other chemical: the breakdown of the gas leading to the generation of an electrical discharge (physical aspect), and the creation of chemically active species (electrons, free radicals, excited species, meta-stables, and ions) that interact with objects placed between the electrodes, resulting in chemical modifications of their surface properties (chemical aspect). These characteristics, along with their relative ease of implementation, have made DBD plasmas widely used in various fields of application, such as industry and biomedicine [24–26].

II.9.1. Treatment of Gaseous Pollutants: NOx Removal

One of the most significant applications of DBDs is the removal of nitrogen oxides (NOx) from exhaust gases. NOx, which includes nitric oxide (NO) and nitrogen dioxide (NO_2), are

major atmospheric pollutants generated from combustion processes in power plants, vehicles, and industrial activities. In DBD reactors, high energy electrons interact with nitrogen and oxygen molecules, leading to the formation of radicals (O, OH, N) that convert NO into less harmful compounds such as N_2 and O_2. When combined with catalysts or additives such as ammonia or hydrocarbons, the process efficiency increases significantly. Thus, DBDs provide an energy efficient, non thermal plasma method for selective non catalytic or catalytic NOx reduction, the operating principle of the DBD reactor used in gaseous pollutants treatment is shown schematically in figure II.3 [25].

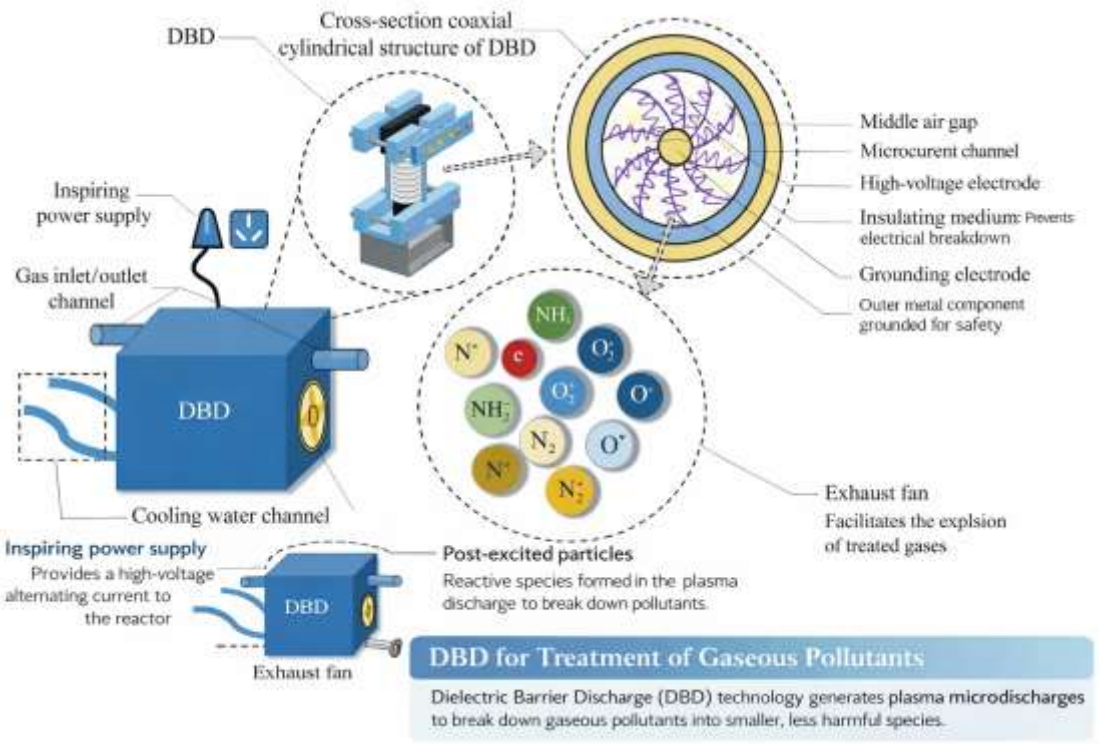

Fig II.4. *DBD for Treatment of Gaseous Pollutants [25]*

II.9.2. Ozone Generation

DBD reactors are widely used for ozone (O_3) production due to their ability to generate high-energy electrons that dissociate O_2 molecules, which then recombine into ozone.

- **Ozone Instability:** Ozone is inherently unstable and decomposes naturally back into O_2. Its half-life strongly depends on temperature, humidity, and the presence of catalytic surfaces.
- **Ozone Behavior with Bacteria, Viruses, and Germs:** Because of its high oxidation potential, ozone effectively inactivates bacteria, viruses, and other microorganisms by damaging their cell membranes and disrupting nucleic acids. This makes ozone an environmentally friendly disinfectant.

- **Ozone Generation:** DBD reactors are the dominant industrial technology for large-scale ozone generation, used in water treatment (see figure II.5), food sterilization, and air purification.
- **Advantages Over Other Disinfection Methods:** Unlike chlorine-based methods, ozone does not leave harmful chemical residues. It also acts faster than UV irradiation and penetrates biofilms more effectively.

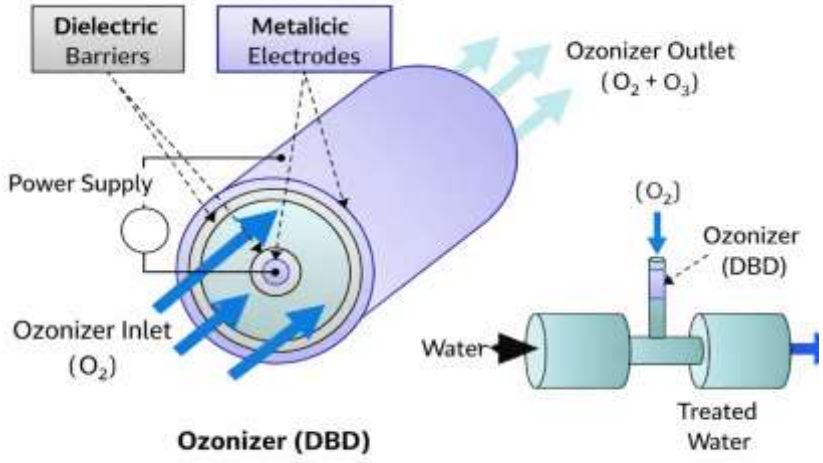

Fig II.5. *Diagram of an Ozone Device used in Water Treatment [25].*

II.9.3. Oxygen Generation

Although DBDs are mainly associated with ozone production, they can also be applied in oxygen enrichment processes. By carefully tuning the plasma conditions, oxygen molecules can be dissociated and recombined into O_2, allowing for selective control of oxygen concentration in a gas streams. This approach is of interest in medical and industrial processes requiring controlled oxygen environments.

II.9.4. Surface Treatment

DBD plasmas are increasingly used for surface modification of materials at atmospheric pressure. The high-energy electrons and reactive species alter the physical and chemical properties of polymer, textile, or metallic surfaces without significant heating. Common modifications include increased wettability, improved adhesion of coatings, and sterilization of medical surfaces. Plasma surface treatments are environmentally friendly alternatives to wet chemical processes, avoiding the use of toxic solvents.

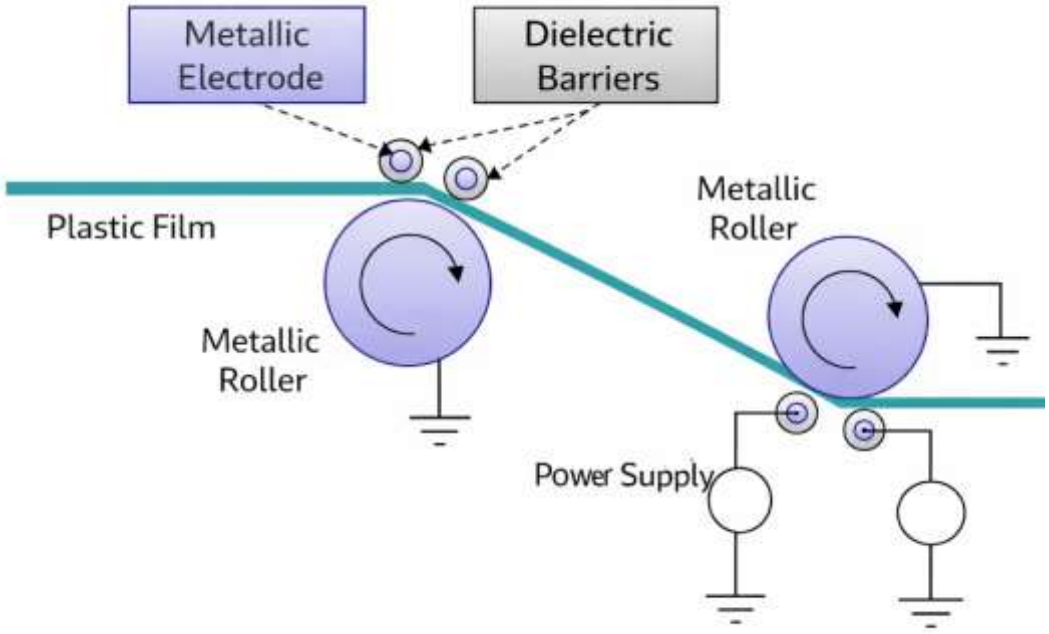

***Fig II.6**. Use of a DBD in the Surface Treatment of Plastics [27].*

II.9.5. Treatment of Gaseous Pollutants Beyond NOx

In addition to nitrogen oxides, DBDs are efficient for treating a wide variety of volatile organic compounds (VOCs), sulfur dioxide (SO_2), and other hazardous gaseous pollutants. The non-thermal plasma produces radicals and excited species that oxidize pollutants into less harmful products such as CO_2 and H_2O. For VOC removal, DBDs are often combined with catalysts to improve selectivity and reduce energy consumption.

II.9.6. Treatment of Liquid Pollutants

DBDs can also be applied in water and wastewater treatment. When operated in contact with liquids, DBD plasmas generate hydroxyl radicals (•OH), ozone, hydrogen peroxide (H_2O_2), and UV radiation, all of which contribute to advanced oxidation processes (AOPs). These species efficiently degrade organic pollutants, pesticides, and pharmaceutical residues, while also inactivating pathogens. Cold plasma water treatment is particularly promising as it avoids chemical additives and can be applied on-site.

II.9.7. Plasma Display Panels (PDPs)

Another industrial application of DBDs is in plasma display panels (PDPs), which were widely used in flat-screen televisions and displays. In PDPs, each pixel contains a miniature

DBD cell filled with a noble gas mixture. When a voltage is applied, the discharge excites the gas atoms, producing UV photons that subsequently excite phosphors to emit visible light. Although PDPs have largely been replaced by LCD and LED technologies, they represent one of the most commercially successful uses of DBDs.

Figure II.7 illustrates the role of DBD plasma in flat-panel displays [26,28,29]. The left panel shows a parallel-electrode DBD configuration, where the discharge occurs between two opposing electrodes separated by dielectric layers. The right panel presents a coplanar-electrode DBD configuration, in which the electrodes are placed on the same substrate and covered by a dielectric, allowing the plasma to spread along the surface. The bottom panel depicts an elementary display cell (pixel) composed of red, green, and blue sub cells, each containing a phosphor material excited by UV radiation to generate visible light. The combination of these subpixels enables full-color image formation.

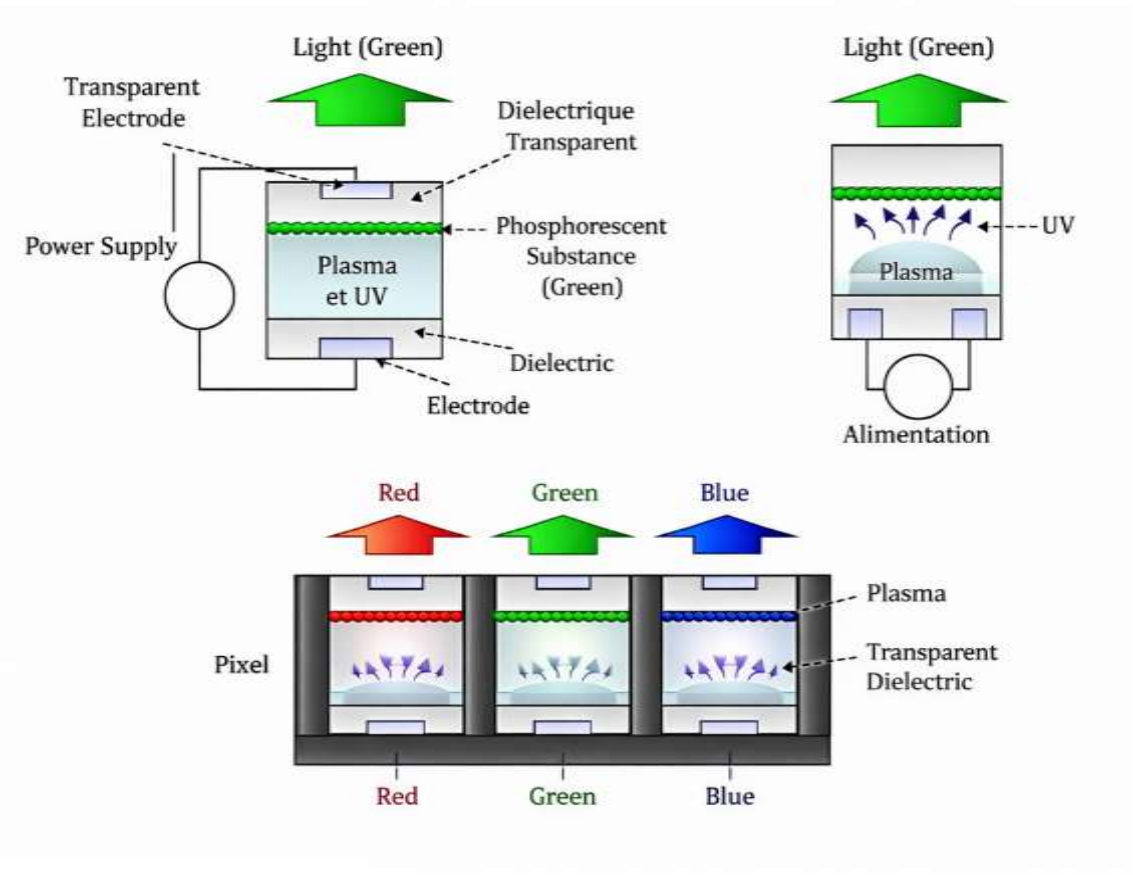

Fig II.7. *Operating Principle of Dielectric Barrier Discharge Plasma in Flat-Panel Displays*

The following figure summarizes the general principle of DBDs and outlines their major applications, as ozone generation, surface treatment, pollution control, NOx or CO_2 removal, excimer formation, plasma screen.

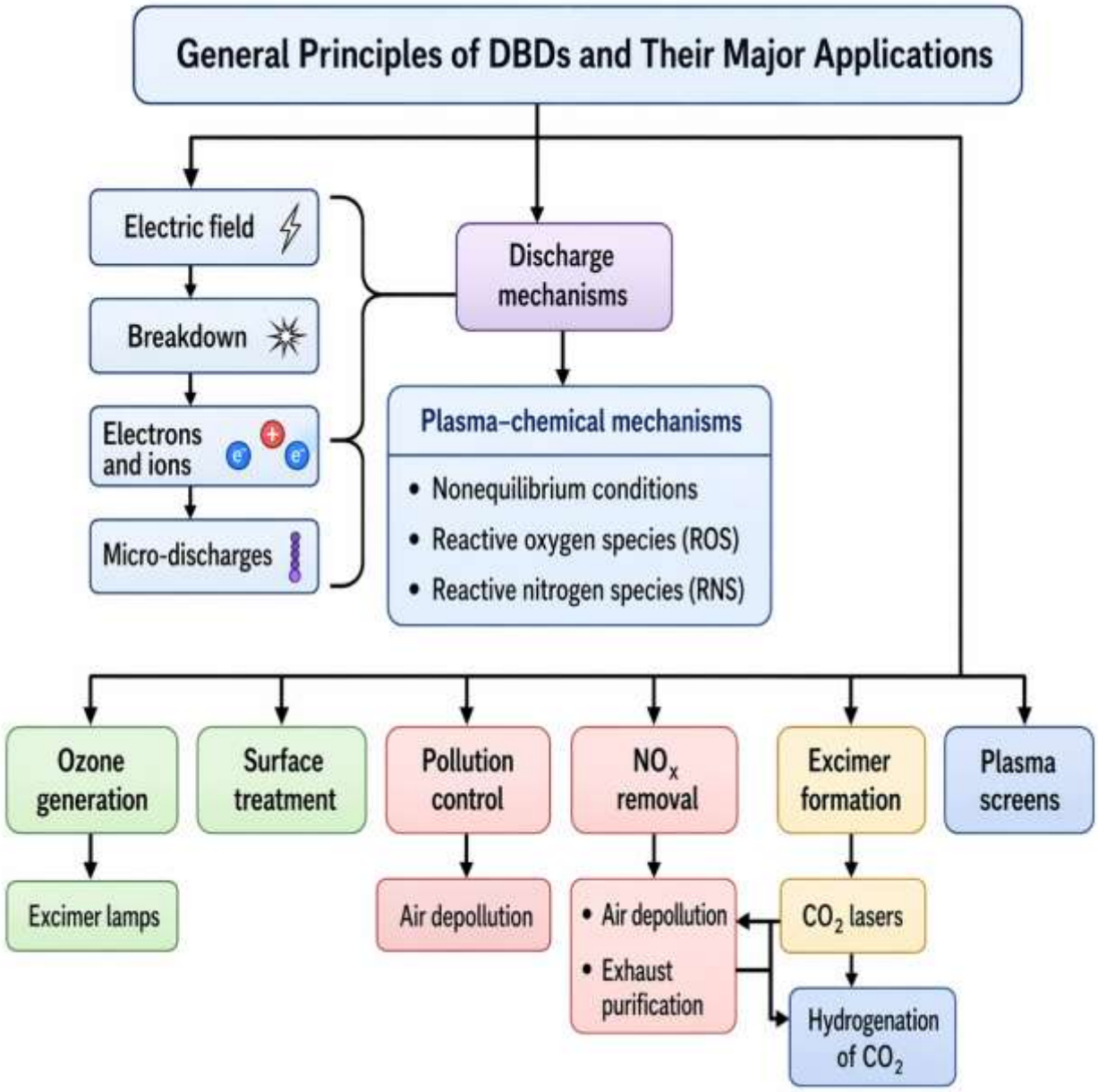

Fig II.8. *General Principle of DBDs and Their Major Applications*

II.10. Conclusion

This chapter presented a comprehensive overview of dielectric barrier discharge (DBD) plasma and its application to nitrogen oxides (NO_x) reduction. The fundamental characteristics of DBD plasmas were first discussed, including discharge mechanisms, reactor configurations, and the distinction between filamentary and diffuse discharge modes. The plasma chemical environment within DBD reactors was then examined, with particular emphasis on the generation of reactive oxygen and nitrogen species and their roles in the oxidation and reduction pathways involved in NO_x conversion.

In addition, various applications of DBD plasmas were reviewed, such as ozone generation, surface modification, and treatment of gaseous and liquid pollutants, with emphasis on environmental remediation. Important considerations related to reactor performance and optimization were also addressed, underscoring the significance of numerical modeling and appropriate reactor design in enhancing NO_x removal efficiency. This comprehensive overview establishes the foundation for Chapter III, where a one-dimensional fluid model is developed to simulate the physical and chemical processes governing NO_x reduction in DBD plasmas.

References

[1] D. P. Subedi, U. M. Joshi, C. S. Wong,"Dielectric barrier discharge (DBD) plasmas and their applications. In Plasma science and technology for emerging economies,*"an AAAPT experience* pp. 693-737,*Singapore: Springer Singapore*, 2017.

[2] L. Abdelhadi, "Modélisation Electrique d'une Décharge à Barrières Diélectriques DBD," *Mémoire de Magister, Université d'Oran des Sciences et de la Technologie (USTO-MB),* Décembre, 2014.

[3] Y. Akishev, *et al*.,"Memory and sustention of micro-discharges in a steady-state DBD: Volume plasma or surface charge," *Plasma Sources Science and Technology*, vol. 20, no. 2, 024005, 2011.

[4] M. Domonkos, P. Tichá, "Low-temperature atmospheric pressure plasma treatment in the polymer and textile industry," *IEEE Transactions on Plasma Science*, vol. 51, no. 7, pp. 1671-1681, 2023.

[5] C. U. Okonkwo, *et al.,*"Non-Thermal Plasmas for Flue Gas Pollutants (Nitrogen Oxides, Volatile Organic Compounds, Elemental Mercury, and Sulfur Dioxide) Abatement," *Plasma Processes and Polymers*, vol. *22*, no. 5, p. 2400247, 2025.

[6] S.G. Farahani, M.Anbia, "Strategies to Reduce NOx Emissions from Flue Gas: Trends and Prospects,"*Water, Air, & Soil Pollution*, vol. 236, no. 11, p.718, 2025.

[7] W.Zhao, *et al.,*"A critical review on surface-modified nano-catalyst application for the photocatalytic degradation of volatile organic compounds," *Environmental Science: Nano*, vol. 9, no. 1, pp. 61-80,2022.

[8] S. Li, *et al.,* "Research status of volatile organic compound (VOC) removal technology and prospect of new strategies: a review," *Environmental Science: Processes & Impacts*, vol. 25, no. 4, pp. 727-740, 2023.

[9] N. Bibinov, "Basics and biomedical applications of dielectric barrier discharge (DBD)," *Biomedical engineering, trends in materials science*, 2011.

[10] A. Lin, *et al.*, "Characterization of non-thermal dielectric barrier discharges for plasma medicine: from plastic well plates to skin surfaces," *Plasma Chemistry and Plasma Processing*, vol. 43, no. 6, pp. 1587-1612, 2023.

[11] T. Nozaki, *et al*., "Combination of DBD and Catalysts for CH_4 and CO_2 Conversion: Basics and Applications, "*Plasma Chemistry and Plasma Processing*, vol. 43, no. 6, pp. 1385-1410, 2023.

[12] M. Li, R. Wang, "Combined Catalytic Conversion of NOx and VOCs: Present Status and Prospects," *Materials*, vol. 18, no. 1, p. 39, 2024.

[13] B. Eliasson, U. Kogelschatz, "Nonequilibrium volume plasma chemical processing," *IEEE transactions on plasma science*, vol. 19, pp. 1063-1077, 1991.

[14] Y. P. Raizer, "Gas discharge physics," 1991.

[15] J. P. N. Naudé, A. Belinger, R. Subilau, "Diagnostic électrique et alimentations des décharges à barrière diélectrique," *Plasma et son environnement, Plasmas Froids en France et au Québec, Publication Missions Ressources et Compétence Technologiques,* 2012.

[16] N. Naudé, "Etude électrique de la physique d'une décharge de Townsend à la pression Atmosphérique et de son interaction avec un générateur : modèle et expérience," *Thèse de Doctorat, Université de Toulouse III - Paul Sabatier*, 2005.

[17] F. L. Yat, "Modélisation d'une Décharge à Barrière Diélectrique (DBD) : Influence des Applications," *Rapport de stage, Université Paul Sabatier*, 2012-2013.

[18] A. Sublet, "Caractérisation de décharges à barrières diélectriques atmosphériques et sub-atmosphériques et application à la déposition de couches d'oxyde de silicium," *Thèse de Doctorat, Ecole polytechnique Fédéral de Lausanne EPFL*, 2007.

[19] I. Enache, "Etude expérimentale et modélisation du transfert de matière dans des décharges de Townsend à pression atmosphérique en mélange HMDSO-N_2O-N_2 et SiH4-N_2O-N_2," *Thèse de Doctorat, Université Paul Sabatier Toulouse 3,* 2007.

[20] N. Ghérardi, "Physico-chimie et régimes des décharges contrôlées par barrière diélectrique en mélanges azote-gaz oxydant-silane. Application à l'activation de surfaces polymères et aux dépôts," *Thèse de Doctorat, Université Paul Sabatier Toulouse 3,* 2000.

[21] R. Maurau, "Etude de l'influence du régime d'une décharge à barrière diélectrique dans un mélange HMDSO/N_2, sur les propriétés d'un procédé de dépôt," *Thèse, Universitè Pierre et Marie Curie, Paris, France*, 2009.

[22] T. Moustafa, "Modélisation dimensionnelle d'une décharge à barrière diélectrique dans l'oxygène pour la production de l'ozone," *Mémoire de Magister, Université d'Oran des Sciences et de la Technologie (USTO-MB)*, Octobre, 2016.

[23] X.Lu, *et al*., "On the chronological understanding of the homogeneous dielectric barrier discharge,"*High Voltage*, vol. *8*, no. 6, pp. 1132-1150, 2023.

[24] A. Chebbah, "Contribution à l'étude de la production de l'ozone par décharge à barrière diélectrique à électrodes planes. Application au traitement des eaux polluées," *Thèse de Doctorat, Université Djilali Liabes de Sidi Bel Abbes*, 2018.

[25] Y. Liu, *et al.*,"NOx removal by non-thermal plasma reduction: experimental and theoretical investigations," *Frontiers of Chemical Science and Engineering*, vol. 16, no. 10, pp. 1476-1484,2022.

[26] T. Callegari, "Modélisation et diagnostics de décharges à barrières diélectriques pour écran

à plasma," *Thèse de Doctorat, Université Paul Sabatier Toulouse 3*, 2000.

[27] C. Khamphan, "Modélisation numérique de décharges contrôlées par barrières diélectriques à la pression atmosphérique : application à l'étude des précurseurs de Poudres en mélange N_2-N_2O-SiH_4," *Thèse de Doctorat, Université Paul Sabatier-Toulouse* 3, 2004.

[28] D. Astanei, *et al.*,"Treatment of polymeric films used for printed electronic circuits using ambient air DBD non-thermal plasma," *Materials*, vol. 15, no. 5, p. 1919, 2022.

[29] R. D. Medina, "Alimentation de puissance d'une lampe exciplexe à décharge à barrière diélectrique, en vue du contrôle du rayonnement," *Thèse de Doctorat, Institut National Polytechnique de Toulouse*, 2008.

Chapter III

Modeling and Simulation Results of Air DBD-Discharge

III.1. Introduction

Due to the transient and non-equilibrium nature of DBD plasmas, as well as the difficulty of directly measuring microscopic plasma parameters under atmospheric conditions, numerical modeling has become an indispensable tool for understanding and optimizing DBD based NO_x treatment.

Modeling provides access to quantities such as electron energy distribution, space charge dynamics, and radical concentrations, which are challenging to capture experimentally. In particular, fluid models allow the description of spatiotemporal evolution of plasma species by solving continuity, transport, and energy equations, coupled with Poisson's equation for the electric field. By incorporating detailed plasma chemistry for NO and NO_2 conversion, these models enable the evaluation of dominant pathways leading to pollutant removal, as well as the identification of conditions that maximize efficiency while minimizing undesired by-products.

The objective of this chapter is therefore to establish the physical and numerical framework used to simulate DBD plasma for NO_x reduction. The model is based on a one-dimensional (1D) fluid description that couples plasma transport equations with a reaction set representing the key chemical processes in air. Special attention is given to the treatment of dielectric charging, micro-discharge self-termination, and the non-equilibrium nature of electron kinetics. This framework provides the foundation for the results and analysis of NOx reduction presented in the last chapter.

III.2. Dielectric Barrier Discharge Modeling

Given the intrinsic complexity of dielectric barrier discharge systems, the literature commonly reports the use of simplified modeling approaches, such as zero dimensional (0D) and one dimensional (1D) models. These reduced order frameworks allow for the quantitative estimation of key plasma parameters, including electron density and electron temperature, while maintaining manageable computational costs. Such models are particularly useful in preliminary analyses, as they facilitate the identification of dominant plasma chemical reactions and the selection of relevant kinetic data. However, due to the simplifying assumptions involved, these approaches lack sufficient spatial and temporal resolution to serve as fully predictive tools. A detailed description of plasma behavior, based on tracking individual particles using stochastic equations is extremely computationally expensive. To overcome this limitation, plasma species are characterized using distribution functions, which provide a statistical representation of their collective behavior.

The distribution function of each particle is obtained by solving the Boltzmann equation, as commonly described in the literature [1–2]:

III.2.1. Distribution function

Each gas particle is characterized by its position vector *r*, which extends from the origin of the reference frame to the particle's center of mass, and by its velocity vector v. The combination of spatial coordinates and velocity components defines a six-dimensional phase space. At a given time t , the expected number of particles $dN(r,v,t)$ contained within an infinitesimal spatial volume element dr^3 around position *r*, and possessing velocities within the differential velocity element dv^3 about *v*, is expressed as:

$$dN(r,v,t) = dr^3 dv^3 f(r,v,t) \tag{III.1}$$

where $f(r,v,t)$ denotes the particle density distribution function.
The local particle number density at position *r* and time *t* is obtained by integrating the distribution function over the entire velocity space, yielding:

$$N(r,t) = \int f(r,v,t) dv^3 \tag{III.2}$$

Furthermore, the mean velocity of particles at a given point in the plasma can be defined as the first order moment of the distribution function with respect to velocity:

$$v = \frac{1}{N(r,t)} \int v f(r,v,t) dv^3 \tag{III.3}$$

III.2.2. Boltzmann equation

The collective transport behavior of charged particle ensembles can be described statistically through the Boltzmann equation [3–4]:

$$\frac{\partial f_i}{\partial t} + \vec{v_i}.\overrightarrow{\nabla_r}.f_i + \frac{\vec{f}_i}{m_i}.\overrightarrow{\nabla_v} f_i = \left(\frac{\partial f_i}{\partial t}\right)_{coll} \tag{III.4}$$

The solution of this equation provides the time- and space-dependent distribution function f_i for each particle species *i*. In the present study, the dominant external force acting on particles charged arise from the applied electric field, which directly governs the evolution of the

corresponding distribution functions. At the same time, the electric field is not prescribed independently but is determined self-consistently by the spatial distribution of charges through Poisson's equation [5]:

$$\nabla \vec{E} = \frac{e}{\varepsilon_0}(n^+ - n^-) \tag{III.5}$$

The numerical solution of the Boltzmann equation is inherently complex, and its coupling with electromagnetic phenomena further increases the computational challenge. As a result, several modeling strategies have been developed to describe electrical discharges.

The most simplified approach is the fluid model, which relies on a number of assumptions but can yield reliable results within a limited range of operating conditions and with relatively low computational cost. At the opposite end, microscopic or particle-based methods directly solve the Boltzmann equation to capture detailed kinetic effects. Between these two extremes, hybrid approaches have been introduced to balance accuracy and computational efficiency. In the hybrid model, fast electrons are treated using a Monte Carlo simulation (more details about Monte Carlo simulation can be found in references [6,7,8], and slow electrons are treated using the fluid model, this fluid model will be described in the following sections.

III.3. Fluid Model

In the fluid description, plasma behavior is represented through macroscopic quantities such as particle density, mean velocity, and average energy for each species. These variables are determined by solving a set of continuity, momentum (or flux), and energy balance equations associated with the different plasma constituents [9].

The fluid equations are derived by taking successive velocity moments of the Boltzmann equation. To ensure a self-consistent description of the discharge, the fluid equations are coupled to Maxwell's equations in the general case, or with Poisson's equation in electrostatic formulations, allowing the electric (and, when relevant, magnetic) fields to be calculated from the charge distributions.

The particle continuity equation can be written as:

$$\frac{\partial n}{\partial t} + \vec{\nabla}_r n\vec{v} = \int_v \left(\frac{\partial f}{\partial t}\right)_{coll} = S = n_e(v_i(r,t) - v_a(r,t)) - r(r,t)\,\mathrm{n_e n_p} \tag{III.6}$$

In this expression, the first term represents the temporal variation of the particle density, while the second term corresponds to the divergence of the particle flux. The term on the right-hand side accounts for source and loss processes, encompassing all collisional mechanisms responsible for the production and destruction of the considered species. The corresponding creation and loss frequencies depend on the gas composition, pressure, and the species distribution functions.

Fluid modeling is particularly well suited for high-pressure plasmas, where frequent collisions tend to reduce nonlocal effects. Nevertheless, nonlocal behavior may still arise in atmospheric-pressure discharges when strong electric fields are present. Despite this limitation, fluid models are widely employed due to their high computational efficiency. Moreover, they allow the inclusion of a large number of species and reactions, making them suitable for investigating complex plasma-chemical mechanisms.

The formulation of fluid models relies on two principal assumptions in order to limit the number of governing equations and to achieve mathematical closure of the system [10].

- The first assumption concerns the truncation order of the moment expansion of the Boltzmann equation. For instance, a first-order formulation retains the conservation equations for particle density and momentum, while a second-order formulation additionally includes the conservation equation for energy density.
- The second assumption relates to the closure conditions required to express higher-order moments in terms of lower-order quantities.

The closure of the system of equations at the first-order moment corresponds to the hypothesis of local field equilibrium, while the closure of this system at the second-order moment corresponds to the hypothesis of local energy equilibrium.

a- Local Field Approximation (LFA)

Under the Local Field Approximation, electron transport coefficients and reaction rate coefficients are assumed to depend solely on the local reduced electric field $E(r,t)/p$, where $E(r,t)$ denotes the electric field at position r and time t, and p is the gas pressure. Accordingly, the electron energy distribution function (EEDF) at a given point is considered equivalent to that obtained in a uniform field characterized by the same reduced electric field. This assumption implies a local equilibrium between the energy gained by electrons from the electric field and the

energy dissipated through collisions [11]. As a result, transport and kinetic coefficients are typically obtained from precomputed databases as functions of E/p.

b- Local Energy Approximation (LEA)

In the Local Energy Approximation, transport properties and reaction rates are expressed as functions of the mean electron energy, which is evaluated by solving the electron energy balance equation within the fluid framework. With advancements in plasma modeling, it has become common practice to solve the coupled set of equations comprising the species continuity equations, the mean electron energy equation, and Poisson's equation, generally used in one-dimensional (1D) or two-dimensional (2D) geometries. To further simplify the model, particle fluxes are often described using the drift diffusion approximation, in which the flux is expressed as the sum of drift and diffusion components while higher order contributions are neglected. Although fluid models do not provide detailed information on full distribution functions, such as ion energy distribution functions, and are limited to averaged quantities, this shortcoming can be alleviated through the use of hybrid modeling approaches [11]. A key advantage of fluid models, which remains unmatched by statistical methods of comparable dimensionality, is their rapid convergence and relatively low computational cost.

III.4. Physical Model and Basic Equations of DBD Discharge

This section outlines the physical model adopted to describe the dielectric barrier discharge, along with the underlying assumptions and the fundamental equations employed. The present work relies on a one dimensional formulation based on a fluid representation derived from the first three velocity moments of the Boltzmann equation. The transport of electrons and ions is modeled in a self consistent manner by coupling these fluid equations with Poisson's equation for the electric field, while additional kinetic equations are used to describe the temporal evolution of excited state populations.

III.4.1. Transport equation

The velocity distribution function provides access to macroscopic plasma quantities; including particle density, mean velocity, and average energy. The particle number density $N(r,t)$ is defined by the following integral:

$$\mathrm{N}(r,t) = \int f(r,v,t)\, d\,v^{3} \tag{III.7}$$

More generally, the mean value of a physical quantity χ is given by:

$$\chi(r,t) = \frac{1}{n_s(r,t)} \int \chi_s f_s(r,v,t) dv^3 \tag{III.8}$$

Macroscopic transport equations can thus be obtained by multiplying the Boltzmann equation by the corresponding quantity χ(*v*) and integrating over the entire velocity space. In this framework, the Boltzmann equation is replaced by a system of three coupled equations governing the evolution of particle densities, average velocities, and electron energy. These equations correspond to the continuity, momentum, and energy balance equations, respectively, and are obtained by taking successive velocity moments of the Boltzmann equation, where χ(*v*) is expressed as a polynomial function of the particle velocity.

A. Continuity equation:

By choosing $\chi(v)=1$, the zeroth-order moment of the Boltzmann equation is obtained, leading to the continuity equation:

$$\frac{\partial n_{e,p}}{\partial t} + \nabla_r n_{e,p} = S_{e,p} \tag{III.9}$$

This equation expresses the conservation of charged particles. Here, *n* denotes the number density of charged species, where subscripts *e* and *p* refer to electrons and positive or negative ions, respectively. The source term *S* accounts for all production and loss mechanisms, including ionization, attachment, and recombination processes, and can be written as:

$$S_{e,p} = n_e \left[\upsilon_i(r,t) - \upsilon_a(r,t) \right] - r(r,\mathrm{t}) n_e n_p \tag{III.10}$$

In this expression, υ_i represents the ionization frequency, υ_a the attachment frequency, and $r(r,t)$ the electron ion recombination coefficient.

The recombination term reflects collisions between charged species, and is generally negligible compared to ionization during the current pulse. Both ionization and attachment frequencies depend on the electron energy distribution function, which is not explicitly known and therefore requires appropriate modeling assumptions.

B. Momentum Transfer Equation

Selecting $\chi(v)= mv$ yields the first order moment of the Boltzmann equation, corresponding to the momentum balance. Under standard simplifying assumptions, this leads to the following momentum transfer equation:

$$n_{e,p} \bar{v}_{e,p} = a n_{e,p} \mu_{e,p} E - \nabla(D_{e,p} N_{e,p}) \tag{III.11}$$

where $\bar{v}_{e,p}$ denotes the mean drift velocity, E is the electric field, and μ and D represent the mobility and diffusion coefficient, respectively. The parameter a in equation (III.11) takes the value −1 for electrons and negative ions and +1 for positive ions. In this formulation, the particle flux consists of a drift component driven by the electric field and a diffusion component resulting from spatial gradients in particle density.

C. Energy Equation:

By setting $\chi(v)=mv^2/2$, the second-order moment of the Boltzmann equation is obtained, leading to the scalar energy balance equation:

$$\frac{\partial n_e \bar{\varepsilon}_e}{\partial t} + \frac{5}{3}\nabla\left[n_e \bar{\varepsilon}_e \bar{V}_e \right] + \nabla q - n_e e \bar{V}_e E = -n_e \bar{\varepsilon}_e \nu_\varepsilon \qquad \text{(III.12)}$$

In this equation, ε denotes the mean energy of the charged particles, ∇q represents the variation of thermal energy, and ν_ε is the energy exchange frequency associated with inelastic and elastic collisions, $\bar{\varepsilon}_e$ is the average energy.

The accumulation of space charge due to electrons and ions significantly alters the local electric field within the discharge gap. These field distortions, in turn, affect the evolution of the particle distribution functions through the force term in the transport equations. Consequently, an accurate description of the discharge requires coupling the fluid equations with Poisson's equation, which governs the spatial and temporal variation of the electric field:

$$\nabla E = \frac{|e|}{\varepsilon_0}(n_p - n_e) \qquad \text{(III.13)}$$

where ε_0 denotes the vacuum permittivity

The coupled system consisting of the continuity, momentum, and energy equations, together with Poisson's equation, provides a comprehensive description of the DBD discharge. However, this system remains mathematically unclosed. To achieve closure, additional assumptions regarding the energy distribution of charged particles must be introduced, allowing transport and reaction coefficients to be expressed in terms of macroscopic plasma parameters.

III.5. Mathematical Model used in our Calculations

The dielectric barrier discharge (DBD) plasma is modeled using a fluid approach, which describes the spatiotemporal evolution of charged and neutral species through conservation laws

coupled with electric field by solving the Poisson equation. The model incorporates momentum continuity equations for each species ions and electrons; the electron energy balance equation is also taken into account in order to govern the non-equilibrium effects. In this model based on Local Energy Approximation (LEA), the electrons transport parameters and reaction rate coefficients are functions of the local electrons average energy, obtained from pre-calculated Boltzmann solutions by including complete set of cross sections.

A. Continuity Equations for Charged and Neutral Species

For each plasma species *j* (electrons, ions, excited neutrals, radicals), the continuity equation expresses the balance between temporal density variation, transport, and volumetric production or loss:

$$\frac{\partial n_j}{\partial t} + \nabla \cdot \Gamma_j = R_j \tag{III.14}$$

where:

- n_j is the number density of species *j*,
- Γ_j is the particle flux,
- R_j represents the net source term (creation minus destruction) due to plasma-chemical reactions.

For electrons (e^-) and ions (N_2^+, O_2^+, NO^+, etc.), R_j includes contributions from ionization, recombination, attachment, detachment, and electron-impact processes. For neutrals (O, O_3, NO, NO_2), it includes dissociation, oxidation, and radical reactions.

The electron flux is expressed using the drift–diffusion approximation (see equation III.11):

$$\Gamma_e = \upsilon_e n_e = -\mu_e n_e E - D_e \nabla n_e \tag{III.15}$$

with:

- μ_e: electron mobility,
- D_e: electron diffusion coefficient,
- E: local electric field.

This relation accounts for both drift transport under the applied electric field and diffusion transport driven by density gradients. It is important to note that the neutral flux only contains the diffusion term due to the density gradient of each neutral type.

B. Electron Energy Balance Equation

Since DBD plasmas are strongly non-equilibrium systems, the electron energy distribution must be separately described. The electron energy density equation is written as the following:

$$\frac{\partial n_\varepsilon}{\partial t} + \nabla \cdot \Gamma_\varepsilon + E \cdot \Gamma_e = R_\varepsilon \tag{III.16}$$

where:

- n_ε: electron energy density,
- Γ_ε: electron energy flux,
- R_ε: net electron energy gain or loss through collisions,
- the term $E.\Gamma_e$: energy gained from the electric field.

❖ The electron energy flux is expressed as:

$$\Gamma_\varepsilon = -\mu_\varepsilon n_\varepsilon E - D_\varepsilon \nabla n_\varepsilon \tag{III.17}$$

where μ_ε and D_ε are the energy mobility and diffusivity, respectively [12].

❖ The mean electron energy is obtained as:

$$\varepsilon = \frac{n_\varepsilon}{n_e} \tag{III.18}$$

The electron energy loss term is calculated by summing the collisional energy losses over all inelastic electron-neutral reactions:

$$R_\varepsilon = \sum_{j=1}^{P} x_j k_j N_n n_e \Delta\varepsilon_j \tag{III.19}$$

Where:

- x_j: mole fraction of target species in reaction j,
- k_j: rate coefficient of reaction j,
- N_n: total neutral particle density,
- $\Delta\varepsilon_j$: energy loss per collision,
- P: probability of inelastic electron–neutral collisions

C. Poisson's Equation

The electric potential distribution in the plasma is computed from Poisson's equation:

$$\nabla \cdot (\varepsilon_0 \varepsilon_r \nabla V) = -\rho_s \tag{III.20}$$

where:

- V: electrostatic potential,
- ε_0: vacuum permittivity,
- ε_r: relative permittivity of the medium (dielectric or gas),
- ρ_s: space charge density.

❖ The space charge density is computed from the plasma species densities as:

$$\rho_s = q(\sum_{k=1}^{N} Z_k n_k - n_e) \tag{III.21}$$

where:

- q: elementary charge,
- Z_k: charge number of ion species k,
- n_k: ion density,
- n_e: electron density.

The dielectric barrier plays a critical role in limiting current and preventing transition to arc discharge. Its response to the applied field is described by:

$$D = \varepsilon_0 \varepsilon_r E \tag{III.22}$$

where D is the electric displacement vector. Surface charge accumulation on the dielectric modifies the local electric field distribution and leads to the self-terminating nature of DBD micro discharges.

❖ The electric field is obtained from the potential:

$$E = -\nabla V \tag{III.23}$$

❖ **Boundary conditions**

The impact of heavy species on the surface of the dielectric barrier represents the most important parameter governing the behavior of the discharge.

- The accumulation of charges on the surface of the dielectric, resulting from variations in the flows of electrons and ions is described as follows [9]:

$$-n(D_1 - D_2) = \rho_s \tag{III.24}$$

$$\frac{d\rho_s}{dt} = J_i + j_e \tag{III.25}$$

with ρ_s is the density of surface charge. On the boundaries, the electric fields displacement is defined by D_1 and D_2, J_i : the total current density of ion, and J_e the total current density of electron.

- At electrode surface, the electron energy is written as [13]:

$$\Gamma_\varepsilon n = \frac{1}{3} v_{e,th} \bar{\varepsilon} n_e \tag{III.26}$$

where n boundary normal vector and $v_{e,th}$: electron thermal. $\bar{\varepsilon}$ is the mean energy of electrons.

- For electron, electron energy, and heavy species beside to both sides of the gap, the boundaries conditions are written as [14]:

$$\begin{cases} -n\Gamma_e = 0 \\ -n\Gamma_\varepsilon = 0 \\ -n\Gamma_k = 0 \end{cases} \tag{III.27}$$

III.6. Surface Reactions

Surface processes are essential to neutralize ions at the dielectric surfaces. A surface interaction coefficient, which indicates the likelihood that a particular species would respond upon coming into touch with the surface, is used to characterize these interactions [15,16]. In mathematics, the following relation describes the flux of particles reacting at the surface:

$$\Gamma_k = \gamma_k \cdot n_k \cdot \sqrt{\frac{k_B . T_k}{2\pi . m_k}} \tag{III.28}$$

where:

- Γ_k is the specie (k) flux of the surface,
- γ_k is the surface interaction coefficient of specie (k),
- n_k is the specie (k) number density,
- k_B is Boltzmann constant,
- T_k is the specie (k) temperature,
- m_k is the mass of specie (k).

This expression accounts for the thermal motion of heavy species and the probability of reaction upon surface contact.

III.7. Simulation conditions

The table III.1 summarizes the DBD reactor geometry dimensions, the electric parameters, and the species atomic data used in the discharge of our model.

Table III.1 Discharge Parameters used in our Model

Parameter	Value
Maximum applied voltage (kV)	9,10,12
Frequency (kHz)	3, 4,5
Resistance (kΩ)	1
Pressure (Torr)	760
Discharge gap (mm)	1
Electrode area (cm^3)	9
Preionization density (m^3)	10^6
Thickness of dielectric (mm)	0.635
Relative permittivity of dielectric (Al_2O_3)	9.96
Molar mass N_2 (g/mol)	28.01340
Molar mass O_2 (g/mol)	31.99880
Molar mass Ar (g/mol)	39.9480
Molar mass NO (g/mol)	30.00610
Polarizability N_2 ($Å^3$)	1.710
Polarizability O_2 ($Å^3$)	1.562
Polarizability Ar ($Å^3$)	1.664
Polarizability NO ($Å^3$)	1.698
Gas temperature (K)	300
Gas mixture percentage (%)	69%N_2,20%O_2,1%Ar,10%NO

III.7.1. Initial Conditions

Initial distributions of electron and ion densities: $n_e=5\times10^4$ cm^3, $n_{i=}10^4 cm^3$**.**

Initial fraction of metastable density: $n_n = 10^{-16}$.

Initial average electronic energy: $\bar{\varepsilon}$ =5V.

III.8. Computational Study

The model developed in this study is a fluid type, self consistent model based on the resolution of the first three moments of the Boltzmann equation, coupled with Poisson's equation. The adaptation of the simulation model to the studied structure is achieved through the introduction of boundary conditions and initial conditions inherent to the system. The model developed for the dielectric barrier discharge is one-dimensional (1D).

Our work focuses on the development of fluid models using COMSOL Multiphysics 6.2, a simulation and modeling environment that integrates multiple physical domains, either coupled or separate. It is based on the finite element method (FEM)**,** which discretizes the studied problem by dividing the different domains into elementary meshes.

The appropriate simulation module, *Plasma*, was chosen according to the basic equations of dielectric barrier discharge plasma presented earlier. Once the geometry of the model is created and the values of constants and variables are predefined, the selection of boundary conditions becomes essential. The determination of the mesh, calculation time, and time step optimizes the accuracy of the simulation.

Through this software, it is possible to visualize both the resolution and the convergence rate used for our system of equations, which allows us to reduce computation time and detect the errors during the resolution process. After completing these steps, the simulation results are ready for analysis [10].

The different simulation procedures of plasma discharge using COMSOL Multiphysics 6.2 are illustrated in Figure III.1.

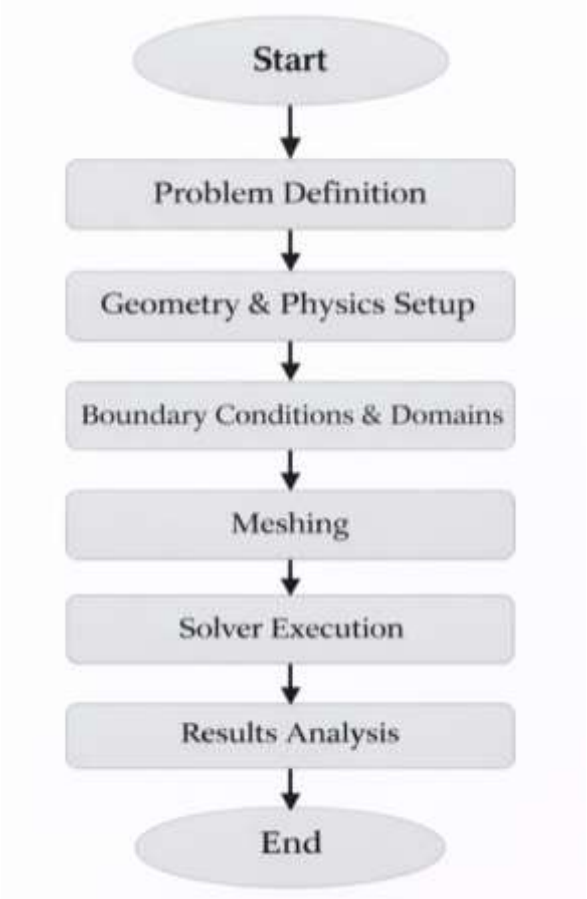

Fig III.1. *COMSOL Multi-physics Calculation Process*

III.9. Results of the 1D Modeling of Air DBD at Atmospheric Pressure

In this section, we present the results obtained from the numerical simulation of a dielectric barrier discharge (DBD) in atmospheric-pressure air, considered as a mixture of nitrogen, oxygen, and argon. The objective of this simulation is to investigate the influence of DBD operating conditions on the electrical characteristics of the plasma generated in air. The governing system of equations, together with the boundary and initial conditions, has already been introduced in the previous section. We conclude this part by presenting the simulation results obtained under a sinusoidal voltage signal.

III.9.1. Kinetic Model Considered in Air Discharge

To model a plasma discharge in air, it is necessary to account for the transport parameters of the main gas components. Since atmospheric air is a mixture of nitrogen (~79%), oxygen (~20%), and argon (~1%), the chemical kinetics involve a variety of elastic collisions, excitations, ionizations, dissociations, and attachment processes. The most relevant reactions for air plasmas can be summarized as follows [17–19]:

Table III.2: Collision Processes Considered in the Simulation of Air Discharge

No.	Reaction	Type	Δε (eV)
1	$e^- + N_2 \Rightarrow e^- + N_2$	Elastic	0
2	$e^- + O_2 \Rightarrow e^- + O_2$	Elastic	0
3	$e^- + Ar \Rightarrow e^- + Ar$	Elastic	0
4	$e^- + N_2 \Rightarrow e^- + N_2^*$	Excitation	6–12
5	$e^- + O_2 \Rightarrow e^- + O_2^*$	Excitation	4.5–10
6	$e^- + Ar \Rightarrow e^- + Ar^*$ (metastable)	Excitation	11.6
7	$e^- + N_2 \Rightarrow 2e^- + N_2^+$	Ionization	15.6
8	$e^- + O_2 \Rightarrow 2e^- + O_2^+$	Ionization	12.1
9	$e^- + Ar \Rightarrow 2e^- + Ar^+$	Ionization	15.8
10	$e^- + O_2 \Rightarrow O^- + O$	Attachment	4–6
11	$e^- + N_2 \Rightarrow e^- + 2N$	Dissociation	9.8
12	$e^- + O_2 \Rightarrow e^- + 2O$	Dissociation	5.1

III.9.2. Cross Section

The electron-impact collision cross sections for nitrogen (N_2), oxygen (O_2), and argon (Ar), adopted from the Triniti, Phelps, and Siglo databases available on the LXCat online platform, are

presented in fig.III.2, fig.III.3, and fig.III.4, respectively, where in figure III.2; the curve 1 represents the effective momentum transfer, curves from 2 to 22 are the excitations for different levels, and curve 23 represents the ionization, in figure III.3; the curve 1 represents the electron attachment, curve 2 represents the effective momentum transfer, curves from 3 to 16 are the excitations for different levels, and curve 17 represents the ionization, and in figure III.4; the curve 1 represents the effective momentum transfer, curve 2 is the excitation process, and the curve 3 represents the ionization with electron impact.

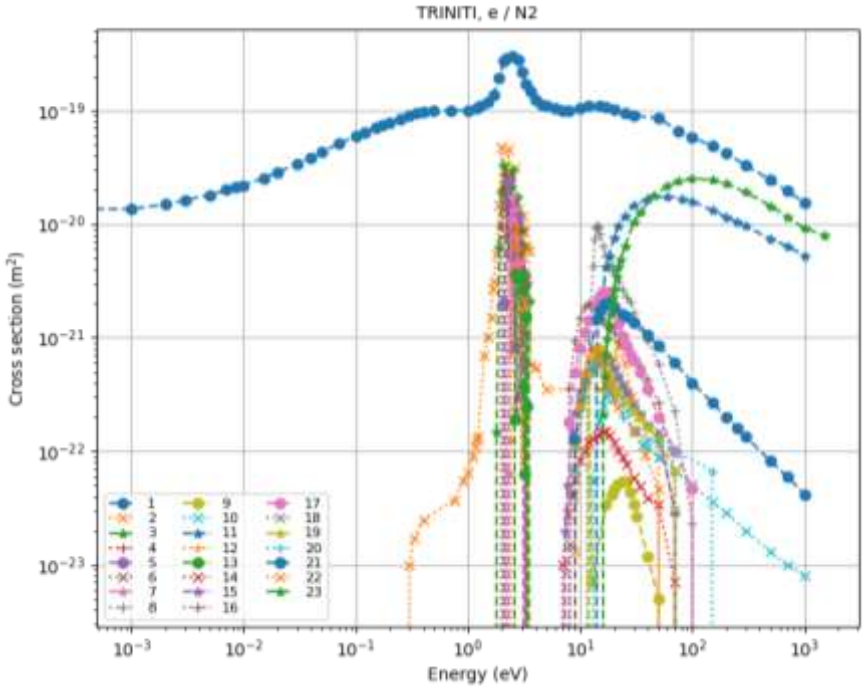

Fig III.2. *Nitrogen cross section (Triniti Data [20]).*

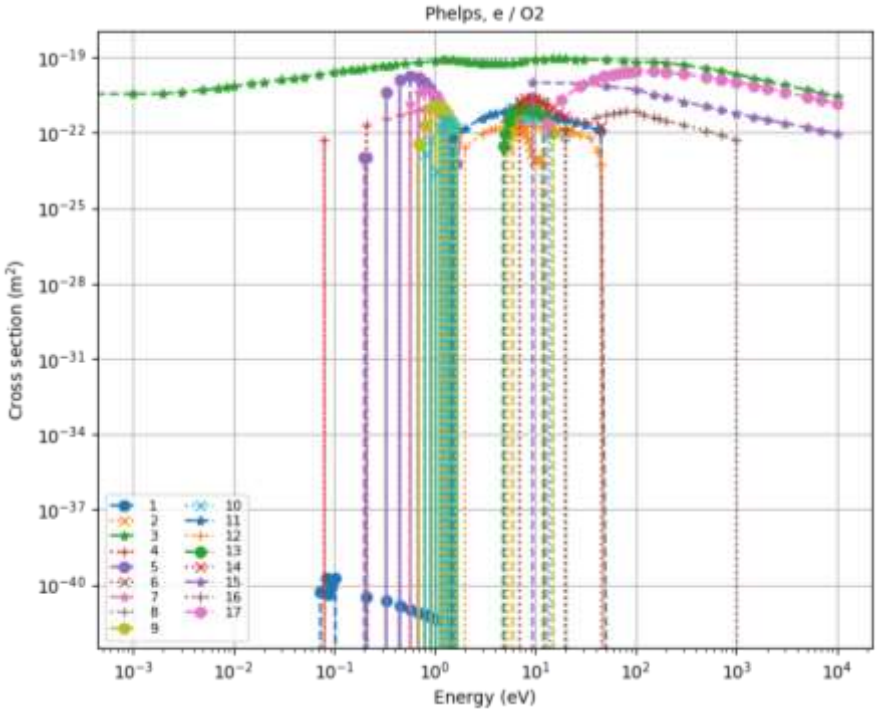

Fig III.3. *Oxygen cross section (Phelps Data [21]).*

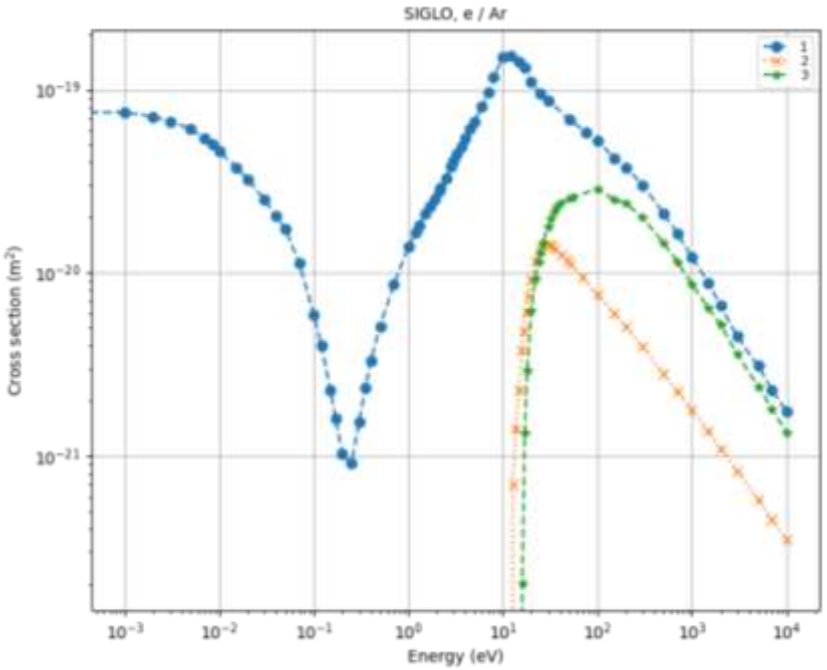

Fig III.4. *Argon cross section _Siglo Data [22].*

These cross sections include the main elastic, excitation, ionization, and dissociation processes relevant to low-temperature. Their accurate representation is essential for determining electron transport coefficients and reaction rate constants, and consequently, the generation of reactive species involved in NO_x conversion.

III.9.3. Studied Geometry for the DBD Discharge

The geometric model of the dielectric barrier discharge (DBD) plasma cell considered in this simulation is shown in Figure III.5. The DBD discharge is established between two parallel electrodes. The upper electrode, connected to an alternating voltage source, is covered with a dielectric layer of Al_2O_3 (thickness: 0.635 mm, permittivity: 9.96), while the lower electrode is grounded and also coated with the same dielectric.

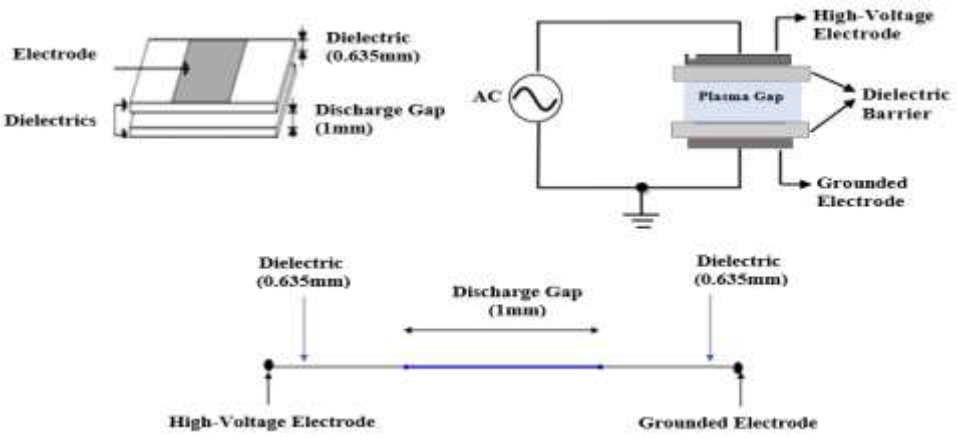

Fig III.5. *Geometric Model of the Dielectric Barrier Discharge (DBD) [23].*

III.10. Simulation Results and Interpretations

This section presents the main results obtained from the numerical simulation of the dielectric barrier discharge (DBD) in an air mixture (N_2–O_2–Ar) at atmospheric pressure. The results are analyzed in terms of the electrical characteristics of the discharge, the temporal evolution of charged and neutral species. Each result is interpreted to provide physical insight into the discharge mechanisms, electron kinetics, and the generation of reactive species, with particular focus on the implications for ozone production and NOx removal.

III.10.1. Temporal Progression of Electrical Characteristics

Figure III.6 illustrates the temporal evolution of the applied voltage and discharge current over two consecutive periods of the DBD operation. The applied voltage follows a sinusoidal waveform with peak amplitudes of ±10 kV, which is typical for AC-driven DBD systems at atmospheric pressure.

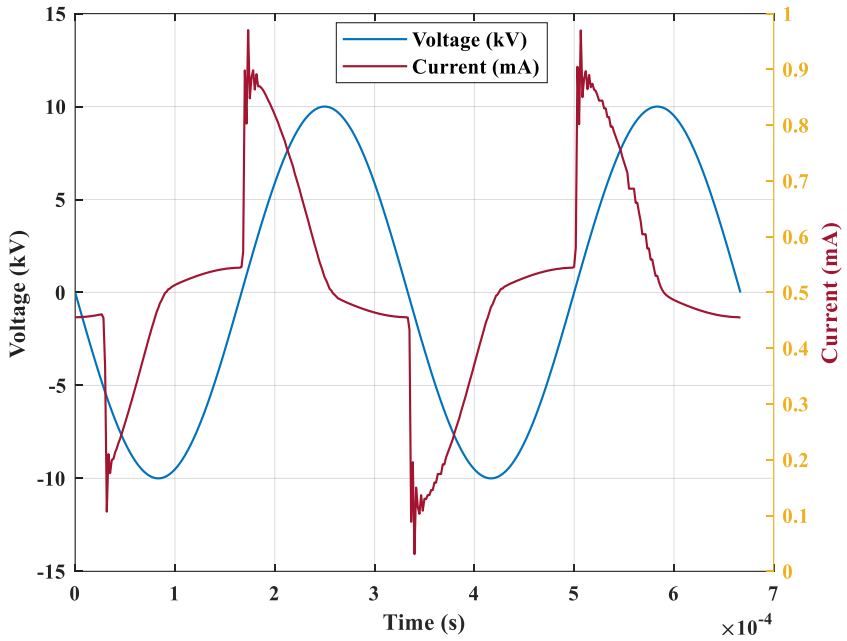

Fig III.6. *Current Discharge and Voltage Waveform in Two Periods of DBD*

In contrast, the discharge current exhibits sharp, transient pulses with peak values of the order of 1 mA. These current spikes are signatures of filamentary micro-discharges occurring near the rising and falling edges of the applied voltage. Each micro-discharge corresponds to a short-lived plasma channel where strong local electric fields accelerate electrons to high energies. In reality, this current represents the superposition of two currents: the discharge current due to the movement of charged particles, where it is dominated by the movement of electrons, and another weak capacitive current due to the temporal variation of the electric field.

The energetic electrons initiate key elementary processes such as electron-impact dissociation of O_2 and N_2, leading to the formation of atomic oxygen (O) and excited nitrogen species. From a NOx reduction perspective, this pulsed discharge regime is particularly favorable, as it maximizes the production of reactive radicals without excessive thermal NO formation. The strong temporal correlation between voltage extrema and current peaks confirms that NOx-relevant chemistry is mainly triggered during these micro-discharge events.

III.10.2. Temporal Evolutions in the Density of Charged Species

Figures III.7 and III.8 present the temporal Fluctuations of positive and negative ion species, together with electrons, during dielectric barrier discharge (DBD) operation.

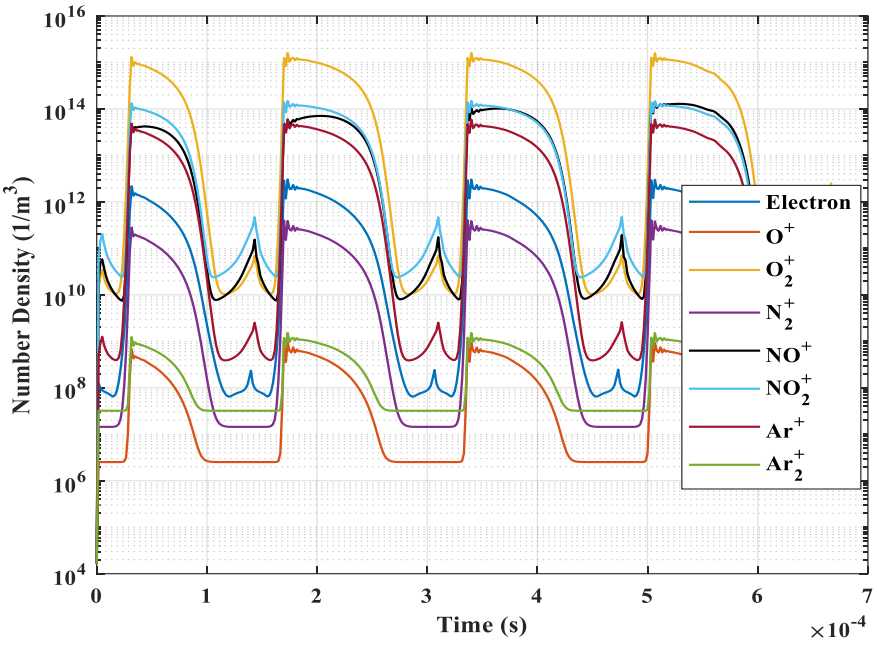

Fig III.7. *Evolution of Positive Charges Densities During Two Periods of DBD*

The results show that electron density oscillates between 10^{10} and 10^{14} m^{-3}, with sharp peaks occurring in phase with the applied voltage, corresponding to micro discharge events. Among positive ions, O_2^+ dominates with densities up to 10^{15} m^{-3}, followed by N_2^+ and NO^+. The formation of O^+ and argon-related ions (Ar^+, Ar_2^+) is comparatively less significant but still contributes to charge balance and energy transfer processes.

For negative ions, O_3^- and O^- exhibit the highest densities, reaching up to 10^{14} m^{-3}, while NO_2^- and O_2^- show moderate concentrations, where the negative ion O- is created mainly by the dissociative attachment of the oxygen molecule O_2 (primary reaction), and the other negative ions are created by secondary reactions.

The temporal profiles highlight that ion production and recombination are strongly synchronized with the applied AC field, where rapid ionization and attachment processes occur during each half-cycle. These charged species, particularly oxygen-related ions, play a crucial role in ozone formation via subsequent three-body recombination and ion–molecule reactions. which play a central role in converting NO into NO_2 and higher nitrogen oxides.

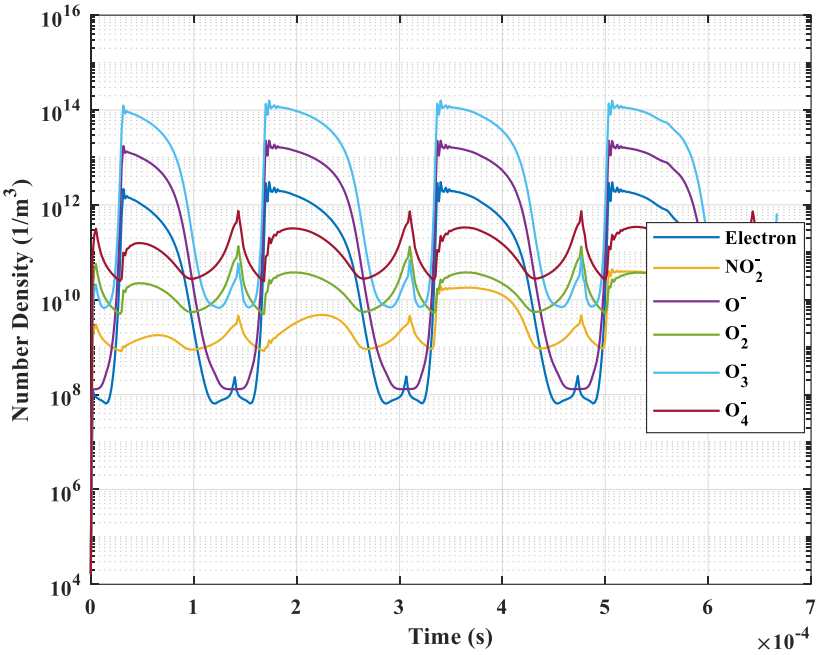

Fig III.8. *Evolution of Negative Charges Densities During Two Periods of DBD*

III.10.3. Temporal Evolution of Exited Species

The temporal variation of excited species within the dielectric barrier discharge (DBD) reactor reveals a strongly pulsed behavior, corresponding to the periodicity of the applied voltage as display in Figures III.9 and III.10.

The simulated densities of excited states of molecular nitrogen (e.g., N_2(A3s), N_2(B3p), N_2(C3p)) and atomic nitrogen states (N(d), N(P)) exhibit sharp increases during discharge pulses, followed by rapid decay, characteristic of short-lived metastable and excited species. Notably, the N_2(a1s) state shows a gradual accumulation, suggesting a relatively longer lifetime or persistent excitation between pulses. Similarly, excited oxygen species such as O(1d), O(1s), and O_2(a1d), which play critical roles in ozone formation and NOx Conversion, follow a comparable pulsed profile. The O_2(b1s) state reaches the highest peak densities (up to 10^{18} m^{-3}), indicating significant dissociation and excitation of molecular oxygen during discharge. Meanwhile, Ar metastable (Ar(s)) are present at lower densities yet contribute to sustaining the discharge via energy transfer processes.

These results demonstrate the tight coupling between electrical pulse dynamics and species excitation, underscoring the importance of discharge timing and energy input in controlling the plasma chemistry and optimizing ozone production and NOx Removal efficiency.

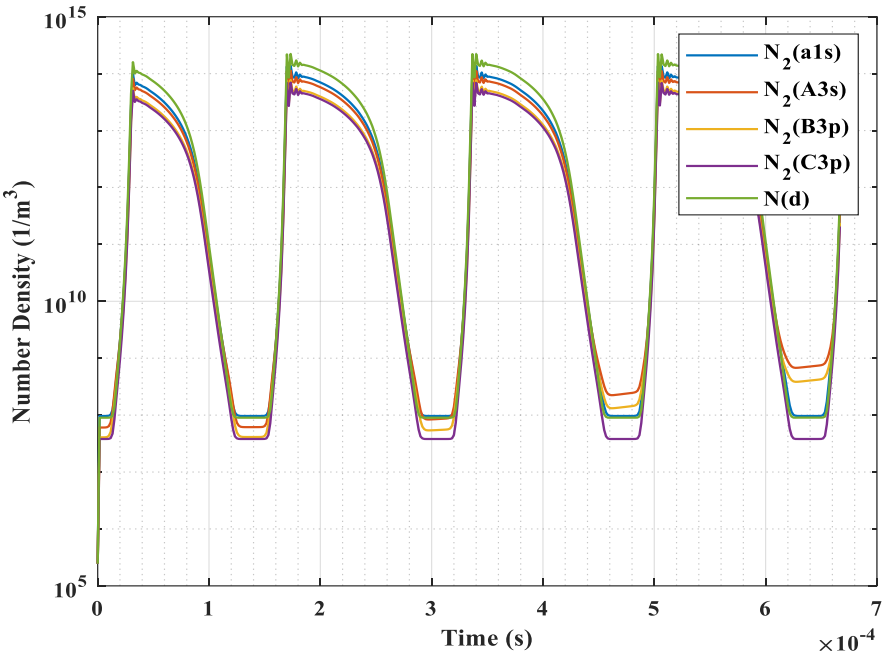

Fig III.9. *Evolution of Excited Nitrogen Species Densities During Two Periods of DBD*

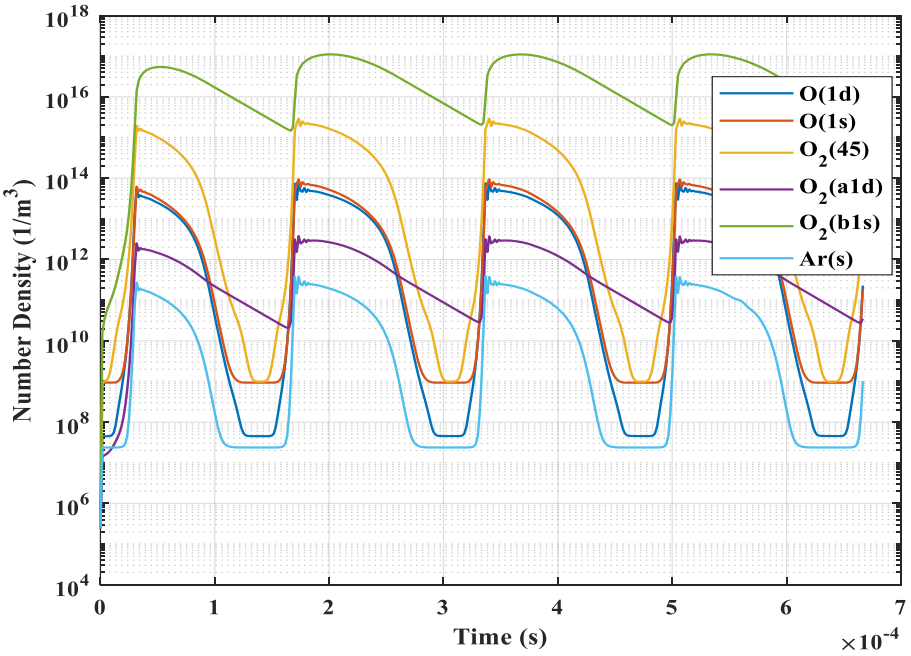

Fig III.10. *Evolution of Excited Oxygen Species Densities During Two Periods of DBD*

III.10.4. Temporal Evolution of Neutral Species

The time variation of neutral species in the post-discharge phase of the DBD system, as depicted in Figure III.11, provides important insights into the chemical mechanisms governing

NO_x reduction. The rapid formation of ozone (O_3), reaching number densities above 10^{21} m^{-3} within the first milliseconds, and this highlights the strong oxidative environment established by the discharge. Ozone acts as a key oxidizing agent for NO, promoting its conversion into higher nitrogen oxides through reactions such as:

$$NO + O_3 \rightarrow NO_2 + O_2. \qquad \text{(III.29)}$$

This pathway represents a critical first step in NO_x transformation within DBD systems.

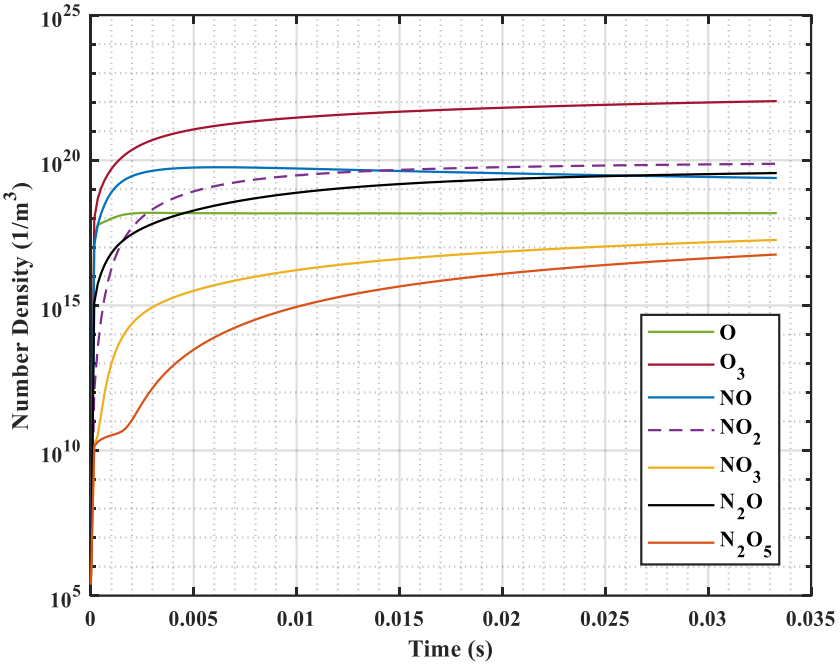

Fig III.11. *Evolution of Neutral Species during 100 Period of DBD in (*79% N_2, 20% O_2, 1% Ar)

Nitric oxide (NO) and nitrogen dioxide (NO_2) exhibit sharp increases during the early post-discharge period, stabilizing at densities on the order of 10^{20} m^{-3}. This behavior reflects the continuous interplay between NO oxidation and subsequent consumption pathways. While NO is rapidly oxidized by O_3 and atomic oxygen, NO_2 serves as an intermediate species that can further react with ozone and other radicals to form more stable nitrogen oxides. The presence of sustained NO_2 levels indicates an active conversion regime rather than simple accumulation.

The gradual formation of secondary nitrogen oxides, including N_2O_3, N_2O_5, and N_2O, with densities ranging from 10^{15} to 10^{20} m^{-3}, is particularly relevant for NO_x removal. These species originate from downstream reactions involving NO_2, ozone, and nitrogen oxides, and represent more stable or condensable products that can be more readily removed from the gas phase. In particular, the formation of N_2O_5 is a key indicator of effective NO_x oxidation, as it may lead to subsequent hydrolysis or surface adsorption in practical systems.

Atomic oxygen (O) concentration increases rapidly to around 10^{18} m^{-3}, and remains relatively stable, indicating its rapid consumption in oxidation reactions. Its role is essential in sustaining ozone production and driving NO to NO_2 conversion, thereby maintaining the oxidative capacity of the plasma-treated gas.

III.11. Conclusion

In this chapter, a comprehensive physical and numerical framework for modeling dielectric barrier discharge (DBD) plasma applied to NO_x reduction was established. A one-dimensional fluid model was developed to describe the non-equilibrium behavior of the plasma, coupling the transport equations of charged and neutral species with Poisson's equation and detailed plasma chemistry relevant to air discharges. The model accounts for key physical mechanisms such as electron energy evolution, space charge dynamics, dielectric surface charging, and the self-termination of micro-discharges. The governing equations, boundary conditions, and numerical solution strategies were presented and discussed, providing a consistent description of the coupled electrical, transport, and chemical processes occurring in DBD plasmas. By integrating plasma chemistry pathways responsible for NO and NO_2 conversion, the model enables the investigation of dominant reaction mechanisms and the influence of operating parameters on NO_x removal efficiency and by-product formation. Generally, this modeling framework constitutes a robust tool for analyzing DBD plasma behavior and optimizing reactor performance under atmospheric conditions. The results obtained from this model and their implications for NO_x reduction are presented and discussed in the following chapter, where the numerical simulations are validated and analyzed in detail.

References

[1] B. Jayaraman, W. Shyy, "Modeling of dielectric barrier discharge-induced fluid dynamics and heat transfer," *Progress in Aerospace Sciences*, vol. *44*, no. 3, pp. 139-191, 2008.

[2] A. V.Likhanskii, *et al*., "Modeling of dielectric barrier discharge plasma actuator in air," *Journal of Applied Physics*, vol. 103, no. 5, 2008.

[3] G. Hagelaar, "Solving the Boltzmann equation to obtain electron transport coefficients and rate coefficients for fluid models," *Plasma Sources Sci. Techno*, vol. 14, p. 722–733, 2005.

[4] R. D. White, "Recent advances in the application of Boltzmann equation and fluid equation methods to charged particle transport in non-equilibrium plasmas," *Journal of Physics D: Applied Physics*, vol. *42*, no. 19, p.194001, 2009.

[5] P. A. Lee, T. M. Rice, "Electric field depinning of charge density waves," In *Basic Notions of Condensed Matter Physics*, pp. 460-470, CRC Press, 2018.

[6] M. Mostafaoui, D. Benyoucef, "Electrical model parameters identification of radiofrequency discharge in argon through 1D3V/PIC-MC model," *Plasma Science and Technology*, vol. 20, no 9, p. 095401, 2018.

[7] D. Benyoucef, Djilali, M. Yousfi, "Particle modelling of low-pressure radio-frequency magnetron discharges including the effects of self-induced electromagnetic fields," *Plasma Sources Science and Technology*, vol. 23, no 4, p. 044007, 2014.

[8] D. Benyoucef and M. Yousfi, "Effects of Increasing Magnetic Field and Decreasing Pressure on Asymmetric Magnetron Radio Frequency Ar/O_2 Discharges," in *IEEE Transactions on Plasma Science*, vol. 41, no. 4, pp. 829-838, 2013.

[9] S. Gadkari, "Fluid model for a partially packed dielectric barrier discharge plasma reactor,"*Physics of Plasmas*, vol. 24, 2017.

[10] M. H. A. Lahouel, " Modélisation et simulation d'une décharge à barrière diélectriques dans un Mélange gazeux à la pression atmosphérique, " *Thèse de Doctorat, Hassiba Benbouali de chlef*, 2021.

[11] M. Bedoui, A. W. Belarbi, "Modélisation numérique d'une décharge luminescente contrôlée par barrière diélectrique, " *African Review of Science, Technology and Developpement*, vol. 1, no. 01, 2016.

[12] M. Chenoui, H.Tebani, D. Benyoucef, "Modeling and Electrical Characterization of CO_2/Ar Dielectric Barrier Discharges at Atmospheric Pressure," *Bulletin of Chemical Reaction Engineering & Catalysis*, vol. 21, no. 1, pp. 38-50, 2026.

[13] Y. M. A. Nedjar, M. Mostefaoui, D. Benyoucef, "One-dimensional fluid modeling of methane dissociation in dielectric barrier discharge: Impact of voltage and dielectric

constant," *Plasma Physics and Technology*, vol. 12, no. 1, pp. 10-15, 2025.

[14] L. S. Wei, "A numerical study of species and electric field distributions in pulsed DBD in oxygen for ozone generation,"*Vacuum*, vol. 125, pp. 123- 132, 2016.

[15] S. Baadj,*et al.*, "Chemical and Electrical Aspects of Homogeneous Discharge in an Argon-Oxygen Mixture for Ozone Generation," *Plasma Medicine*, vol. 13, no. 4,2023.

[16] M. Ghassemi, "*Dielectric Barrier Discharge (DBD) Dynamic Modeling for High Voltage Insulation*," *Electrical Insulation Conference, Annapolis, Maryland, USA*, 2011.

[17] K. H. Becker," Non-equilibrium air plasmas at atmospheric pressure,"*CRC press*, 2004.

[18] M. Capitelli, "Plasma kinetics in atmospheric gases," *Springer Science & Business Media*, vol. 31, 2013.

[19] K. C. Cossel, "Gas-phase broadband spectroscopy using active sources: progress, status, and applications, "*Journal of the Optical Society of America B*, vol. 34, no. 1, p. 104, 2016.

[20] Triniti Database, www.lxcat.net, retrieved on May 4, 2025

[21] Phelps Database, www.lxcat.net, retrieved on May 4, 2025

[22] SIGLO Database, www.lxcat.net, retrieved on May 4, 2025

[23] N. Labdouni, D. Benyoucef, H. Tebani, "Cold Plasma Modeling for Air Pollution Control: NOx Removal in Dielectric Barrier Discharge Reactors," *Bulletin of Chemical Reaction Engineering & Catalysis*, vol. 21, no. 1, pp. 180-190, 2026.

Chapter IV

Application of DBD-Discharge for NO Reduction in Air

IV.1 Introduction

The present chapter aims to provide a comprehensive investigation into the impact of frequency and voltage on the execution of dielectric barrier discharge (DBD) reactors for NO elimination in N_2–O_2– Ar– NO gas mixtures. Particular emphasis is placed on examining the spatiotemporal distribution of electrons and reactive particles within the plasma, thereby improving the fundamental understanding of discharge mechanisms relevant to atmospheric chemistry and advanced plasma technologies. The numerical simulation results offer detailed insights into the temporal evolution of key electrical parameters, as well as the behavior of charged, excited, and neutral species. Additionally, the study tracks the dynamic changes in the mole fraction of NO, enabling a deeper analysis of the chemical kinetics governing its removal. These findings contribute to the optimization of plasma-based systems for environmental remediation and other plasma-assisted processes.

IV.2. The Mixture's Chemical Kinetics Model

The plasma's chemical dynamics are extremely complicated in the N_2-O_2-Ar-NO combination examined in this work. The model incorporates all of the nitrogen-based reactions in Table IV.2 and the oxygen-related reactions mentioned in Table IV.3. Beyond these, it incorporates more than 240 chemical pathways involving interactions with nitrogen, oxygen, and argon atomic and molecular species. The simulation accounts for 34 distinct plasma species presented in table IV.1, including electrons, neutral atoms and molecules, ions, and excited states. These species and their associated reactions encompass dissociation, ionization, recombination, excitation, and charge exchange processes, ensuring a comprehensive description of plasma kinetics under atmospheric pressure conditions. The simulation results forms the foundation for a thorough comprehension of the production and destruction mechanisms of reactive particles, notably those involved in NO_X conversion, and is critical for accurate prediction of plasma behavior under varying electrical and gas mixture conditions.

Table IV.1 Species Taken into Account for the Plasma Model

Electrons	e
Neutral species	N, O, O_3, NO, NO_2, NO_3, N_2O, N_2O_5
Positive species	Ar^+, Ar_2^+, NO^+, NO_2^+, O_2^+, O^+, N_2^+
Negative species	O^-, O_2^-, O_3^-, O_4^-, NO^-, NO_2^-
Exited species	N_2(a1s), N_2(A3s), N_2(B3p), N_2(C3p), N(d), N(p), O(1d), O(1s), O_2(a1d), O_2(b1s), O_2(45), Ar(s)

- **Ions Mobilities**

The electron mobility is computed based on electron-neutral collision cross sections, which are incorporated into the simulation through a Boltzmann solver or from validated experimental data [1]. In contrast, the ion mobilities for the gaseous mixtures studied in this work are determined using polarization theory. This approach allows the estimation of the reduced mobility of an ion through the following relation [2]:

$$\mu_m = \frac{36.10^{-4}}{\sqrt{\alpha.\mathrm{M}_r}}.\frac{T}{T_0} \quad \text{in } (\mathrm{m}^2/\mathrm{V.\ s}) \tag{IV.1}$$

$$M_r = \frac{\mathrm{m}_i.\mathrm{m}_n}{m_i + m_n} \tag{IV.2}$$

with:

α : The polarizability coefficient of the neutral molecule in atomic unit

M_r: The reduced mass of the ion(m_i)/neutral(m_n) in atomic unit

T : The gas temperature

T_0 : Initial temperature

For the mixtures N_2/O_2/Ar/NO

The mobility of charged species in the N_2/O_2/Ar/NO mixture was calculated using Blanc's law, which assumes additive momentum transfer collision frequencies in multicomponent gases. According to this formulation, the inverse mobility in the mixture, $1/\mu_{Air/NO}$ is obtained as the mole-fraction-weighted sum of the inverse mobilities in each pure gas component, i.e.

$$\frac{1}{\mu_{Air/NO}} = \frac{F_{N_2}}{\mu_{N_2}} + \frac{F_{O_2}}{\mu_{O_2}} + \frac{F_{Ar}}{\mu_{Ar}} + \frac{F_{NO}}{\mu_{NO}} \tag{IV.3}$$

where F_i represents the mole fraction of species i, and μ_i denotes the mobility of the same charged particle in the pure gas i at the reference temperature and pressure. This approach provides an effective mobility for the mixture that accounts for the relative contributions of all background gases while preserving the physical influence of each component.

- **Cross Section of Electron-NO**

The cross sections for NO by using the Hayashi compilation from the LXcat website are plotted in figure IV.1. In the last figure, the curve 1 represents the electron attachment, curve 2 represents the effective momentum transfer, curves from 3 to 9 are the excitations for different levels, and curve 10 represents the ionization

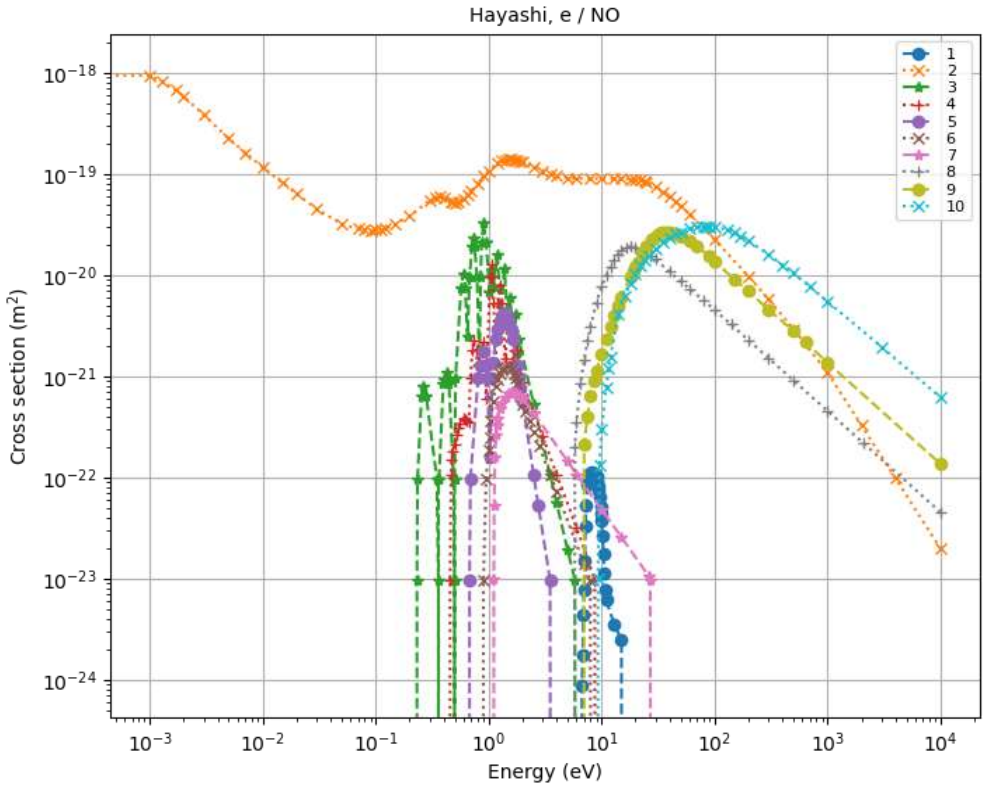

Fig IV.1. *NO Cross Section _Hayashi Data [3]*

IV.3. Chemical Reactions of Heavy Species

Tables IV.2 through IV.6 summarize the primary reactions responsible for the formation and destruction of heavy species in the plasma, along with their corresponding rate coefficients. These reactions include both two-body and three-body processes involving nitrogen, oxygen, argon, and their mixtures. The rate constants are expressed in units of m^3/s for bimolecular reactions and m^6/s for termolecular (three-body) reactions.

The reaction rate coefficients k^f employed in the present model are given using the modified Arrhenius formula [4]:

$$k^f = A\left(\frac{T}{T_0}\right)^n e^{E_a/RT} \qquad \text{(IV.4)}$$

In this expression, *A* is the pre-exponential factor, which captures the frequency of effective molecular collisions, The exponential term incorporates the activation energy *Ea*, representing the minimum energy threshold that must be overcome for the reaction to proceed. The activation energy is expressed in units consistent with the product of the universal gas constant *R* and the absolute temperature *T*, with *T* given in Kelvin and T_0=300K, the temperature *T* controls the thermal energy available to the reacting molecules, while *R* denotes the universal gas constant. Arrhenius coefficients form the basis for accurate modeling of the chemical evolution of heavy species in dielectric barrier discharge plasmas. The compiled reaction sets allow coupling the continuity equations of the species to the transport and energy equations of the plasma, thus ensuring a consistent description of the plasma chemistry at atmospheric pressure.

Table IV.2. Reaction set for Nitrogen with their Rate Coefficients

No	Reaction	Rate Coefficient (m^6/s), (m^3/s)	Ref
	Electron Impact Reactions with Nitrogen		
E1	$e+N_4 => N_2+0.38N_2(A3s) +0.38N_2(B3p) +0.24N2(C3p)$	2e-12*(0.026/Te)^0.5	[5]
E2	$e+N_3^+=>N_2+N$	2e-13*(0.026/Te)^0.5	[6]
E3	$e+N_2^+=>1.143N+0.086N(p)+0.771N(d)$	1.6e-13*(0.026/Te)^0.37	[6]
E4	$e + N_2=> e+N_2$	Cross Section	[7]
E5	$e+ N_2=> e+N_2$	Cross Section	[7]
E6	$e+ N_2=> e+N_2$	Cross Section	[7]
E7	$e+ N_2=> e+N_2$	Cross Section	[7]
E8	$e+ N_2=> e+N_2$	Cross Section	[7]
E9	$e+ N_2=> e+N_2$	Cross Section	[7]
E10	$e+ N_2=> e+N_2$	Cross Section	[7]
E11	$e+ N_2=> e+N_2$	Cross Section	[7]
E12	$e+ N_2=> e+N_2$	Cross Section	[7]
E13	$e+ N_2=> e+N_2$	Cross Section	[7]
E14	$e+ N_2=> e+N_2$	Cross Section	[7]
E15	$e+ N_2=> e+N_2(A3s)$	Cross Section	[7]
E16	$e+ N_2(A3s) => e+N_2$	Cross Section	[7]
E17	$e+ N_2=> e+N_2(A3s)$	Cross Section	[7]
E18	$e+ N_2=> e+N_2(B3p)$	Cross Section	[7]
E19	$e+ N_2(B3p) => e+N_2$	Cross Section	[7]
E20	$e+ N_2=> e+N_2$	Cross Section	[7]
E21	$e+ N_2=> e+N_2(A3s)$	Cross Section	[7]
E22	$e+ N_2=> e+N_2$	Cross Section	[7]
E23	$e+ N_2=> e+N_2(a1s)$	Cross Section	[7]
E24	$e+ N_2(a1s) => e+N_2$	Cross Section	[7]

E25	e+ N_2=> e+0.88N_2+0.12N+0.12N	Cross Section	[7]
E26	e+ N_2=> e+N_2	Cross Section	[7]
E27	e+ N_2=> e+N_2(C3p)	Cross Section	[7]
E28	e+ N_2(C3p) => e+N_2	Cross Section	[7]
E29	e+ N_2=> e+N_2	Cross Section	[7]
E30	e+ N_2=> e+N_2	Cross Section	[7]
E31	e+ N_2=> e+0.7N+0.7N(d)+0.3N_2	Cross Section	[7]
E32	e+ N_2=> e+e+N_2^+	Cross Section	[7]
E33	e+ N_2=> e+ e+ N+N^+	Cross Section	[7]
E34	e+ N_2(A3s) => e+e+N_2^+	Cross Section	[8]
E35	e+ N_2(B3p) => e+e+N_2^+	Cross Section	[8]
E36	e+ N_2(C3p) => e+e+N_2^+	Cross Section	[8]
E37	e+ N_2(a1s) => e+e+N_2^+	Cross Section	[8]
E38	e+ N=> e+N	Cross Section	[7]
E39	e+ N=> e+N(d)	Cross Section	[7]
E40	e+ N(d)=> e+N	Cross Section	[7]
E41	e+ N=> e+N(p)	Cross Section	[7]
E42	e+ N(p)=> e+N	Cross Section	[7]
E43	e+ N=> e+e+N^+	Cross Section	[7]
E44	e+ N(d)=> e+N(p)	Cross Section	[7]
E45	e+N(p)=>e+N(d)	Cross Section	[7]
E46	e+ N(d)=> e+e+N^+	Cross Section	[7]
E47	e+ N(p)=> e+e+N^+	Cross Section	[7]

Nitrogen Reactions

N1	N_2(A3s) + N_2(a1s) => e+N_4^+	5e-17	[5]
N2	N_2(a1s) + N_2(a1s) => e+N_4^+	2e-16	[5]
N3	N_2(a1s) + N(p) => e+N_3^+	1e-17	[5]
N4	N(d)+ N(p) => e+N_2^+	1.92e-21*(T^0.98)/(1-exp(-3129/T))	[9]
N5	N(p)+ N(p) => e+N_2^+	3e-21*(T^0.98)/(1-exp(-3129/T))	[10]
N6	N^++ N_2+ N_2=> N_3^++N_2	1.7e-41*(300/T) ^2.1	[6]
N7	N^++N+N_2=>N_2^++N_2	1e-41*(300/T)	[6]
N8	N_2^++N_2+N_2=>N_4^++N_2	5.2e-41*(300/T)^2.2	[6]
N9	N_2^++N+N_2=>N_3^++N_2	1.7e-41*(300/T)^2.1	[6]
N10	N_4^++N_2=>N_2^++N_2+N_2	2.1e-22*exp(T/121)	[6]
N11	N_4^++N=>N^++N_2+N_2	1e-17	[6]
N12	N_3^++N=>N_2^++N_2	6.6e-17	[6]
N13	N_2^++N=>N^++N_2	7.2e-19*(T/300)	[6]
N14	N^++N=>N_2^+	3.71e-24*(T/300)^0.24*exp(-26.12/T)	[6]
N15	N_2^++N_2(A3s) =>N_3^++N	3e-16	[6]
N16	N+N+N_2=>0.31N_2(A3s) +0.44N_2(B3p) +1.25N_2	8.26e-46*exp(490/T)	[5]
N17	N_2(A3s) +N_2(A3s) =>N_2(C3p) +N_2	1.5e-16	[5]
N18	N_2(A3s) +N_2(A3s) =>N_2(B3p) +N_2	7.7e-17	[5]

N19	$N_2(A3s) + N_2 => N_2 + N_2$	2e-24	[5]
N20	$N_2(B3p) + N_2 => 0.95N_2(A3s) + 1.05N_2$	3e-17	[5]
N21	$N_2(C3p) + N_2 => N_2(B3p) + N_2$	1.15e-17	[5]
N22	$N_2(C3p) + N_2 => N_2(a1s) + N_2$	1e-17	[11]
N23	$N_2(a1s) + N_2 => N_2(B3p) + N_2$	1.9e-19	[5]
N24	$N_2(A3s) + N => N_2 + N(p)$	4e-17*(300/T)^0.66	[5]
N25	$N(p) + N_2 => N + N_2$	3e-22	[10]
N26	$N(p) + N => N(d) + N$	1.8e-18	[9]
N27	$N(d) + N_2 => N + N_2$	1e-19*exp(-510/T)	[10]
N28	$N + N + N => 0.31N_2(A3s) + 0.44N_2(B3p) + 0.25N_2 + N$	3.35e-43*T^-0.5	[5]
N29	$N(p) + N + N_2 => 0.31N_2(A3s) + 0.44N_2(B3p) + 0.25N_2$	8.26e-46*exp(490/T)	[5]
N30	$Nd + N + N_2 => 0.31N_2(A3s) + 0.44N_2(B3p) + 0.25N_2$	8.26e-46*exp(490/T)	[5]
N31	$N_4^+ + N => N_3^+ + N_2$	1e-15	[6]
N32	$N(p) + N_2 => N(d) + N_2$	1.8e-24	[10]

Table IV.3. Reaction set for Oxygen with their Rate Coefficients.

No	Reaction	Rate Coefficient (m^6/s), (m^3/s)	Ref
	Electron Impact Reactions with Oxygen		
E1	$e + O_2 => e + O_2$	Cross Section	[12]
E2	$e + O_2 => O + O^-$	Cross Section	[12]
E3	$e + O_2 => e + O_2$	Cross Section	[12]
E4	$e + O_2 => e + O_2$	Cross Section	[12]
E5	$e + O_2 => e + O_2$	Cross Section	[12]
E6	$e + O_2 => e + O_2$	Cross Section	[12]
E7	$e + O_2 => e + O_2$	Cross Section	[12]
E8	$e + O_2 => e + O_2$	Cross Section	[12]
E9	$e + O_2 => e + O_2$	Cross Section	[12]
E10	$e + O_2 => e + O_2(a1d)$	Cross Section	[12]
E11	$e + O_2(a1d) => e + O_2$	Cross Section	[12]
E12	$e + O_2 => e + O_2(b1s)$	Cross Section	[12]
E13	$e + O_2(b1s) => e + O_2$	Cross Section	[12]
E14	$e + O_2 => e + O_2(45)$	Cross Section	[12]
E15	$e + O_2(45) => e + O_2$	Cross Section	[12]
E16	$e + O_2 => e + O + O$	Cross Section	[12]
E17	$e + O_2 => e + O + O(1d)$	Cross Section	[12]
E18	$e + O_2 => e + O + O(1s)$	Cross Section	[12]
E19	$e + O_2 => e + e + O_2^+$	Cross Section	[12]
E20	$e + O_2 => e + e + O + O^+$	Cross Section	[12]
E21	$e + O_2(a1d) => e + O + O$	Cross Section	[12]
E22	$e + O_2(a1d) => 2e + O_2^+$	Cross Section	[12]
E23	$e + O_2(b1s) => e + O + O$	Cross Section	[12]

E24	$e+O_2(b1s) => 2e+O_2^+$	Cross Section	[12]
E25	$e+O_2(45) => e+O+O$	Cross Section	[12]
E26	$e+O_2(45) => 2e+O_2^+$	Cross Section	[12]
E27	e+O=>e+ O(1d)	Cross Section	[12]
E28	e+O(1d) =>e+O	Cross Section	[12]
E29	e+O=>e+O(1s)	Cross Section	[12]
E30	e+O(1s) =>e+O	Cross Section	[12]
E31	$e+O=>2e+O^+$	Cross Section	[12]
E32	e+O(1d) =>e+O1s	Cross Section	[12]
E33	$e+O(1d) => 2e+O^+$	Cross Section	[12]
E34	$e+O(1s) => 2e+O^+$	Cross Section	[12]
E35	$e+O_3=>e+O_3$	Cross Section	[12]
E36	$e+O_3=>O_2^-+O$	Cross Section	[12]
E37	$e+O_3=>O^-+O_2$	Cross Section	[12]
E38	$e+O_3=>2e+O_3^+$	Cross Section	[12]
E39	$e+O^-=>2e+O$	Cross Section	[12]
E40	$e+O_2=>e+O_2$	Cross Section	[12]
E41	$e+O_2=>O+O^-$	Cross Section	[12]
E42	$e+O_2=>e+O_2$	Cross Section	[12]

Oxygen Reactions

O1	$O^-+O=>O_2+e$	1.9e-16	[13]
O2	$O^-+O_2=>O_3+e$	5e-21	[13]
O3	$O^-+O_3=>O_3^-+O$	8e-16	[13]
O4	$O_2^-+O=>O_3+e$	1.5e-16	[13]
O5	$O_2^-+O=>O^-+O_2$	1.5e-16	[13]
O6	$O_2^-+O_2=>O_2+O_2+e$	2.7e-16*(T/300)^0.5*exp(-5590/T)	[13]
O7	$O_2^-+O_3=>O_3^-+O_2$	3.5e-16	[13]
O8	$O_3^-+O=>O_2+O_2+e$	1e-16	[13]
O9	$O_3^-+O=>O_2^-+O_2$	2.5e-16	[13]
O10	$O_3^-+O_3=>O_2+O_2+O_2+e$	1e-16	[13]
O11	$O_2^-+O_2+O_2=>O_4^-+O_2$	3.5e-42*(300/T)	[13]
O12	$O_4^-+O_2=>O_2^-+O_2+O_2$	1e-16*exp(-1044/T)	[13]
O13	$O_4^-+O=>O_3^-+O_2$	4e-16	[13]
O14	$O_4^-+O=>O^-+O_2+O_2$	3e-16	[13]
O15	$O^-+O_2+O_2=>O_3^-+O_2$	1.1e-42*(300/T)	[13]
O16	$O^++O_2=>O_2^++O$	2e-17*(300/T)^0.5	[13]
O17	$O^++O_3=>O_2^++O_2$	1e-16	[13]
O18	$O_2^++O_2+O_2=>O_4^++O_2$	2.4e-42*(300/T)^3.2	[13]
O19	$O_4^++O=>O_2^++O_3$	3e-16	[13]
O20	$O_4^++O_2=>O_2^++O_2+O_2$	3.3e-12*((300/T)4)*exp(-5030/T)	[13]
O21	$O^++O+O_2=>O_2^++O_2$	1e-41	[13]

O22	$O_4^+ + O_2(a1d) \Rightarrow O_2^+ + O_2 + O_2$	1e-16	[13]
O23	$O_4^+ + O_2(b1s) \Rightarrow O_2^+ + O_2 + O_2$	1e-16	[13]
O24	$O_4^- + O_2(a1d) \Rightarrow O_2^- + O_2 + O_2$	1e-16	[13]
O25	$O_4^- + O_2(b1s) \Rightarrow O_2^- + O_2 + O_2$	1e-16	[13]
O26	$O_2^- + O_2(a1d) \Rightarrow O_2 + O_2 + e$	7e-16	[13]
O27	$O^- + O_2(a1d) \Rightarrow O_3 + e$	6.1e-17	[13]
O28	$O^- + O_2(a1d) \Rightarrow O_2^- + O$	7.3e-16*exp(-890/T)	[13]
O29	$O_2^- + O_2(b1s) \Rightarrow O_2 + O_2 + e$	3.6e-16	[13]
O30	$O + O_3 \Rightarrow O_2 + O_2$	1.43e-20*(T/300)^4.13	[13]
O31	$O + O + O_2 \Rightarrow O_2 + O_2$	1.56e-45*(T/300)^-3	[13]
O32	$O + O_2 + O_2 \Rightarrow O_3 + O_2$	6e-46*(T/300)^-1.7	[13]
O33	$O_2(a1d) + O_3 \Rightarrow O_2 + O_2 + O$	3.5e-21*(T/300)^5.8	[13]
O34	$O_2(a1d) + O_2 \Rightarrow O_2 + O_2$	2.2e-24*(T/300)^0.8	[13]
O35	$O_2(a1d) + O \Rightarrow O_2 + O$	7e-22	[13]
O36	$O_2(b1s) + O_3 \Rightarrow O_2 + O_2 + O$	1.5e-17	[13]
O37	$O_2(b1s) + O_3 \Rightarrow O_2(a1d) + O_3$	3.3e-18	[13]
O38	$O_2(b1s) + O_2 \Rightarrow O_2(a1d) + O_2$	4.3e-28*T2.4*exp(-241/T)	[13]
O39	$O_2(b1s) + O \Rightarrow O_2(a1d) + O$	8.1e-20	[13]
O40	$O_2(b1s) + O \Rightarrow O_2 + O(1d)$	8.1e-20	[13]
O41	$O_2(45) + O_2 \Rightarrow O_2(b1s) + O_2(b1s)$	2.9e-19	[13]
O42	$O_2(45) + O \Rightarrow O_2(b1s) + O(1d)$	9e-18	[13]
O43	$O(1d) + O_2 \Rightarrow O_2(a1d) + O$	0.25*6.4e-18*exp(67/T)	[14]
O44	$O(1d) + O_2 \Rightarrow O_2(b1s) + O$	2.56e-17*exp(67/T)	[14]
O45	$O(1d) + O_2 \Rightarrow O_2 + O$	0.75*6.4e-18*exp(67/T)	[14]
O46	$O(1d) + O_3 \Rightarrow O_2 + O + O$	1.2e-16	[14]
O47	$O(1d) + O_3 \Rightarrow O_2 + O_2$	1.2e-16	[14]
O48	$O(1s) + O_2 \Rightarrow O + O_2(45)$	0.69*4.3e-18*exp(-850/T)	[14]
O49	$O(1s) + O_2 \Rightarrow O(1d) + O_2$	0.31*4.3e-18*exp(-850/T)	[14]
O50	$O(1s) + O_3 \Rightarrow O(1d) + O + O_2$	0.5*4.3e-16	[14]
O51	$O(1s) + O_3 \Rightarrow O_2 + O_2$	0.5*4.3e-16	[14]
O52	$O(1s) + O_2(a1d) \Rightarrow O_2(b1s) + O(1d)$	2.9e-17	[14]
O53	$O(1s) + O_2(a1d) \Rightarrow O_2(45) + O$	1.1e-16	[14]
O54	$O(1s) + O_2(a1d) \Rightarrow O + O + O$	3.2e-17	[14]
O55	$O(1s) + O \Rightarrow O(1d) + O$	5e-17*exp(-300/T)	[14]
O56	$O^- + O^+ \Rightarrow O + O$	7.51e-14*(300/T)^0.5	[13]
O57	$O^- + O_2^+ \Rightarrow O + O + O$	7.51e-14*(300/T)^0.5	[13]
O58	$O^- + O_4^+ \Rightarrow O + O_2 + O_2$	7.51e-14*(300/T)^0.5	[13]
O59	$O_2^- + O^+ \Rightarrow O_2 + O$	7.51e-14*(300/T)^0.5	[13]
O60	$O_2^- + O_2^+ \Rightarrow O_2 + O + O$	7.51e-14*(300/T)^0.5	[13]
O61	$O_2^- + O_4^+ \Rightarrow O_2 + O_2 + O_2$	7.51e-14*(300/T)^0.5	[13]
O62	$O_3^- + O^+ \Rightarrow O_3 + O$	7.51e-14*(300/T)^0.5	[13]
O63	$O_3^- + O_2^+ \Rightarrow O_3 + O + O$	7.51e-14*(300/T)^0.5	[13]

O64	$O_3^-+O_4^+=>O_3+O_2+O_2$	7.51e-14*(300/T)^0.5	[13]
O65	$O_4^-+O^+=>O_2+O_2+O$	7.51e-14*(300/T)^0.5	[13]
O66	$O_4^-+O_2^+=>O_2+O_2+O_2$	7.51e-14*(300/T)^0.5	[13]
O67	$O_4^-+O_4^+=>O_2+O_2+O_2+O_2$	7.51e-14*(300/T)^0.5	[13]
O68	$O_2^-+O_2^++O_2=>O_2+O_2+O_2$	2e-37*(300/T)^2.5	[13]
O69	$O_2^-+O^++O_2=>O_2+O+O_2$	2e-37*(300/T)^2.5	[13]
O70	$O^-+O^++O_2=>O+O+O_2$	2e-37*(300/T)^2.5	[13]
O71	$O_2^-+O^++O_2=>O_3+O_2$	2e-37*(300/T)^2.5	[13]
O72	$O^-+O_2^++O_2=>O_3+O_2$	2e-37*(300/T)^2.5	[13]
O73	$O^-+O^++O_2=>O_2+O_2$	2e-37*(300/T)^2.5	[13]
O74	$O_3+O_2=>O_2+O+O_2$	7.3e-16*exp(-11400/T)	[13]
O75	$O_2(b1s) =>O_2(a1s)$	1.5E-3	[15]
O76	$O_2(b1s) =>O_2$	8.5E-2	[15]
O77	$O_2(a1s) =>O_2$	2.6E-4	[15]
O78	$O_2(45) =>O_2$	11	[15]

Table IV.4. Reactions Nitrogen-Oxygen with rate coefficient

No	Reaction	Rate Coefficient (m^6/s), (m^3/s)	Ref
	Electron Impact Reactions with NO		
E1	$e+ NO =>NO^-$	Cross Section	[3]
E2	$e+NO=>e+NO$	Cross Section	[3]
E3	$e+NO=>e+NO$	Cross Section	[3]
E4	$e+NO=>e+NO$	Cross Section	[3]
E5	$e+NO=>e+NO$	Cross Section	[3]
E6	$e+NO=>e+NO$	Cross Section	[3]
E7	$e+NO=>e+NO$	Cross Section	[3]
E8	$e+NO=>e+NO$	Cross Section	[3]
E9	$e+NO=>e+e+NO^+$	Cross Section	[3]
	Nitrogen-Oxygen Reactions		
R1	$N^++O^-=>N+O$	2.6e-13	[16]
R2	$N^++O_2^-=>N+O_2$	4e-13	[16]
R3	$N_2^++O^-=>N_2+O$	4e-13	[16]
R4	$N_2^++O_2^-=>N_2+O_2$	1.6e-13	[16]
R5	$N_2+O_2^- =>O_2+N_2+e$	1.9e-18*exp(-4990/T)	[16]
R6	$N^++O=>O^++N$	1e-18	[16]
R7	$N^++O_2=>N+O_2^+$	3e-16	[16]
R8	$N_2^++N=>N^++N_2$	1e-17	[16]
R9	$N_2+O^+ =>N_2^++O$	4.9e-15	[16]
R10	$N_2+O+O =>O_2+N_2$	2.76e-46*exp(720/T)	[16]

R11	$N_2^+ + O \Rightarrow O^+ + N_2$	6e-18	[16]
R12	$N_2^+ + O_2 \Rightarrow O_2^+ + N_2$	4.7e-18	[16]
R13	$N_2^+ + O_3 \Rightarrow O_2^+ + O + N_2$	1e-16	[16]
R14	$N_2 + O + O_2 \Rightarrow O_3 + N_2$	6.2e-46	[16]
R15	$N + O^- \Rightarrow NO + e$	2.6e-16	[16]
R16	$NO + O^- \Rightarrow NO_2 + e$	2.6e-16	[16]
R17	$N + O_2^- \Rightarrow NO_2 + e$	5e-16	[16]
R18	$N^+ + O_2 \Rightarrow NO^+ + O$	2.6e-16	[16]
R19	$N^+ + O_3 \Rightarrow NO^+ + O_2$	5e-16	[16]
R20	$N^+ + NO \Rightarrow NO^+ + N$	5.1e-16	[16]
R21	$N^+ + NO \Rightarrow N_2^+ + O$	5e-17	[16]
R22	$N^+ + NO_2 \Rightarrow NO + NO$	5e-16	[16]
R23	$NO^+ + O^- \Rightarrow NO + O$	4.9e-13	[16]
R24	$NO^+ + O_2^- \Rightarrow NO + O_2$	4e-13	[16]
R25	$N_2^+ + O \Rightarrow NO^+ + N$	1.4e-35	[16]
R26	$N_2^+ + O_2 \Rightarrow NO^+ + NO$	1e-23	[16]
R27	$N_2 + O^+ \Rightarrow NO^+ + N$	1.2e-18	[16]
R28	$NO + O^+ \Rightarrow NO^+ + O$	1e-18	[16]
R29	$NO_2 + O^+ \Rightarrow NO^+ + O_2$	5e-16	[16]
R30	$N + O_2^+ \Rightarrow NO^+ + O$	1.8e-16	[16]
R31	$N_2 + O_2^+ \Rightarrow NO^+ + NO$	1e-22	[16]
R32	$NO + O_2^+ \Rightarrow NO^+ + O_2$	3.5e-16	[16]
R33	$NO + O + O_2 \Rightarrow NO_2 + O_2$	8.6e-44	[16]
R34	$NO + O + N_2 \Rightarrow NO_2 + N_2$	1e-43	[16]
R35	$NO_2 + O \Rightarrow NO + O_2$	1.3e-17*(T/1000)^0.18	[16]
R36	$N + NO_2 \Rightarrow N_2 + O + O$	9.1e-19	[16]
R37	$N + NO_2 \Rightarrow 2NO$	6e-19	[16]
R38	$NO_2 + N \Rightarrow N_2 + O_2$	7e-19	[16]
R39	$NO + NO + O_2 \Rightarrow 2NO_2$	1.4e-50	[16]
R40	$NO + O_3 \Rightarrow NO_2 + O_2$	4.6e-20	[16]
R41	$N^+ + NO_2 \Rightarrow NO_2^+ + N$	3e-16	[16]
R42	$NO_2 + O_2^+ \Rightarrow NO_2^+ + O_2$	6e-16	[16]
R43	$NO^+ + O_3 \Rightarrow NO_2^+ + O_2$	1e-20	[16]
R44	$NO_2^+ + NO \Rightarrow NO^+ + NO_2$	2.9e-16	[16]
R45	$N + NO_2 \Rightarrow N_2O + O$	3e-18	[16]
R46	$NO_2 + O_3 \Rightarrow NO_3 + O_2$	1.7e-22	[16]
R47	$NO_2^+ + O^- \Rightarrow NO + O_2$	4e-13	[16]
R48	$NO_2^+ + O_2^- \Rightarrow NO_2 + O_2$	4e-13	[16]
R49	$NO_3 + O \Rightarrow NO_2 + O_2$	1e-17	[16]

R50	$NO+NO_3=>2NO_2$	2e-17	[16]
R51	$NO+NO_3=>2NO+O_2$	2.71e-17*(T)^-0.23 *exp(-947/T)	[16]
R52	$NO_2+NO_3<=>N_2O_5$	1.1e-18	[16]
R53	$NO_3+NO_3=>2NO_2+O_2$	1.2e-21	[16]
R54	$NO^++N_2O_5=>NO_2^++2NO_2$	5.9e-16	[16]
R55	$N_2O_5+O_2^+ =>NO_2^++NO_3+O_2$	8.8e-16	[16]
R56	$N_2O_5+N_2=>NO_2+NO_3+N_2$	1.6e-25	[16]
R57	$N_2O_5+O_2=>NO_2+NO_3+O_2$	1.6e-25	[16]
R58	$e+NO^+=>N+O$	4e-13*(300/Te)^1.5	[16]
R59	$e+NO^+=>N(d)+O$	2e-13*(Te)^-0.5	[17]
R60	$e+NO^+=>N+O(1d)$	2e-13*(Te)^-0.5	[17]
R61	$e+NO_2^+=>NO+O$	2e-13*(Te)^-0.5	[17]
R62	$e+NO_2^+=>NO+O(1d)$	2e-13*(Te)^-0.5	[17]
R63	$N+O^- =>NO+e$	0.26e-15	[17]
R64	$NO+O^- =>NO_2+e$	0.26e-15	[17]
R65	$N_2+O^- =>N_2O+e$	5e-19	[17]
R66	$e+NO=>e+N+O$	6.4e-16	[17]
R67	$N_2(A3s)+O_2=>O+O+N_2$	1.5e-18	[18]
R68	$N_2(A3s)+NO_2=>NO+O+N_2$	1e-18	[18]
R69	$N_2(A3s)+N_2O=>2N_2+O$	0.8e-16	[18]
R70	$N_2(A3s)+O_2=>N_2O+O(1d)$	0.3e-19	[18]
R71	$N_2(A3s)+O_2=>N_2O+O$	2e-20*(T/300)^0.55	[18]
R72	$N_2(A3s)+O=>NO+N(d)$	7e-18	[18]
R73	$N(d)+NO_2=>NO+NO$	1e-18	[18]
R74	$N(d)+O_2=>NO+O$	5.2e-18	[18]
R75	$N(d)+NO=>N_2+O$	1.8e-16	[18]
R76	$NO+O(1d) =>O_2+N$	1.7e-16	[18]
R77	$NO_2+O(1d) =>O_2+NO$	2.5e-16	[18]
R78	$N_2O+O(1d) =>2NO$	7.2e-17	[18]
R79	$NO_2+O(1d) =>NO+O_2$	0.49e-16	[18]
R80	$N_2O+ O(1d) =>N_2+O_2$	4.4e-17	[18]
R81	$N+O_3=>NO+O_2$	5e-22	[18]
R82	$N+NO=>N_2+O$	1.8e-17*(T/300)^0.5	[18]
R83	$N+O+N_2=>NO+N_2$	1e-44*(300/T)^0.5	[18]
R84	$N+O+O_2=>NO+O_2$	1e-44*(300/T)^0.5	[18]
R85	$NO_2+O+O_2=>NO_3+O_2$	8.9e-44*(T/300)^-2	[18]
R86	$NO_2+O+N_2=>NO_3+N_2$	8.9e-44*(T/300)^-2	[18]
R87	$N+NO_2=>N_2+O+O$	0.9e-18	[18]
R88	$N+NO_2=>N_2O+O$	3e-18	[18]

R89	$N+O+O \Rightarrow O_2+N$	3.2e-45*(300/T)^0.41	[18]
R90	$N+O \Rightarrow NO^++e$	2.33e-24*(T)^1.5*exp(-319000/T)	[18]
R91	$NO+O \Rightarrow O_2+N$	7.5e-18*(T/300)^-0.5	[18]
R92	$N+O_2 \Rightarrow NO+O$	3.2e-18*(T/300)*exp(-3150/T)	[18]
R93	$NO+O_3 \Rightarrow NO_2+O_2$	2.5e-19*exp(-765/T)	[18]
R94	$NO+O_3 \Rightarrow NO_3+O$	1.2e-19*exp(-2450/T)	[18]
R95	$N_2+O+O \Rightarrow N_2+O_2$	2.76e-46*exp(720/T)	[18]
R96	$NO+NO_3 \Rightarrow 2NO+O_2$	6.2e-11*(300/T)*exp(-25000/T)	[18]
R97	$N_2+O \Rightarrow NO+N$	3e-16*exp(-38370/T)	[18]
R98	$NO+N_2 \Rightarrow N+O+N_2$	8.7e-15*exp(-75994/T)	[18]
R99	$NO+O \Rightarrow N+O+O$	17.4e-14*exp(-75994/T)	[18]
R100	$NO+NO \Rightarrow N+O+NO$	17.4e-14*exp(-75994/T)	[18]
R101	$NO_2+O_2 \Rightarrow NO+O_3$	2.8e-18*exp(-25400/T)	[18]
R102	$NO_3+O_2 \Rightarrow NO_2+O_3$	1.5e-18*exp(-15020/T)	[18]
R103	$NO+O^+ \Rightarrow O_2^++N$	3e-16	[18]
R104	$NO_2+O^+ \Rightarrow NO_2^++O$	1.6e-15	[18]
R105	$N_2^++NO \Rightarrow NO^++N_2$	3.3e-16	[18]
R106	$N_2^++NO_2 \Rightarrow NO_2^++N_2$	3.3e-16	[18]
R107	$N_2^++NO_2 \Rightarrow NO^++N_2O$	5e-17	[18]
R108	$N_2^++N_2O \Rightarrow NO^++N+N_2$	4e-16	[18]
R109	$N_2+O_2^+ \Rightarrow NO^++NO$	1e-23	[18]
R110	$N+O_2^+ \Rightarrow NO^++O$	1.2e-16	[18]
R111	$N_2O+O^+ \Rightarrow NO^++NO$	2.3e-16	[18]
R112	$N_2^++O_2^- \Rightarrow N_2+O_2$	2e-12*(T/300)^-0.5	[18]
R113	$NO^++O_2^- \Rightarrow NO+O_2$	2e-12*(T/300)^-0.5	[18]
R114	$NO_2^++O_2^- \Rightarrow NO_2+O_2$	2e-12*(T/300)^-0.5	[18]
R115	$NO^++O^- \Rightarrow NO+O$	3e-12*(T/300)^-0.5	[18]
R116	$NO_2^++O^- \Rightarrow NO_2+O$	3e-12*(T/300)^-0.5	[18]
R117	$N_2^++O^- \Rightarrow N_2+O$	3e-12*(T/300)^-0.5	[18]
R118	$N+O_2 \Rightarrow NO+O$	8.9e-23	[19]
R119	$N(d)+O_2 \Rightarrow NO+O(1d)$	6e-18*exp(T/300)^0.5	[19]
R120	$NO+O_2(a1d) \Rightarrow NO+O_2$	2.5e-17	[16]
R121	$N+O_2(a1d) \Rightarrow NO+O$	2e-20*exp(-600/T)	[16]
R122	$N_2(A3s) + O_2 \Rightarrow N_2+O+O$	2.54e-18	[16]
R123	$N_2(A3s) +O_2 \Rightarrow N_2O+O$	7.8e-20	[16]
R124	$N_2(A3s) +O_2^- \Rightarrow N_2+O_2+e$	2e-15	[16]
R125	$N_2(B3p) +O_2^- \Rightarrow N_2+O_2+e$	2.5e-16	[16]
R126	$N_2(B3p) +O^- \Rightarrow N_2+O+e$	1.9e-15	[16]
R127	$N_2(A3s) +O^- \Rightarrow N_2+O+e$	2.2e-15	[16]

R128	$NO+N_2(B3p) \Rightarrow NO+N_2(A3s)$	2.4e-16	[16]
R129	$N_2+O_2(b1s) \Rightarrow N_2+O_2(a1d)$	4.9e-21*exp(-253/T)	[16]
R130	$NO+O_2(b1s) \Rightarrow NO+O_2(a1d)$	4e-19	[16]
R131	$N(p)+NO \Rightarrow N_2(A3s) +O$	3.4e-17	[16]
R132	$N^+ + O_2 \Rightarrow NO^+ + O$	2.5e-17	[16]
R133	$N(d)+O^+ \Rightarrow N^+ + O$	1.3e-16	[18]
R134	$NO_2^+ + e \Rightarrow NO + O$	2e-13*(300/T)^0.5	[17]
R135	$N_2O^+ + e \Rightarrow N_2 + O$	2e-13*(300/T)^0.5	[17]
R136	$NO_2 + e \Rightarrow NO + O^-$	1e-17	[17]
R137	$N_2(A3s) + N_2O \Rightarrow N_2 + N + NO$	1e-17	[16]
R138	$N_2O + O(1d) \Rightarrow NO + NO$	7.2e-17	[17]
R139	$N^+ + NO \Rightarrow O^+ + N_2$	1e-18	[17]
R140	$N^+ + N_2O \Rightarrow NO^+ + N_2$	5.5e-16	[17]
R141	$N_2O + O^+ \Rightarrow N_2O^+ + O$	4e-15	[13]
R142	$N_2O + O^+ \Rightarrow O_2^+ + N_2$	2e-17	[13]
R143	$N_2^+ + N_2O \Rightarrow N_2O^+ + N_2$	5e-16	[13]
R144	$N + O_2^+ \Rightarrow NO^+ + O$	1.2e-16	[13]
R145	$NO + O_2^+ \Rightarrow NO^+ + O_2$	4.4e-16	[13]
R146	$NO_2 + O_2^+ \Rightarrow NO^+ + O_3$	1e-17	[13]
R147	$NO_2 + O_2^+ \Rightarrow NO_2^+ + O_2$	6.6e-16	[13]
R148	$N_3^+ + O_2 \Rightarrow O_2^+ + N + N_2$	2.3e-17	[13]
R149	$N_3^+ + O_2 \Rightarrow NO_2^+ + N_2$	4.4e-17	[13]
R150	$N_3^+ + NO \Rightarrow NO^+ + N_2 + N$	7e-17	[13]
R151	$N_3^+ + NO \Rightarrow N_2O^+ + N_2$	7e-17	[13]
R152	$N_2O^+ + NO \Rightarrow NO^+ + N_2O$	2.9e-16	[13]
R153	$N_4^+ + O_2 \Rightarrow O_2^+ + N_2 + N_2$	2.5e-16	[13]
R154	$NO + O_4^+ \Rightarrow NO^+ + O_2 + O_2$	1e-16	[17]
R155	$NO_2 + O_2^- \Rightarrow NO_2^- + O_2$	8e-16	[13]
R156	$NO_2 + O^- \Rightarrow NO_2^- + O$	1.2e-13	[13]
R157	$N_2O + O^- \Rightarrow NO^- + NO$	2e-16	[13]
R158	$NO_2 + O_3^- \Rightarrow O_3 + NO_2^-$	7e-16	[13]
R159	$NO^- + O_2 \Rightarrow O_2^- + NO$	5e-16	[17]
R160	$NO_3 + O_2^- \Rightarrow O_2 + NO_3^-$	5e-16	[18]
R161	$N_2O + O_2^- \Rightarrow O_3^- + N_2$	5e-16	[18]
R162	$NO_2 + O^- \Rightarrow NO^- + NO$	1.2e-15	[18]
R163	$N_2O + O^- \Rightarrow N_2O^- + O$	2e-18	[18]
R164	$NO + O_3^- \Rightarrow NO_3^- + O$	1e-17	[18]
R165	$NO + O_3^- \Rightarrow NO_2^- + O_2$	2.6e-18	[18]
R166	$NO_2 + O_3^- \Rightarrow NO_2^- + O_3$	7e-16	[18]

R167	$NO_2+O_3^-=>NO_3^-+O_2$	2e-17	[18]
R168	$NO_3+O_3^-=>NO_3^-+O_3$	5e-16	[18]
R169	$NO^-+O_2=>O_2^-+NO$	5e-16	[13]
R170	$NO^-+NO_2=>NO_2^-+NO$	7.4e-22	[13]
R171	$NO^-+N_2O=>NO_2^-+N_2$	2.8e-20	[13]
R172	$NO_2^-+O_3=>NO_3^-+O_2$	1.8e-17	[13]
R173	$NO_2^-+NO_2=>NO_3^-+NO$	4e-18	[13]
R174	$NO_2^-+NO_3=>NO_3^-+NO_2$	5e-16	[13]
R175	$NO_2^-+N_2O_5=>NO_3^-+NO_3+NO$	7e-16	[13]
R176	$NO_3^-+NO=>NO_2^-+NO_2$	3e-21	[13]
R177	$NO+ O_4^- =>NO_3^-+O_2$	2.5e-16	[13]
R178	$N + O_2(a1d) =>NO+O$	1e-22	[18]
R179	$N_2+O(1d) =>O+N_2$	2.6e-17	[18]
R180	$N_2(A3s) +O=>NO+N$	7e-20	[16]
R181	$N_2(a1s) +O_2=>N_2+O+O$	2.8e-17	[16]
R182	$N_2(a1s) +NO=>N_2+N+O$	3.6e-16	[16]
R183	$N_2(A3s) +N_2(a1s) =>N_4^++e$	5e-17	[16]
R184	$N_2(a1s) +N_2(a1s) =>N_4^++e$	2e-16	[16]
R185	$N_2+O_2(a1d) =>O_2+N_2$	1.7e-16	[16]
R186	$N_2(A3s) +N_2=>2N_2$	2.7e-17	[16]
R187	$N_2(A3s) +NO_2=>NO+O+N_2$	1e-18	[16]
R188	$N_2(A3s) +N_2O=>2N_2+O$	8e-17	[16]
R189	$N_2(A3s) +N_2O=>N_2+N+NO$	8e-17	[16]

Table IV.5. Reaction set for Argon with Rate Coefficient

No	Reaction	$\Delta\varepsilon$ (eV)	Rate coefficient (m^6/s), (m^3/s)	Ref
	Electron Impact Reactions with Argon			
E1	$e+Ar=>e+Ar$	0	Cross section	[20]
E2	$e+Ar=>e+Ar(s)$	11.50	Cross section	[20]
E3	$e+Ar(s)=>e+Ar$	-11.50	Cross section	[20]
E4	$e+Ar=>2e+Ar^+$	15.80	Cross section	[20]
E5	$e+Ar(s)=>2e+Ar^+$	4.427	Cross section	[20]
	Argon Reactions			
A1	$Ar(s)+Ar=>Ar+Ar$		1807	[19]
A2	$Ar^++Ar+Ar =>Ar_2^++Ar$		2.5e-43*(300/T)^1.5	[19]
A3	$Ar(s)+Ar(s)=>e+Ar+Ar^+$		3.3734e8	[19]
A4	$e+Ar_2^+=>Ar+Ar$		7.34e-14*Te^-0.67*(T/300)^ -0.58	[19]

Table IV.6. Reaction set for Argon & Oxygen& Nitrogen with Rate Coefficient

No	Reaction	Rate Coefficient (m^6/s), (m^3/s)	Ref
R1	$Ar^+ + O^- \Rightarrow Ar + O$	7.51e-14*(300/T)^0.5	[21]
R2	$Ar^+ + O_2^- \Rightarrow Ar + O_2$	7.51e-14*(300/T)^0.5	[21]
R3	$Ar^+ + O_3^- \Rightarrow Ar + O_3$	7.51e-14*(300/T)^0.5	[21]
R4	$Ar^+ + O_4^- \Rightarrow Ar + 2O_2$	7.51e-14*(300/T)^0.5	[21]
R5	Ar(s) +Ar => Ar+ Ar	1807	[21]
R6	$Ar(s) + O_2 \Rightarrow Ar + O + O$	0.46*2.2e-16	[21]
R7	$Ar(s) + O_2 \Rightarrow Ar + O + O(1d)$	0.52*2.2e-16	[21]
R8	$Ar(s) + O_2 \Rightarrow Ar + O + O(1s)$	0.02*2.2e-16	[21]
R9	Ar(s) +O =>Ar + O	4.1e-17	[19]
R10	$Ar + O + O_2 \Rightarrow O_3 + Ar$	3.9e-46*(300/T)^1.9	[21]
R11	$Ar + O_2(b1s) \Rightarrow O_2 + Ar$	1.5e-23	[21]
R12	$Ar^+ + Ar + Ar \Rightarrow Ar_2^+ + Ar$	2.5e-43*(300/T)^1.5	[21]
R13	$Ar_2^+ + O^- \Rightarrow 2Ar + O$	7.51e-14*(300/T)^0.5	[21]
R14	$Ar_2^+ + O_2^- \Rightarrow 2Ar + O_2$	7.51e-14*(300/T)^0.5	[21]
R15	$Ar_2^+ + O_3^- \Rightarrow 2Ar + O_3$	7.51e-14*(300/T)^0.5	[21]
R16	$Ar_2^+ + O_4^- \Rightarrow 2Ar + 2O_2$	7.51e-14*(300/T)^0.5	[19]
R17	$Ar(s) + Ar(s) \Rightarrow e + Ar + Ar^+$	3.3734e8	[19]
R18	Ar+O(1d) =>Ar+O	2.0947e-17*exp(-309.4467/T)	[21]
R19	$Ar^+ + O_2 \Rightarrow Ar + O_2^+$	6.3e-17*exp(T/300)^-0.78	[21]
R20	$Ar^+ + O \Rightarrow Ar + O^+$	6.4e-18	[21]
R21	Ar+ O(1s) =>Ar+ O(1d)	5e-23	[21]
R22	$Ar + 2O \Rightarrow Ar + O_2(A)$	9.85e-41	[21]
R23	$Ar + O_2(A) \Rightarrow Ar + O_2$	3e-24*exp(-200/T)	[21]
R24	$Ar + O_2(B) \Rightarrow Ar + O_2(A)$	1e-23	[21]
R25	$Ar + O_4^+ \Rightarrow Ar + O_2^+ + O_2$	3e-23	[21]
R26	$O_2 + Ar_2^+ \Rightarrow 2Ar + O_2^+$	1.2e-16	[21]
R27	$Ar + 2O \Rightarrow Ar + O_2$	4.5e-40*exp(630/T)	[19]
R28	$e + Ar_2^+ \Rightarrow 2Ar$	7.34e-14*(Te)^-0.67*(T/300)^-0.58	[40]
R29	$Ar + O_2(B) \Rightarrow O_2 + Ar$	1e-22	[21]
R30	Ar+O =>O+Ar	3e-19	[21]
R31	$Ar^+ + O_2(A) \Rightarrow Ar + O_2^+$	5e-17	[21]
R32	$Ar^+ + O_2(B) \Rightarrow Ar + O_2^+$	5e-17	[21]
R33	$Ar + O^+ \Rightarrow Ar^+ + O$	2.1e-17	[21]
R34	$Ar + O_2^+ \Rightarrow Ar^+ + O_2$	2.1e-17	[21]
R35	Ar+O(1d) =>Ar+O	5e-18	[21]
R36	$Ar + 2O \Rightarrow Ar + O_2$	2.45e-43*(T)^-0.63	[21]

R37	$Ar+NO+O \Rightarrow Ar+NO_2$	1e-43*(T/300)^-1.6	[19]
R38	$Ar+NO_2+O \Rightarrow Ar+NO_3$	9e-44*(T/300)^2*exp(-0/T)	[19]
R39	$Ar+N_2+N_2^+ \Rightarrow Ar+N_4^+$	1.8e6	[19]

IV.4. Surface Reactions

In addition to the gas-phase chemical reactions described previously, a set of surface-mediated reactions has been incorporated into the model to account for interactions at the reactor walls or electrode surfaces. These interfacial reactions are summarized in Table IV.7 and include processes such as adsorption, desorption, recombination, and heterogeneous oxidation of reactive species. Surface reactions play a significant role in modeling the overall plasma chemistry, particularly for species with high reactivity, such as atomic oxygen and nitrogen radicals. They can act as additional pathways for the removal or generation of certain species, influencing both the concentrations of gas phase radicals and the formation of stable by products. By integrating these surface mechanisms, the model provides a more comprehensive and realistic description of the dielectric barrier discharge under atmospheric-pressure conditions.

Table IV.7. Surface Reactions

Reaction	Formula	Reaction	Formula
01	$N^+ \Rightarrow N$	21	$O(1d) \Rightarrow O$
02	$N_2^+ \Rightarrow N_2$	22	$O(1s) \Rightarrow O$
03	$N_3^+ \Rightarrow N_2+N$	23	$O_2(a1d) \Rightarrow O_2$
04	$N_4^+ \Rightarrow N_2+N_2$	24	$O_2(a1s) \Rightarrow O_2$
05	$N \Rightarrow 0.5N_2$	25	$O_2(b1s) \Rightarrow O_2$
06	$N(d) \Rightarrow N$	26	$O_2(45) \Rightarrow O_2$
07	$N(p) \Rightarrow N$	27	$O^+ \Rightarrow O$
08	$N_2(A) \Rightarrow N_2$	28	$O_2^+ \Rightarrow O_2$
09	$N_2(A3s) \Rightarrow N_2$	29	$O_3^+ \Rightarrow O_2+O$
10	$N_2(B3p) \Rightarrow N_2$	30	$O_4^+ \Rightarrow O_2+O_2$
11	$N_2(C3p) \Rightarrow N_2$	31	$O \Rightarrow 0.5O_2$
12	$N_2(a1s) \Rightarrow N_2$	32	$O^- \Rightarrow O$
13	$NO^+ \Rightarrow NO$	33	$O_2^- \Rightarrow O_2$
14	$NO^- \Rightarrow NO$	34	$O_3^- \Rightarrow O_2+O$
15	$NO_2 \Rightarrow O_2+N$	35	$O_4^- \Rightarrow O_2+O_2$
16	$NO_2^+ \Rightarrow O_2+N$	36	$NO_3^- \Rightarrow N+O_3$
17	$NO_2^- \Rightarrow N+O_2$	37	$N_2O^- \Rightarrow N_2O$
18	$NO_3^+ \Rightarrow O_3+N$	38	$Ar^+ \Rightarrow Ar$
19	$N_2O \Rightarrow O+N_2$	39	$Ar_2^+ \Rightarrow Ar+ Ar$
20	$N_2O^+ \Rightarrow N_2O$	40	$Ar(s) \Rightarrow Ar$

IV.5. Results & Discussion

This section presents the results obtained from the numerical modeling of a dielectric barrier discharge (DBD) reactor operating in air-based gas mixtures composed of 69% N_2, 20% O_2, 1% Ar, and 10% NO at atmospheric pressure, with the primary goal of investigating NO removal. The simulations consider a DBD configuration in which a sinusoidal voltage is applied across two parallel, planar electrodes, each measuring 3cm×3cm. Both electrodes are coated with a dielectric material characterized by a relative permittivity of 9.96 and a thickness of 0.635 mm.

The working gases are introduced into a narrow 1 mm discharge gap, maintained at 1 atm, while the reactor is energized with a peak voltage of 10 kV at a frequency of 3 kHz. The initial NO mole fraction is set to 10%, and the temporal evolution of the plasma and reactive species is tracked throughout the discharge period.

IV.5.1 Temporal Evolution of Electrical Parameters

Figure IV.2 presents the temporal evolution of voltage and current during a representative cycle of the electrical system under investigation over three different periods. The voltage waveform follows sinusoidal profile, with peak amplitudes reaching approximately ±10 kV, consistent with a high-voltage alternating signal. In contrast, the current exhibits a distinctly non-sinusoidal behavior, characterized by sharp transients and irregular oscillations, with peak values exceeding (peak ≈ 0.9 mA).

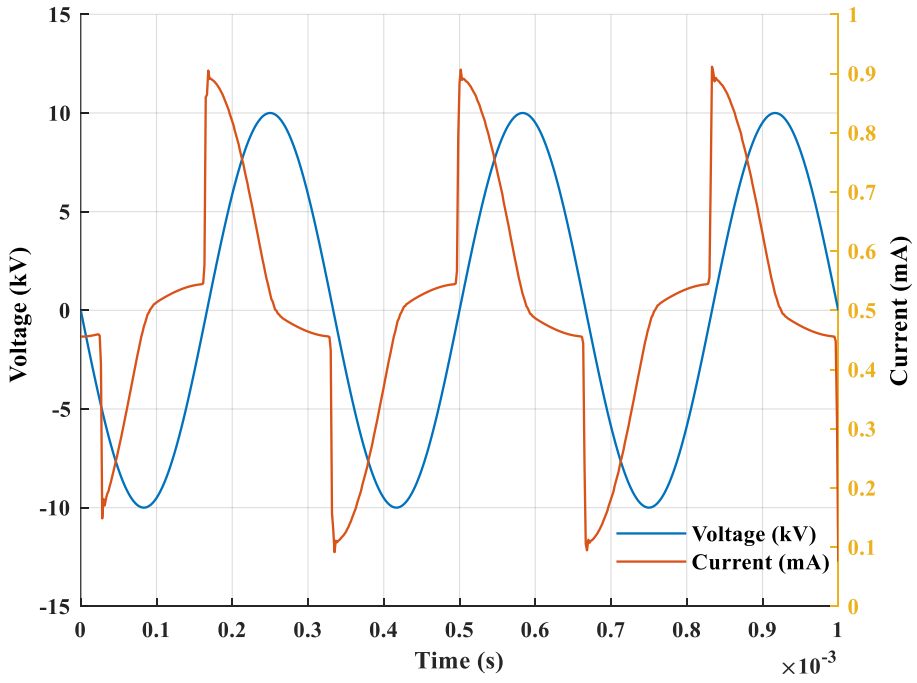

Fig. IV.2 *Discharge Current and Voltage Waveform in Three Periods of DBD Discharge*

These current spikes occur in synchronization with specific phases of the voltage signal, particularly near the voltage zero-crossings and extrema. This suggests the presence of nonlinear conduction phenomena; they induced by the breakdown of insulating media and dielectric barrier discharges.

IV.5.2. Evolution of Charged Particles Densities

Figures IV.3 and IV.4 present the time-resolved number densities of positive and negative charged particles, respectively, over a 1 ms under periodic electrical excitation.

1. Positive Charged Species

The dominant positive ion observed is NO^+, which reaches peak densities on the order of 10^{17} m^{-3}, significantly exceeding those of other ions. The positive ion densities of others such as O_2^+, N_2^+, and O^+ exhibit synchronized oscillations, with peak values ranging from 10^{12} to 10^{14} m^{-3}. The rare gas ions Ar^+ and Ar_2^+ remain nearly constant, with lower densities ($\sim 10^8$ m^{-3}), reflecting their more inert chemical behavior under the studied discharge conditions.

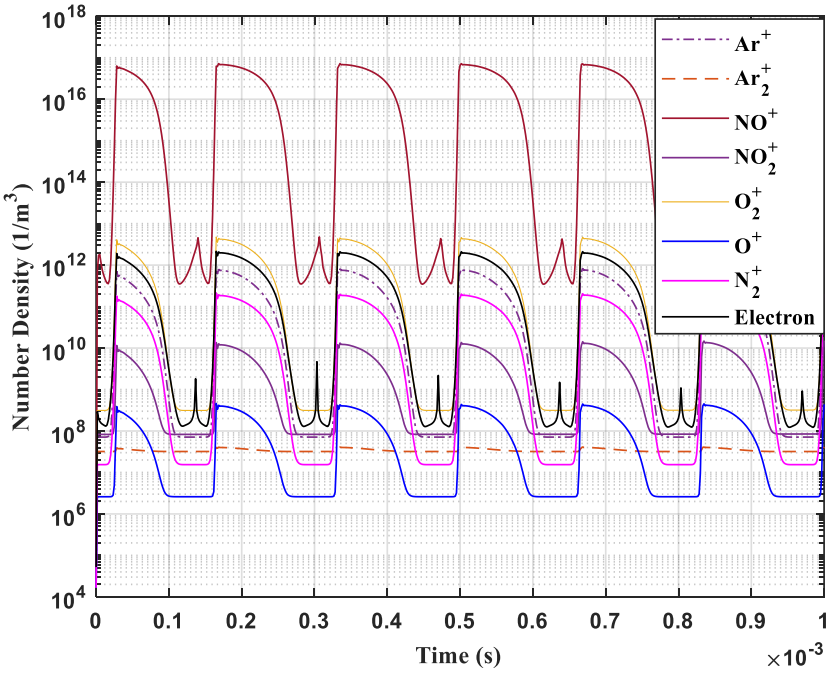

Fig IV.3 *Evolution of Positive Charges Densities During Three Periods of DBD Discharge*

2. Negative Charged Species

Among the negative ions, $\mathbf{NO_2^-}$ and $\mathbf{O^-}$ dominate the charge carrier population, with densities peaking around 10^{12} m^{-3}. Other anionic species such as $\mathbf{O_2^-}$, $\mathbf{O_3^-}$, $\mathbf{O_4^-}$, and $\mathbf{NO^-}$ also exhibit notable presence, contributing to the overall electronegativity of the plasma. The periodic

rise and fall in their concentrations are anti correlated with the electron density, consistent with electron attachment processes being more effective during relaxation phase.

The presence of multiple ions, especially oxygen containing ones, reflects a chemically rich plasma environment with active dissociation, attachment, and recombination reactions. The formation of these species is susceptible to electron energy and gas composition, reinforcing the complex temporal chemistry driven by the applied voltage.

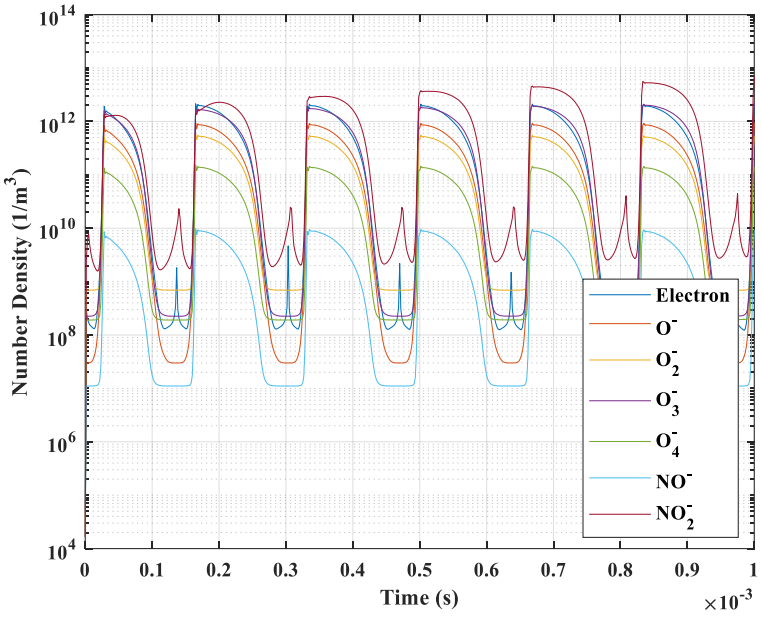

Fig IV.4 *Evolution of Negative Charges Densities During Three Periods of DBD Discharge*

Together, these figures reveal highly dynamic and chemically active plasma in which ionization, attachment, and recombination processes vary rapidly within each voltage cycle. The clear phase dependence and distinct behavior of individual species provide key insights into discharge kinetics, offering a foundation for optimizing plasma-driven applications in gas processing.

The electron density closely follows the similar temporal trend as the dominant molecular ions, particularly NO^+ and O_2^+, indicating a strong coupling between ionization processes and the applied voltage waveform. The stepwise variation and recurrent peaks in densities suggest periodic ionization and recombination events modulated by the applied electric field.

IV.5.3 Evolution of Exited Particles

Figures IV.5 and IV.6 depict the time-dependent behavior of important excited atomic and molecular types in a dielectric barrier discharge (DBD) plasma, which shed light on the discharge's energy distribution and excitation kinetics.

a. Excited Nitrogen States

Figure IV.5 shows the temporal evolution of several excited nitrogen states, including singlet and triplet metastable and radiative levels such as **N_2(A3s)**, **N_2(B3p)**, and **N_2(C3p)**, along with their related population states (**N_2(a1s)**, **N_2(d)**, **N_2(p)**). The results reveal a periodic generation of excited species that is closely synchronized with the applied voltage waveform. The **N_2(A3s)** state, a long-lived metastable, exhibits the highest density (peaking around 6×10^{13} m^{-3}, with a sharp increase at each discharge pulse followed by exponential decay, characteristic of excitation during the breakdown phase and subsequent quenching or radiative decay. The **C-state (N_2(C3p))** and **B-state (N_2(B3p))** also shows similar trends but with slightly lower densities, consistent with their shorter lifetimes and higher energy thresholds.

The sequential appearance and decay of these excited states confirm that nitrogen plays a dominant role in energy transfer processes in the plasma. These species are also indicators of electron impact excitation and serve as precursors for vibrational and dissociative processes.

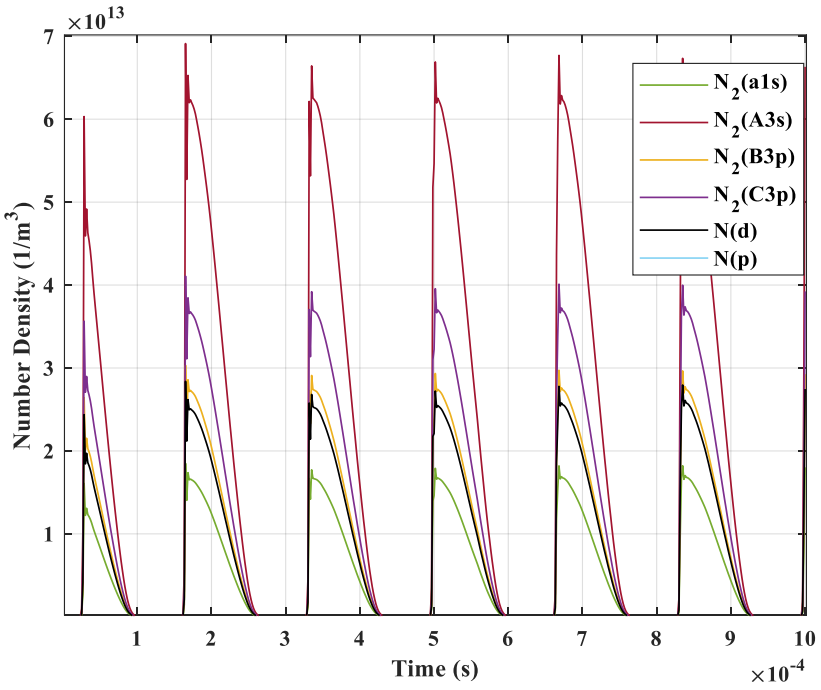

Fig IV.5 *Evolution of Excited Nitrogen Species Densities During Three Periods of DBD.*

b. Excited Oxygen and Argon Species

Figure IV.6 presents the number densities of electronically excited oxygen and argon states, including **O(1s), O(1d), O_2(b1s), O_2(a1d),** and **O_2(45),** as well as excited **Ar(s)** levels. Oxygen species exhibit significantly higher peak densities, reaching up to 10^{17} m^{-3}, particularly

for **O_2(45)** and **O_2(b1s).** Their behavior shows apparent periodicity aligned with the applied voltage cycles, indicating strong electron impact excitation during discharge phases.

Although less concentrated (~10^{10} m^{-3}), the excited argon species follow a similar temporal trend, showing a delayed response compared to oxygen due to differences in excitation thresholds and cross-sections. The persistence of Ar(s) may play a role in sustaining the plasma via Penning ionization, especially in mixtures with nitrogen and oxygen.

These observations suggest that oxygen contributes more significantly to the pool of reactive excited species due to its high electron affinity and multiple accessible energy levels. The rapid quenching of oxygen states between discharge cycles highlights the transient nature of these excitations and their strong coupling to the pulsed electric field.

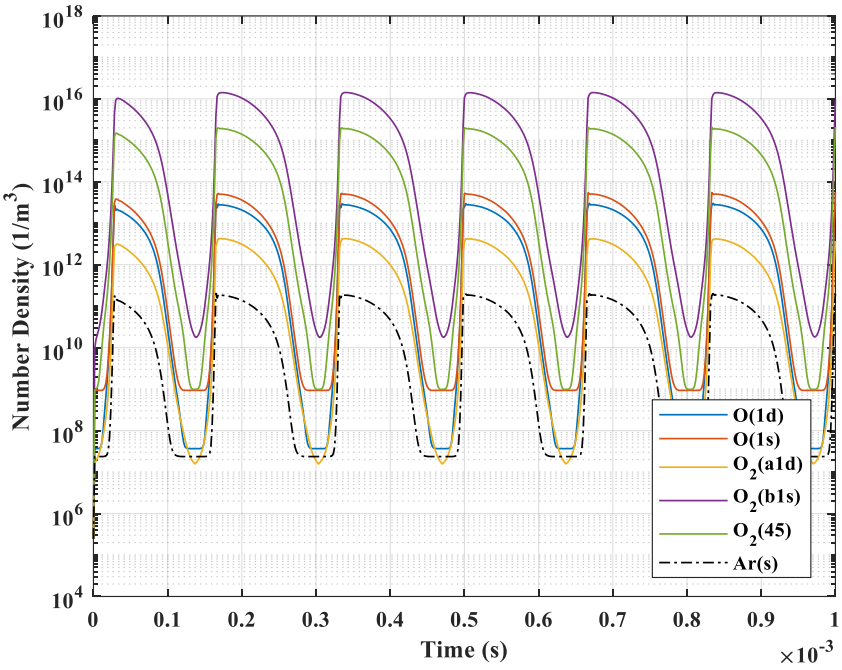

Fig IV.6 *Evolution of Excited Oxygen Species Densities During Three Periods of DBD.*

IV.5.4. Temporal Evolution of Neutral Particles during NO Removal in DBD

Figure IV.7 illustrates the temporal variation of different neutral gas-phase particles involved in the removal of nitric oxide (NO) within a dielectric barrier discharge (DBD) plasma over a 100 ms period. The number densities are plotted on a logarithmic scale to capture the broad dynamic range of concentrations, spanning from 10^5 to 10^{25} m^{-3}.

❖ ***NO Depletion and Reaction Pathways***

The most prominent feature is the progressive decline in NO concentration, starting from a high initial value (~10^{24} m^{-3}) and decreasing by multiple orders of magnitude during the

simulation. This strong depletion indicates the effective destruction of NO by plasma activated processes, including reactions with atomic oxygen and nitrogen species and the formation of higher order nitrogen oxides.

Concurrently, NO_2 rapidly accumulates and reaches a quasi-steady state at around 10^{21} m^{-3}, suggesting that NO is primarily oxidized to NO_2 in the early stages. This is consistent with the well-known reaction:

$$NO + O \rightarrow NO_2 \quad \text{(IV.6)}$$

❖ ***Formation of Secondary Products***

As the discharge progresses, further oxidation leads to the formation of NO_3, N_2O_5, and O_3, which exhibit slower but steady increases in concentration. Notably:

- **NO_3** increases gradually and stabilizes near 10^{18} m^{-3}, indicating its role as a secondary oxidation product.
- **N_2O_5** and **O_3** show delayed formation but reach similar concentrations, highlighting the multi-step reaction pathways involving NO_2 and O atoms or radicals.
- **N_2O** forms rapidly and stabilizes early, reflecting the contribution of recombination and neutral-neutral reactions in the nitrogen cycle.

The atomic oxygen (O) and atomic nitrogen (N) species, which are critical intermediates, remain relatively low in concentration but increase modestly during the early discharge stages before plateauing. These atoms facilitate the initiation and propagation of NO decomposition and oxidation reactions.

❖ ***Ozone (O_3) as a Key Oxidizing Agent***

The generation of ozone (O_3) is particularly significant in the discharge process. During the latter stages of discharge, O_3 emerges as a primary oxidizing species, attaining peak concentrations on the order of 10^{22} m^{-3}. Beyond its direct involvement in the oxidation of NO and NO_2, ozone participates in the formation of higher nitrogen oxides, such as NO_3 and N_2O_5, thereby influencing the overall nitrogen chemistry within the reactor.

The temporal evolution of reactive species indicates that NO removal in DBD plasma proceeds through a cascade of rapid radical mediated reactions during the early phase, followed by slower oxidation and recombination processes that produce more stable nitrogen-containing by-products. The dynamic interplay among NO, NO_2, atomic oxygen (O), O_3, and other

intermediate nitrogen oxides underscores the complexity of the reaction network. These observations highlight the critical role of plasma operating conditions including electric field strength, gas composition, and discharge time in governing both the efficiency of pollutant abatement and the nature and yield of secondary products.

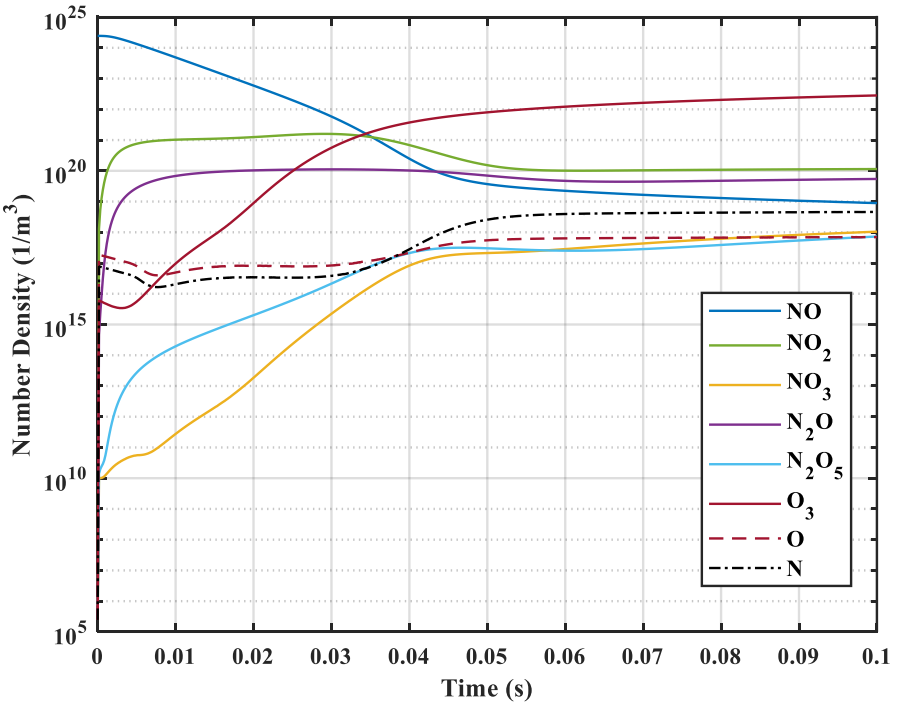

Fig IV.7 *Neutral Species Evolution in DBD During NO Removal in (*69% N_2, 20% O_2, 1% Ar,10% NO)

IV.5.5. Temporal Variation Mole Fraction of NO

Figure 8 presents the time dependent evolution of the nitric oxide (NO) mole fraction for several initial inlet concentrations, namely 10%, 7.5%, 5%, and 2.5%, in an atmospheric-pressure dielectric barrier discharge reactor. For all investigated cases, a rapid decrease in NO concentration is observed as the discharge progresses, clearly demonstrating the strong capability of plasma-assisted processes to promote NO conversion under non-thermal conditions.

At higher initial concentrations, particularly for the 10% NO case, the reduction occurs extremely rapidly during the early stages of the discharge. This behavior can be attributed to the enhanced frequency of interactions between NO molecules and energetic electrons, as well as with highly reactive plasma-generated species such as atomic oxygen (O), ozone (O_3), and electronically excited nitrogen states. These reactive agents significantly accelerate NO oxidation and dissociation pathways, resulting in an abrupt decline of NO concentration shortly after plasma ignition. Remarkably, the simulations indicate that, after approximately 0.025 s of treatment, more than 99% of the initial NO is eliminated in all cases, independent of the initial

mole fraction. This finding highlights the ability of the DBD reactor to achieve near complete NO removal within a very short effective residence time.

For lower initial NO concentrations, such as 2.5%, the temporal decay profile exhibits a comparatively smoother slope, reflecting reduced collision probabilities and reaction rates due to the lower availability of NO molecules. Nevertheless, complete or near complete removal is still attained within the same characteristic time interval. This observation reveals a nonlinear relationship between NO depletion kinetics and initial concentration, arising from the complex coupling between electron driven processes, reactive species densities, and competing plasma chemical reactions.

Overall, these results confirm the high chemical reactivity and operational efficiency of dielectric barrier discharge plasmas for NO abatement. The insights gained from the temporal behavior of NO removal provide valuable guidance for optimizing key reactor parameters, including discharge power, operating time, and gas residence duration, thereby supporting the development of efficient plasma based solutions for environmental pollution control.

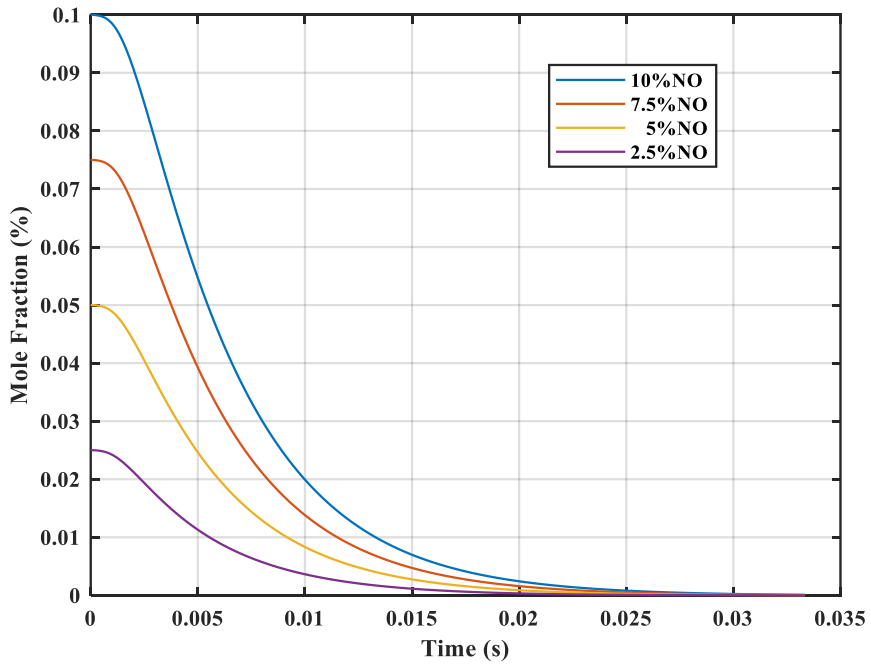

Fig IV.8 *Temporal Variance of NO Mole Fraction Over 100 DBD Discharge Periods*

IV.5.6. Effect of Voltage on the NO Removal

The NO mole fraction's temporal change under dielectric barrier discharge (DBD) circumstances is depicted in figure 9 for three distinct applied voltages: 8 kV, 10 kV, and 12 kV, starting with a 10% NO concentration and a fixed frequency of 3 kHz.

The results clearly demonstrate that increasing the applied voltage enhances the NO removal efficiency. This trend is attributed to the higher electrical field strength at increased voltages, which in turn leads to greater electron energy. As a result, more energetic electrons are available to initiate dissociation and oxidation reactions involving NO, producing reactive species such as O, O_3, and N that contribute to NO decomposition. At **0.025 seconds**, the NO mole fraction has significantly dropped for all voltage levels; however, the rate of decay is noticeably faster at 12 kV, indicating accelerated NO conversion due to more intense plasma activity. In contrast, at 8 kV, the removal is slower and less efficient, due to insufficient energy to fully activate the gas-phase chemistry within the short residence time.

These findings highlight the critical role of voltage in optimizing DBD reactors for NO_x abatement. Higher voltages promote more effective plasma generation, which enhances reaction kinetics and shortens the time required for near-complete NO removal. However, practical considerations such as energy efficiency, thermal effects, and dielectric material limits must be considered when scaling up the voltage in industrial implementation.

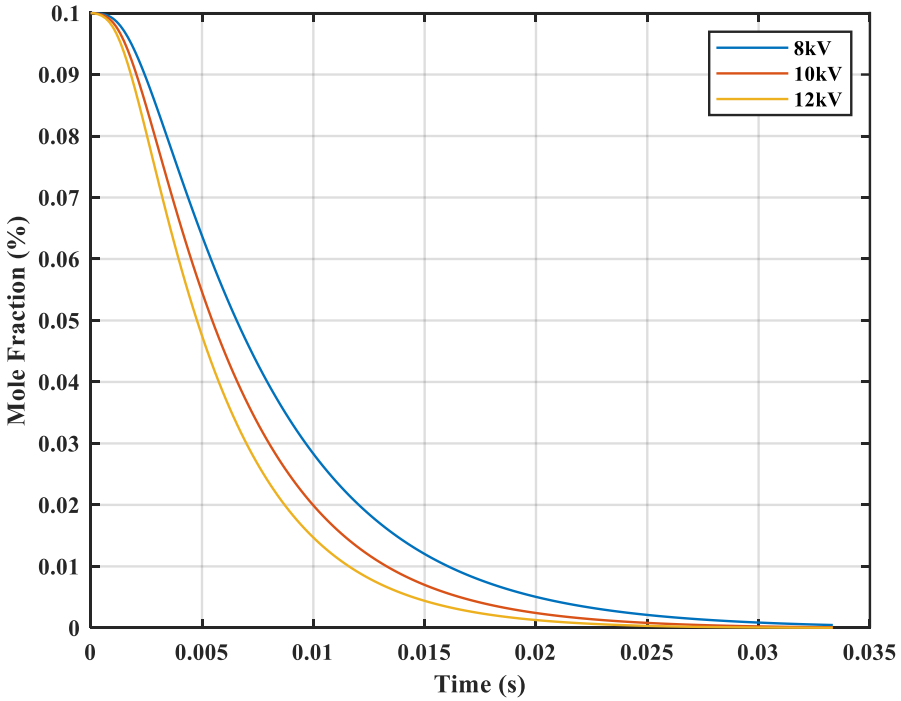

Fig IV.9 *Impact of Voltage on NO Removal Over 100 DBD Discharge Periods*

IV.5.7. Effect of Frequency on the NO Removal

Graph 10 illustrates the temporal variation of NO mole fraction under DBD conditions for three applied frequencies: 2kHz, 3kHz, and 4kHz, with a constant voltage of 10 kV and an initial NO concentration of 10%.

Increasing the frequency enhances the NO removal efficiency. As frequency rises, the number of discharge cycles per second increases, which results in a more frequent generation of energetic electrons and reactive plasma species. These reactive species, including O, O_3, and excited N_2/O_2 states, play a critical role in NO decomposition through oxidation and dissociation mechanisms. At **0.025 s**, the NO mole fraction is significantly lower for higher frequencies, indicating faster NO degradation. The curve for 4 kHz drops more rapidly compared to 2 kHz and 3 kHz, demonstrating that higher frequency facilitates more effective plasma driven chemical reactions. This is because a higher frequency enhances the average power density and discharge uniformity, both of which promote better gas treatment efficiency.

These results affirm that frequency is a key control parameter for optimizing DBD reactors in NO_x abatement applications.

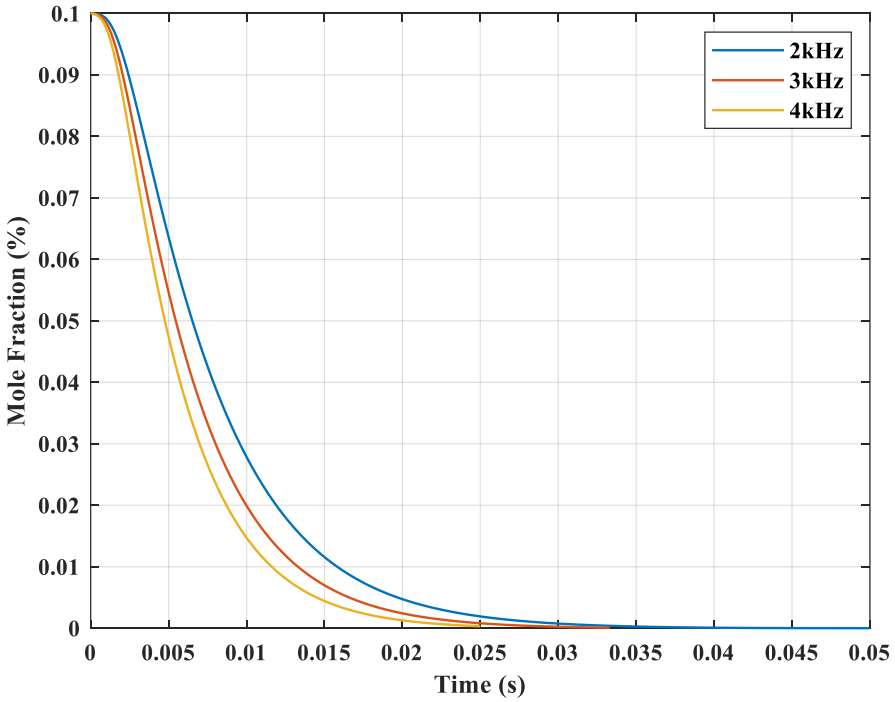

Fig IV.10 *Impact of Frequency on NO Removal Over 100 DBD Discharge Periods*

IV.6. Conclusion

This chapter presented a detailed numerical investigation of the application of dielectric barrier discharge (DBD) plasma for nitric oxide (NO) removal in air and N_2–O_2–Ar–NO gas mixtures. The influence of operating parameters, particularly applied voltage and excitation frequency, on discharge behavior and plasma chemistry was systematically analyzed. The simulation results demonstrated that both parameters play a critical role in controlling the electrical characteristics of the discharge, the formation of reactive species, and the overall efficiency of NO conversion. The spatiotemporal distributions of electrons, charged particles, and key reactive radicals were examined, providing valuable insight into the underlying discharge mechanisms and non-equilibrium plasma dynamics. The evolution of NO mole fraction revealed the dominant chemical pathways responsible for NO removal, highlighting the importance of reactive oxygen and nitrogen species generated under specific operating conditions. These findings elucidate the complex interplay between electrical excitation, plasma kinetics, and pollutant conversion.

References

[1] B. Parent, F. M. F. Rodriguez, "Progress in electron energy modeling for plasma flows and discharges, "Physics *of Fluids*, vol. 36, no. 8, 2024.

[2] E. Carbone, "Data needs for modeling low-temperature non-equilibrium plasmas: the LXCat project, history, perspectives and a tutorial," *Atoms*, vol. 9, no. 1, p. 16, 2021.

[3] Hayashi database, www.lxcat.net, retrieved on May 4, 2025.

[4] M. H. A. Lahouel, D. Benyoucef, A. Gadoum, "One Dimensional Modeling of Dielectric Barrier Discharge in Pure Oxygen at Atmospheric Pressure Using Comsol Multiphysics," *1st International Symposium on Materials, Energy and Environment, El Oued, Algeria*, 2020.

[5] K. W. Cheng,*et al*., "Fluid modeling of a nitrogen atmospheric-pressure planar dielectric barrier discharge driven by a realistic distorted sinusoidal alternating current power source," *Japanese Journal of Applied Physics*, vol. 51, no.11, 116001, 2012.

[6] F. Massines, "Physics and chemistry in a glow dielectric barrier discharge at atmospheric pressure: diagnostics and modelling," *Surface and Coatings Technology*, vol. 174, pp. 8-14, 2003.

[7] Triniti database, www.lxcat.net, retrieved on May 4, 2025

[8] J. Bacri, A. Medani, "Electron diatomic molecule weighted total cross section calculation," *Physica*, vol. 101, no. 3, pp. 399-409,1980.

[9] C. Lazarou, *et al*., "Numerical modeling of the effect of the level of nitrogen impurities in a helium parallel plate dielectric barrier discharge," *Plasma Sources Science and Technology*, vol. 24, no. 3, 2015.

[10] I. H. Tsai, C. C. Hsu," Numerical simulation of downstream kinetics of an atmospheric-pressure nitrogen plasma jet," *IEEE Transactions on Plasma Science*, vol. 38, no. 12, pp. 3387-3392, 2010.

[11] Y. H. Choi, J. H. Kim, Y. S. Hwang, "One-dimensional discharge simulation of nitrogen DBD atmospheric pressure plasma," *Thin solid films*, vol. 506, pp. 389-395,2006.

[12] Phelps database, www.lxcat.net, retrieved on May 4, 2025

[13] I. A. Kossyi, *et al*., "Kinetic scheme of the non-equilibrium discharge in nitrogen-oxygen mixtures," *Plasma Sources Science and Technology*, vol. 1, no. 3, p. 207, 1992.

[14] Morgan database, www.lxcat.net, retrieved on May 4, 2025

[15] J. K. Lefkowitz, *et al*., "Species and temperature measurements of methane oxidation in a nanosecond repetitively pulsed discharge," *Philosophical Transactions of the Royal Society A: Mathematical, Physical and Engineering Sciences*, vol. 373, no. 2048, 2015.

[16] O. Eichwald, *et al*., "Coupling of chemical kinetics, gas dynamics, and charged particle

kinetics models for the analysis of NO reduction from flue gases," *Journal of Applied Physics*, vol. 82, no. 10, pp. 4781-4794, 1997.

[17] M. H. A. Lahouel, " Modélisation et simulation d'une décharge à barrière diélectriques dans un Mélange gazeux à la pression atmosphérique, " *Thèse de Doctorat, Hassiba ben Bouali de chlef*, 2021.

[18] M. Benyamina, "Etude de la production de l'ozone dans les décharges couronne ». *Université d'Oran de la Sciences et de la Technologie (USTOMB)*, 2014.

[19] N. Vichiansan, *et al.,* "Simulation of simple 2D plasma jet model for NO, OH, and H2O2 production via Multiphysics in laminar flow and transport of diluted species through design of experiment method," *AIP Advances*, vol. 11, no. 3, mars 2021.

[20] SIGLO database, www.lxcat.net, retrieved on May 4, 2025.

[21] D. Liu, *et al.*," Main species and chemical pathways in cold atmospheric-pressure Ar^+ H_2O plasmas," *Plasma Sources Science and Technology*, vol. 26, no. 4, p. 045009, 2017.

General Conclusion

General Conclusion

This thesis demonstrated the strong potential of Dielectric Barrier Discharge (DBD) plasma as an effective non-thermal technology for nitrogen oxides (NO_x) reduction under atmospheric-pressure conditions. The originality of this work lies in the development of a self-consistent numerical framework coupling plasma physics, charged particle transport, electric field evolution, and detailed plasma chemistry in air-based gas mixtures relevant to NO removal.

Using COMSOL Multiphysics, a one-dimensional fluid model was successfully implemented to investigate the temporal evolution of electrons, ions, excited species, and neutral reactive particles involved in the discharge process. The simulations revealed that NO_x conversion is primarily governed by electron-impact reactions and by the generation of reactive oxygen and nitrogen species such as O, N, and O_3, which strongly influence the oxidation and dissociation pathways of nitrogen oxides.

One of the major outcomes of this work is the identification of the operating conditions leading to enhanced NO removal efficiency. The study established that both the applied voltage and excitation frequency play a decisive role in controlling plasma activity, electron energy, and reactive species production. Under optimized operating conditions corresponding to an applied voltage of 10 kV and an excitation frequency of 3 kHz, the developed model predicted a NO reduction efficiency approaching 99%, confirming the high capability of DBD plasma for atmospheric pollutant treatment.

The obtained results also highlighted the dominant contribution of ozone-assisted oxidation pathways, together with secondary reactions involving NO_2, NO_3, N_2O, and N_2O_5. The temporal evolution of these species demonstrated the existence of a complex and highly coupled plasma-chemical reaction network responsible for NO conversion. Another important contribution of this work is the proposal of a predictive numerical framework for evaluating the influence of discharge parameters on NO_x removal performance. This model provides valuable physical insight into plasma-assisted depollution mechanisms and constitutes a useful basis for reactor optimization and future industrial applications.

Despite these promising results, some limitations remain associated with the one-dimensional approximation adopted in this study. The 1D model cannot fully reproduce filamentary structures, multidimensional transport phenomena, and spatial non-uniformities characteristic of real DBD discharges. Therefore, extending the model toward 2D or 3D configurations would improve the realism and predictive capability of the simulations.

Furthermore, although the numerical results are physically coherent and consistent with trends reported in the literature, experimental validation remains essential to confirm the predicted discharge behavior, species evolution, and NO_x conversion efficiency under real operating conditions.

Future Works

While the results obtained in this thesis are promising, several opportunities for further development and improvement remain. The following perspectives outline potential directions for future research:

- **Extending the Model to 2D or 3D Geometries**

A multidimensional model would capture lateral non-uniformities, filament interactions, and surface effects more realistically. This would allow better prediction of streamer branching, power deposition, and reactor-scale inhomogeneities.

- **Coupling Plasma with Catalysts (Plasma–Catalysis)**

Coupling the DBD with catalytic surfaces or packed-bed materials could enhance NO oxidation/reduction pathways, reduce energy consumption, and minimize undesired by-products (e.g., O_3, N_2O). Modeling supported by targeted experiments represents a promising advancement.

- **Experimental Validation**

Although the numerical results are highly informative, experimental campaigns would be essential to validate the spatial and temporal distributions of species, confirm the predicted NO removal pathways and assess long-term reactor stability and energy efficiency.

- **Industrial-Scale Integration**

Finally, scaling up DBD technology for industrial exhaust treatment requires addressing, energy efficiency for removed NO_x molecules, gas flow effects and residence times, durability of dielectric materials, and compact reactor designs adapted to real flue-gas condition.

Overall, this work confirms that DBD plasma represents a promising, flexible, and environmentally friendly technology for NO_x abatement. Beyond the numerical results themselves, the developed model contributes to a deeper understanding of the coupling between plasma physics and chemical kinetics and provides a scientific framework for future optimization, plasma-catalysis integration, and industrial-scale environmental applications.